

LEWIS
GRANT
111-02
234609
P-230

Turbulent Swirling Jets With Excitation

Rahmat Taghavi and Saeed Farokhi
*The University of Kansas Center for Research, Inc.
Lawrence, Kansas*

March 1988

Prepared for
Lewis Research Center
Under Grant NCC-3-56



(NASA-CR-180895) TURBULENT SWIRLING JETS
WITH EXCITATION Interim Report (Kansas
Univ. Center for Research) 230 p CSCL 01A

N89-29329

Unclass
0234609

G3/02

TABLE OF CONTENTS

	<u>Page</u>
CHAPTER ONE: INTRODUCTION.....	1
1.1 EFFECT OF INITIAL TANGENTIAL VELOCITY DISTRIBUTION ON THE MEAN EVOLUTION OF A SWIRLING TURBULENT JET.....	1
1.2 CONTROLLED EXCITATION OF A COLD TURBULENT SWIRLING FREE JET.....	3
1.3 PRESENT CONTRIBUTION.....	4
CHAPTER TWO: LITERATURE REVIEW.....	6
2.1 FREE SWIRLING FLOWS (EXPERIMENTAL STUDIES).....	6
2.2 CONFINED SWIRLING FLOWS (EXPERIMENTAL STUDIES).....	15
2.3 THEORETICAL STUDIES OF SWIRLING FLOWS.....	29
2.4 VORTEX BREAKDOWN.....	33
2.5 AERODYNAMIC EXCITATION OF FREE SHEAR FLOWS.....	36
2.6 MEASUREMENT TECHNIQUES IN SWIRLING FLOWS.....	38
2.6.1 Multihole Probe Techniques.....	38
2.6.2 Hot-Wire Techniques.....	44
CHAPTER THREE: EXPERIMENTAL FACILITIES AND INSTRUMENTATION.....	49
3.1 JET FACILITY.....	49
3.1.1 Swirl Generator.....	49
3.1.2 Air Supply and Control System.....	52

TABLE OF CONTENTS, continued

	<u>Page</u>
3.1.3 Excitation Section.....	53
3.1.4 Exit Nozzle.....	53
3.2 INSTRUMENTATION.....	53
3.2.1 Five-Hole Pitot Probe.....	53
3.2.2 Hot-Wire Anemometry.....	54
3.2.3 Microphone.....	55
3.2.4 Probe Positioning.....	55
3.2.5 Data Acquisition System.....	56
CHAPTER FOUR: EXPERIMENTAL PROCEDURE.....	58
4.1 MEAN FLOW MEASUREMENTS.....	58
4.2 FLUCTUATING FLOW MEASUREMENTS.....	59
4.3 OVERALL SOUND PRESSURE LEVEL MEASUREMENTS.....	60
4.4 EXCITABILITY EXPERIMENTS.....	60
4.5 SUMMARY OF THE TESTS.....	61
CHAPTER FIVE: RESULTS AND DISCUSSION.....	62
5.1 SYSTEM EVALUATION.....	62
5.1.1 Instrumentation.....	62
5.1.2 Swirl Generator.....	63
5.2 EFFECT ON INITIAL MEAN TANGENTIAL VELOCITY DISTRIBUTION ON THE EVOLUTION OF FREE SWIRLING TURBULENT JETS.....	64
5.2.1 Mean Flow Field.....	64
5.2.2 Fluctuating Flow Field.....	70

TABLE OF CONTENTS, continued

	<u>Page</u>
5.3 EXCITABILITY EXPERIMENTS.....	71
5.4 EFFECT OF SCREEN.....	74
CHAPTER SIX: SUMMARY AND CONCLUSIONS.....	76
CHAPTER SEVEN: RECOMMENDATIONS FOR FUTURE WORK.....	78
7.1 SWIRLING FLOW INVESTIGATION.....	78
7.2 ACOUSTIC EXCITATION.....	78
CHAPTER 8: REFERENCES.....	80
FIGURES.....	94
TABLES.....	138
APPENDICES:	
A. FIVE-HOLE PROBE CALIBRATION PROCEDURE.....	A.1
B. HOT-FILM CALIBRATION PROCEDURE.....	B.1
C. COMPUTER PROGRAMS.....	C.1
D. BLUEPRINTS.....	D.1

LIST OF SYMBOLS

<u>Symbol</u>	<u>Definition</u>	<u>Dimension</u>
I. Latin		
a	Speed of sound	ft/sec
b	Effective jet width	inch
C	Constant	---
D	Nozzle exit diameter	inch
f	Frequency	Hz
G	Degree of swirl $\left(\frac{W_{mo}}{U_{mo}}\right)$	---
G_x	Axial momentum flux	$\frac{\text{lbm} \cdot \text{ft}}{\text{sec}^2}$
G_θ	Angular momentum flux	$\frac{\text{lbm} \cdot \text{ft}^2}{\text{sec}^2}$
HIP	Half impact pressure $P_5 - \frac{1}{4} (P_1 + P_2 + P_3 + P_4)$	psig
L	Vortex core diameter	inch
M	Mach number	---
MAN (A)	Manifold (A)	---
MAN (C)	Manifold (C)	---
\dot{m}	Mass flow rate	lbm/sec
N	Number of elbows	---
NPPD	Normalized pitch pressure difference $\left(\frac{P_3 - P_1}{\text{HIP}}\right)$	---

LIST OF SYMBOLS, continued

<u>Symbol</u>	<u>Definition</u>	<u>Dimension</u>
NSPD	Normalized static pressure difference $\frac{\frac{1}{4} (P_1 + P_2 + P_3 + P_4) - P_s}{HIP}$	---
NTPD	Normalized total pressure difference $\left(\frac{P_5 - P_t}{HIP}\right)$	---
OASPL	Overall Sound Pressure Level	dB
P	Pressure	psig
P ₁ ,...P ₅	Five-hole pitot probe pressure outputs	psig
P _t	Total pressure	psig
P _s	Static pressure	psig
P _∞	Ambient pressure	psia
Q̇	Volumetric flow rate	ft ³ /sec
R	Gas constant	ft • lb _f /lbm • °R
R	Nozzle exit radius	inch
Re	Reynolds number	---
r	Radial distance between the measuring point and jet axis	inch
r _{1/2}	Half velocity radius (where U = $\frac{1}{2}$ U _m)	inch
r _{1/10}	One-tenth velocity radius (where U = $\frac{1}{10}$ U _m)	inch
S	Swirl number $\left(\frac{G_\theta}{G_x \cdot R}\right)$	---
St	Strouhal number	---
T	Temperature	°R, °F
U, V, W	Time mean axial, radial, and tangential velocity components	ft/sec

LIST OF SYMBOLS, continued

<u>Symbol</u>	<u>Definition</u>	<u>Dimension</u>
u, v, w	Fluctuating axial, radial, and tangential velocity components (rms)	ft/sec
V	Total time mean velocity	ft/sec
x, r, θ	Axial, radial, and azimuthal cylindrical polar coordinates	---
x_0	Location of the "jet effective origin"	inch
Y	Radial distance from the jet center in Y direction	inch
 II. <u>Greek</u>		
α	Half jet angle ($\tan \alpha = \frac{r_{1/2}}{x}$)	degrees
β	Yaw angle	degrees
δ	Pitch angle	degrees
ϕ	Vane angle	degrees
γ	Specific heat ratio	---
Γ	Circulation	ft ² /sec
ρ	Density	slug/ft ³
μ	Micro	---
Ω	Vorticity	1/sec
ω	Frequency	Hz
ψ	Stream function	---
 III. <u>Subscripts</u>		
a	Mass averaged	
AMB	Ambient	
f	Fundamental	

LIST OF SYMBOLS, continued

<u>Symbol</u>	<u>Definition</u>	<u>Dimension</u>
m	Local maximum	
m_0	Local maximum at $x/D = 0$	
P	Relative to probe sensing tip diameter	
rms	Root mean square	
s	Static, tangential	
x	Quantity on the jet axis, axial	
θ	Tangential	
θ	Angular	
0	at $x/D = 0$	
t	Total	
∞	Ambient	

1. INTRODUCTION

Two major distinct problems are investigated in this report which are introduced as follows:

1.1 EFFECT OF INITIAL TANGENTIAL VELOCITY DISTRIBUTION ON THE MEAN EVOLUTION OF A SWIRLING TURBULENT FREE JET

Turbulent jets with swirl exhibit distinctive characteristics absent in their nonrotating counterparts. A subsonic swirl-free jet, for example, experiences theoretically no static pressure gradient in the axial or radial direction. Hence, in this case, the mechanism for jet spread is dominated by the turbulent mixing at the interface between the jet and the ambient fluid. A turbulent jet with strong swirl, on the other hand, is primarily driven in the near field ($x/D < 5$) by the static pressure gradients in both axial and radial direction, i.e. mainly an inviscid phenomenon. Turbulent mixing then becomes a dominant factor only when the strong pressure gradients are weakened through rapid initial jet spread (i.e. a jet in near pressure equilibrium). The occurrence of flow reversal in the jet, or what is known as vortex breakdown, is a fascinating phenomenon observed in high-intensity swirling flows, which we will briefly discuss in this report. The absence of a potential core, by definition, in a swirling jet is another feature which distinguishes the rotating from the nonrotating jets.

The nondimensional parameter describing the integrated swirl strength in a jet is the swirl number S , and is defined as

$$S \equiv G_{\theta} / G_x R \quad (1)$$

$$\text{where } G_{\theta} \equiv 2\pi \int_0^{\infty} \rho U W r^2 dr; \text{ jet torque,} \quad (2)$$

$$G_x \equiv 2\pi \int_0^{\infty} [\rho U^2 + (p - p_{\infty})] r dr; \text{ jet axial thrust,} \quad (3)$$

and R is the nozzle exit radius. The inclusion of the turbulent shear and normal stresses, $\rho \overline{u w}$ and $\rho \overline{u^2}$, in the integrands of the jet torque and thrust expressions, i.e. Equations (2) and (3), respectively, provide for total jet thrust and torque as described in Reference [1]. However, our swirl number definition excludes Reynolds stresses. By definition, the swirl number is an integrated quantity; hence, it is possible to generate swirling jets with different initial tangential velocity profiles ranging from solid body rotation [i.e. $W_0(r) = c \cdot r$] to near free-vortex flow [i.e. $W_0(r) \approx c/r$] with constant "S." Moreover, as the static pressure field is coupled to the tangential velocity distribution, through the momentum equations, and dominates the swirling jet evolution in the near field, vastly different mean jet behavior (e.g. mean centerline velocity decay) should be observable in swirling jets with constant "S." Chigier and Beer [1] and Pratt and Keffer [2], among others, have acknowledged the above problem and claimed that the method by which the swirl is generated, meaning initial velocity distribution, would affect the evolution of swirling flows. They reached the conclusion that "swirl number cannot be the sole universal criterion of similarity for swirling jets unless the flows

are generated by geometrically similar swirl generators." There have been some attempts in the past towards the study of effects of initial axial velocity distributions in swirling jet evolution [3,4]; but to our knowledge, this is the first comprehensive experimental investigation of the effects of initial tangential velocity distribution.

1.2 CONTROLLED EXCITATION OF A COLD TURBULENT SWIRLING FREE JET

Controlled excitation of free shear flows has been under extensive theoretical and experimental investigations over the past decade. This technique has been vastly used to study flow instabilities, large-scale coherent structures, and flow control. Among the flows mainly studied are axisymmetric jets and boundary layers. Acoustic drivers as well as mechanical devices and heat strips have been used as a means of excitation [5].

It is already understood that acoustic excitation at the "right" Strouhal number ($f \cdot D/U$) has significant effects on mixing characteristics of jets, provided that the excitation amplitude is beyond a certain minimum "threshold level." Acoustic excitation is also found to significantly influence the flow separation over an airfoil at some specific Strouhal numbers [6, 7].

There has not been any experimental investigation of the effect of excitation on swirling flows. As swirling flows are present in many practical applications, the effect of controlled excitation, if any, may improve the flow quality through devices such as

turbomachinery and jet engine diffusers, and over delta wings at high angles of attack, etc.

1.3 PRESENT CONTRIBUTION

To conduct the swirling flow experiments, a unique swirl generator was designed, built, and incorporated in an existing cold jet facility at NASA-Lewis Research Center. The system is capable of generating flows at a wide range of swirl numbers with controllable initial tangential velocity distributions. Distinctly different swirl velocity profiles, ranging from solid-body rotation to a profile predominated by a free-vortex distribution, with identical swirl numbers, were produced.

A five-hole pitot probe was designed and fabricated; and the necessary instrumentation, controls, and software were developed for mean flow measurements. Single, constant-temperature, hot-wire anemometers, and microphones, were used to take limited turbulence data and measure overall sound pressure levels, respectively, along the jet centerline.

With the above capability, the effects of mean initial tangential velocity distribution on the evolution of a free swirling jet is experimentally investigated. Two flows with identical initial swirl numbers, Mach numbers, and mass flow rates but with different initial swirl profiles are compared up to a distance of 12 nozzle diameters downstream of the nozzle exit. Major differences are noticed in the behavior of these flows.

Another objective of the present investigation is to obtain a basic understanding of the response of cold swirling turbulent free jets to acoustic excitation. To our knowledge, this is the first attempt to study the effect of excitation on a swirling jet. As a first step, a free swirling turbulent jet with a swirl number of 0.35 is excited internally by plane acoustic waves; and the results are compared with a similar jet without swirl. The mass flux is kept constant in the two cases. Only experimental results are presented in this report, and further studies are needed to understand the mechanism of interaction.

2. LITERATURE REVIEW

From a large body of experimental and theoretical work on the swirling turbulent flows and aerodynamic excitation of free shear flows, only a few were selected for the purpose of review in this report. The literature review which follows is divided into six parts with some interdependence as follows:

- a) Free swirling flows (experimental studies)
- b) Confined swirling flows (experimental studies)
- c) Theoretical studies of swirling flows
- d) Vortex breakdown
- e) Aerodynamic excitation of free shear flows
- f) Measurement techniques in swirling flows.

2.1 FREE SWIRLING FLOWS (EXPERIMENTAL STUDIES)

As might be expected, the evolution of a subsonic swirling turbulent jet issuing from a nozzle into ambient fluid depends on the method of swirl generation. This fact was acknowledged by Chigier and Beer [1], and Pratt and Keffer [2], and others. The design of swirl generators in practice today use the following principles of swirl production:

- a) Fixed or adjustable vanes
- b) Axial-plus-tangential entry swirl generator
- c) Spinning , fully developed pipe flow
- d) Flow through a rotating perforated plate

References [8, 9] can be consulted on the details of various swirl generator designs and their corresponding limitations and efficiencies. Because of the experimental nature of this report, the method of swirl generation and the measurement techniques used in most references is emphasized.

Rose [10] was the first to present measurements in a free swirling jet emerging from a rotating pipe into a reservoir of motionless air. Because of the relatively low viscosity of air, it was possible to generate only weak swirl by this method. The pipe was 100 diameters long and was rotating at 9500 rpm. Near the pipe discharge, the flow was roughly a fully developed turbulent pipe flow in solid body rotation. Mean velocity and one component of Reynolds normal stresses were measured using a single hot-wire anemometer. Flow direction measurements were made with a special x-meter. He showed that compared to nonswirling jets, the jet with swirl spreads at a larger angle, entrains reservoir fluid more rapidly, and consequently displays a more rapid reduction of mean-velocity and growth of turbulence intensity.

Pratt and Keffer [2] generated a swirling jet, with swirl number of 0.3, by air flow through a rotating pipe similar to that of Rose [10]. A pipe 47 diameters long was rotated at speeds of up to 8700 rpm. A single constant-temperature hot-wire probe is used for measurement of mean velocity and turbulent fluctuations. Static pressure measurements are made with a special disk probe. Their measurements show that the flow achieves self similarity for the

mean velocities rather quickly, while the normal turbulence intensities reach a self-similar state after a longer period of jet development. They also conclude that the method by which swirl is generated would have an influence upon the flow, and the region immediately downstream from the nozzle exit would be particularly sensitive. They claim that only for geometrically similar swirl generators, as well as comparable average swirl numbers, would a high degree of equivalence be expected throughout the entire flow field. A similar idea was also addressed by Chigier and Beer [1]. Pratt and Keffer also extended their study to a pair of swirling jets having opposite rotation [11]. The double swirling jet was produced by discharging air through a pair of rotating pipes similar to Reference [2]. mean flow and turbulence intensities were measured by multi-orientation of a single, normal constant-temperature hot wire. This required that for every data point, the wire be positioned in three mutually orthogonal planes. It was concluded that the tangential component of the mean velocity decayed rapidly in the streamwise direction. At a downstream station of about 35 nozzle diameters, the resultant flow of the pair of swirling jets had most of the characteristics of a single free jet without swirl.

Chigier and Chervinsky [12, 13] have performed theoretical and experimental studies of turbulent swirling jets issuing from a round orifice. They used boundary layer approximations and assumptions of similar profiles to integrate the equations of motion for

incompressible turbulent flows. Swirl was generated by an axial-plus-tangential entry swirl generator, and mean flow data were taken by means of a five-hole spherical impact tube. The similarity assumption was experimentally demonstrated to hold in a swirling jet, for weak and moderate swirls ($S < 0.4$), for $x/D > 4$. For strongly swirling flows, where the mean axial velocity distribution shows a central trough, or what is also known as a double hump profile, the similarity was not observed until 10 diameters. For $x/D > 10$, the location of the maximum mean axial velocity shifted back to the jet centerline, from which point the similarity was observed. The measured mean axial velocity and static pressure profiles were described by Gaussian error curves and the mean tangential velocity profile was expressed in terms of third-order polynomials. The empirical constants in the data-fit expressions of Chigier and Chervinsky are functions of the degree of swirl in the jet defined as

$$G \equiv W_{mo} / U_{mo} \quad (4)$$

the ratio of maximum mean tangential-to-axial velocity at the nozzle exit.

Kerr and Fraser [14] have studied swirling jets generated by vane swirlers in a boiler furnace and in a model burner, respectively. A probe made to the design of Hiatt and Powell [15] was used to measure mean velocity magnitude and direction. Their system allowed direct measurement of nozzle torque and jet reaction thrust. They found that the angular momentum was conserved along

the length of the jet up to about 19 nozzle diameters and was equal to the measured torque. By dimensional analysis they found that the entrainment rate was a function of a dimensionless group (torque/[thrust \times nozzle diameter]) which is called the swirl number. By assuming error curves to fit axial velocity profiles, and half velocity radius to vary linearly with axial distance, relationships giving decay of axial velocity and jet half angle versus swirl number are obtained.

Design aspects of annular and hubless vane swirlers is studied by Mathur and MacCallum [16]. They claim that $\tan\phi$ alone may be taken as a measure of the degree of swirl for jets issuing from vane swirlers (for hubless swirlers $S = 2/3 \tan\phi$ where ϕ is the vane angle in degrees). They noticed that for vane angles of 45 degrees and higher, the sub-atmospheric pressure in the central zone of the jet near the nozzle is strong enough to induce recirculation. Static pressures were measured with a disk-type probe to the design of Miller and Comings [17].

Measurements of stress tensor components in free isothermal swirling jets have been made by some researchers [18-21]. Elsner and Drobniak [18] concentrated on flows at low swirl numbers where no recirculation could exist. They conclude that the greater the swirl number, the higher is the overall level of turbulence fluctuations at the nozzle exit, and the more intense is their decay further downstream. Their results indicate that the presence of swirl not only affects the mean evolution but also modifies the

turbulence structure of the swirling jet. It is concluded by them that the average size of largest eddies is greater in the presence of swirl but the difference decreases as the measuring station is moved further downstream. It is also noticed that the influence of swirl upon the turbulent microscale depends on the position of the control plane. In the near field, the average size of the smallest eddies decreases for higher swirl intensities while in the downstream region this influence becomes quite opposite. In general, they concluded that the presence of swirl intensifies the energy transfer process in the near-field of the jet while in the far-field region this influence becomes quite opposite.

Syred et al. [19] used single-wire, six-orientation, hot-wire technique to measure mean velocity and all turbulent stress tensor components in a very strongly swirling free isothermal jet and from these values derived effective viscosity distributions. These distributions show significant radial variations and considerable anisotropy of turbulence. Local turbulence intensities are found to be extremely high in and near the central recirculation zone. Neither upstream nor downstream stagnation points could be found by this method.

One of the latest measurements of mean velocity and turbulent intensities in a free isothermal swirling jet is made by Sislian and Cusworth [20]. Strong swirling motion, at a swirl number of 0.79, was imparted to the axial flow by fixed, flat, guide vanes placed at the nozzle exit. Three mean velocity and six turbulent stress

tensor components were measured using laser Doppler velocimetry. The location and extent of the recirculation region is established. They noticed that inside the recirculation zone, the fluid rotates as a rigid body. The normal Reynolds stress results showed substantial deviations from isotropy. These stresses are significantly larger than the Reynolds shear stresses, which clearly shows the need to consider the three normal stresses in any turbulence models of such flows. The distributions of all Reynolds stresses exhibit double peaks. These peaks are produced in regions with high gradients of mean velocity, i.e. near the edge of recirculation zone and at the edge of the jet flow boundary (shear) layer.

Measured values of mean velocity, all stress tensor components, and probability density distributions of fluctuating velocity are reported for isothermal turbulent coaxial jets, with and without swirl, by Ribeiro and Whitelaw [21]. The jets were emerging into stagnant surroundings from a long pipe and an annulus concentric with the pipe. Swirl could be introduced into the annular flow by tangential air slots. Measurements were made with a crossed hot-wire probe. Since practical limitations of hot-wire anemometry imply that the probe axis must coincide with the mean flow direction if a reasonable level of accuracy is to be achieved, the direction of the flow was determined using a 45° slanting sensor hot-wire prior to taking measurements. Their results show that the nonswirling coaxial flow configurations approach a self-similar

state in a much smaller distance than that of the round jet. This is due to the mixing layer and vortex shedding that occur in the region downstream of the separation wall between the two streams. In the presence of swirl, the coaxial jet is found to develop at a faster rate. They concluded that the introduction of swirl was responsible for a considerable increase in the jet mixing, and the process appeared to be dictated initially by the centrifugal forces and gradually taken over by the increased turbulent mixing.

Measurements of the free swirling flows with combustion was first taken by means of water-cooled multihole pitot probes. Chigier and Chervinsky [22] used a five-hole hemispherical water-cooled pitot probe for studying a turbulent burning free jet. The swirling jet was generated by an axial-plus-tangential entry swirl generator identical to the one used in References [12] and [13]. Flames were stabilized at about four diameters downstream from the burner exit, in the shape of an annular ring, and were unconfined for a distance of 24 diameters. The measurements made in this region, for three different swirl numbers, show that the decay of axial and swirl velocities is slower in a flame than in cold swirling jets. The normalized mean tangential velocity profiles are in the form of a Rankine-type vortex and can be described by a third-order polynomial. The normalized axial velocity profiles have a similar form which can be shown in the form of error curves. The maximum temperature is found to be in the main reaction zone and not on the jet axis.

Many problems encountered in the use of water-cooled pressure probes and hot-wire anemometry for measurements in complex turbulent swirling flows with combustion and flame are overcome by the advent of linear, nonintrusive technique of laser Doppler velocimetry (LDV) [23-25]. Chigier and Dvorak [23] made an experimental study of unconfined turbulent swirling jets under flame and no-flame conditions. Swirl is generated by passing air through four tangential slots. Axial and circumferential components of the mean velocity as well as three normal turbulent stresses are measured, using a laser anemometer with frequency shift. Substantial changes in flow patterns are detected as a consequence of combustion by direct comparison of velocity profiles under flame and no-flame conditions. The kinetic energy of turbulence per unit mass under flame conditions is higher than the corresponding cold conditions in almost all regions of the flame.

Fujii et al. [24] were the first to measure three mean velocity and all the six stress components in an unconfined swirling jet under isothermal and combusting conditions using laser Doppler velocimetry. Swirl was generated by passing compressed air through a row of adjustable vanes. A drastic alteration of mean profiles was recognized as a result of combustion.

Radial and tangential components of mean velocity are of the same order of magnitude outside of the hot bubble, which implies that the outward movement of the reacting flow is predominant. The virtual origin moved upstream when combustion commenced, indicating

lesser spread of axial velocity in the reacting flow. Turbulence levels are increased as a consequence of combustion, and the region of anisotropy of turbulence is significant.

Claypole and Syred [25] present some detailed results including velocities (measured by laser Doppler anemometry), temperature, and species concentration in swirling jets with and without combustion and compare the aerodynamics of these flows. Swirl is induced by passing air through eight tangential slots. Their isothermal results are similar to other researchers' [1]; but once the combustion is established in the recirculation zone, there appears to be little correlation between isothermal flow and flow with combustion. Although the recirculation zone is larger with combustion, the recirculated mass flow is far lower (8% as opposed to 30%), because the elevated temperatures produce considerable reduction in density. The recirculation zone is shorter and wider in the reacting flow than in the isothermal state. They also found out that the effects of combustion on the flow increases with swirl strength. Advances in all aspects of swirling flows with and without combustion are extensively reviewed in References [26] and [27].

2.2 CONFINED SWIRLING FLOWS (EXPERIMENTAL STUDIES)

The phenomenon of swirling flow in round and annular tubes has been extensively studied in the past by a number of researchers. One of the initial interests was the study of energy separation

effect of vortex flow obtained in the so-called vortex tube (Ranque-Hilsch tube). This device was first patented by George Ranque in 1931 and introduced into the United States in 1945 [28]. It was a simple device in which a particular type of vortex motion could be studied. Afterwards, with increased practical applications, confined swirling flows were investigated in different configurations. The studies of confined swirling flows may be arbitrarily divided into two classifications [29]:

1. Swirling flows in large length-to-diameter ratio tubes where circumferential wall effects interact strongly with the swirling flow; and
2. Swirling flows in short, large-diameter chambers where end-wall effects interact with the swirling flow to produce strong secondary reverse flow (e.g. combustion).

The works reported in References [29-32] fall into the first category. The phenomenon of swirling incompressible flow (water) through a tube has been studied by King et al. [29]. Swirl is introduced by injection of the total fluid stream through two symmetric tangential inlets. Separate static and stagnation probes which could be oriented into axial-tangential resultant flow vector were designed (this was based on the assumption that the time averaged radial velocity component was less than 1% of the axial and tangential velocities. Dimensionless static pressure, axial velocity, and tangential velocity profiles are obtained at different stations along the pipe. The initial forced vortex decayed into a

free vortex further downstream, while the total vorticity was decreased by friction. A region of reverse axial flow is noted in the center of the tube, the radius of which decreases with increasing downstream distance to zero. The turbulent Navier-Stokes equations are simplified to some extent by an order of magnitude analysis using the profiles developed in this study. Even though the simplified set is still indeterminate due to the presence of shear stress terms.

In the investigation of Yajnik and Subbaiah [30], the effects of variable initial swirl on turbulent pipe flow are examined. The initial swirl produced by adjustable guide vanes is small and amounts to a swirl number of less than 0.16; consequently, flow reversal does not take place. Turbulence field is not studied, and mean flow measurements are made with conventional five-hole conical-head and two-dimensional three-tube probes. The skin friction at the pipe wall is found to obey the logarithmic skin-friction law whose additive coefficient depends on swirl angle.

Weske and Sturov [31] examined the decay of swirl and turbulence field in pipe flow. Swirl is generated by rotating part of the pipe at 3000 rpm, generating solid-body rotation. The three components of mean velocity and six components of the Reynolds stress tensor are measured by hot-wire anemometry. The swirl number investigated is substantially larger than those studied by Yajnik and Subbaiah [30] and ranges from 0 to 3; consequently, flow similarity is not found. The turbulence field is found to decay quickly; however, its decay is a strong function of swirl number.

Sukhovich [32] performed an experimental investigation in a thermally insulated tube having a length-to-diameter ratio of 41. A stream of air was supplied to the working zone by a nozzle located at the end of the tube, and the secondary swirling flow was admitted into the tube through an annular gap formed by the outer surface of the nozzle and the inner surface of the working tube. Static pressure, as well as the axial and tangential components of the mean velocity, is determined from readings of a special precalibrated cylindrical probe. The distribution of the coefficients of turbulent heat and momentum transport in this confined swirling flow is determined from measurements of the time-averaged velocity, static pressure, and temperature. The calculations show that axial and tangential components of friction stresses are anisotropic and the coefficients of turbulent transport depend on the coordinates and parameters describing the swirl number. At higher gradients of angular velocity, the transport coefficient for tangential component of momentum is lower than the transport coefficient for axial component of momentum.

Now some studies related to the second category of confined swirling flows are reviewed. Mathur and MacCallum [33] studied the characteristics of a swirling jet in a model of square cross section. They used an isothermal-air model to obtain time-mean velocity profiles with a five-hole pitot probe and a water model to obtain qualitative data. They found that the initial rates of spread of confined swirling jets is more rapid than that of free

swirling jets; also, that the central toroidal recirculation zone is much stronger in confined jets than in free jets.

Extensive experimental and numerical studies have been performed at Oklahoma State University on confined swirling flows [34-43]. Throughout the entire research project an annular adjustable vane swirler having 10 blades with a hub-to-tip diameter ratio of 0.25 was used. The vanes were wedge shaped to give a constant pitch-to-chord ratio of 0.68. Vane angle could be adjusted between zero and 70 degrees.

The performance of the vane swirler was investigated by Sander and Lilley [34]. They show that the assumption of flat axial profile with zero radial velocity becomes progressively less realistic as the swirler blade angle increases. At strong swirl, the central recirculation zone extends even upstream of the exit plane, almost to the swirler vanes. Nonaxisymmetry was found in all swirl cases investigated.

Five-hole pitot probes were used to measure mean velocity components and static and total pressures in some of these studies [34-36]. Rhode et al. [35] measured the time-mean velocity components using a five-hole pitot probe. They investigated the effects of sidewall expansion angle and swirl number on the time-mean flow field. The effect of sidewall expansion angle is found to be negligible for the central recirculation zone. The effect of swirl number is to shorten the length of central recirculation zone and to generate the central toroidal recirculation zone, the length

of which is found to increase for increasing swirl number. Their study only included weak and moderate swirl strengths. This work is extended by Yoon and Lilley [36] to include higher swirl strengths and to study the effect of different contraction nozzles placed at various axial locations in the test chamber. They found that a strong contraction nozzle of area ratio 4 greatly affects the size and shape of the central toroidal recirculation zone.

Turbulence measurements have been made by six-orientation hot-wire technique [37-39], crossed wire [40], and triple hot-wire [41]. Janjua et al. [37] made measurements in an isothermal nonswirling, and in weakly swirling, confined jets using the above techniques. The measurements were used to calculate the time mean velocity components of normal and shear turbulent stresses. The swirling jet results presented were quite limited but did show that around regions of recirculation large values of turbulence intensity and shear existed even for moderate swirl. They also performed an uncertainty analysis on the hot-wire technique. This involved changing certain input parameters to the data reduction and determining the percentage change in output parameters. The most inaccurate term is found to be \overline{uw} .

Jackson and Lilley [38] extended the data base given in Reference [37] to higher swirl numbers and more axial measurement stations. Effects of a strong contraction nozzle of area ratio 4 were also included. Throughout the flow field, the most dramatic effect of swirl was to increase values of three turbulent shear

stress terms. Turbulence levels and shear stresses were found to increase along the jet centerline near the exit of the contraction nozzle. Finally, the accuracy and directional sensitivity of the single wire technique was studied by Jackson and Lilley [39]. The variation of input parameters and their effect on the output data has shown that the least accurate output quantities are the shear stresses, in particular the $x\theta$ component. The directional sensitivity analysis has shown that the technique adequately measures the properties of a flow field independent of the dominant flow direction except when the flow is predominantly in the direction of the probe holder.

McKillop and Lilley [40] made measurements of time mean turbulence quantities in a complex axisymmetric nonreacting, nonswirling, confined flow field using a crossed hot-wire anemometer. Their measurements indicated that the crossed hot wire used could not handle axial flow reversal (without prior knowledge and probe re-orientation), and the experimental technique was inadequate for the measurement of time-mean velocity. Nevertheless, the crossed hot-wire technique gave more accurate results for the turbulent shear stress, and thus turbulent viscosity, than the multi-orientation single-wire technique.

Turbulence measurements in a swirling confined jet flow field using a triple hot-wire probe have been performed by Janjua and McLaughlin [41]. The probe was operated by three separate but closely matched constant-temperature anemometers. They noticed that

the mean velocities measured by the triple-wire probe were in good agreement with five-hole probe results, and that the turbulent normal and shear estimates obtained were in general agreement with the corresponding measurements performed with the six-orientation, single-hot-wire technique. The above activities plus some numerical techniques and a computer code development for swirling turbulent recirculating flows are reviewed in References [42] and [43].

So far, the swirling flows through cylindrical ducts with constant diameter have been studied. Gore and Ranz [44] have made an analytical and experimental study of backflows in swirling fluids moving axially through expanding cross sections. A motor-driven perforated plate generated swirling flow with solid-body rotation. A single, constant-temperature hot-wire anemometer was used for velocity measurements. Tufts and smoke traces indicated flow directions, and light-weight spinners gave values of angular velocity. They found that backflows appear when the swirl number exceeds some critical value. When the flow was bypassed through a diffuser with large angle, separation occurred when no swirl was present. At high swirl numbers, the flow near the wall was accelerated and separation disappeared. This is what happens in most liquid fuel burners where primary combustion air is made to swirl and fill an expanding flow cross section. The resulting backflow stabilizes combustion by recirculating hot gases.

References [45] and [46] deal with the confined swirling flows through annular chambers. Scott and Rask [45] carried out their experimental study in an open circuit wind tunnel designed for swirl flows. Airfoil-shaped guide vanes imparted swirling motion to the flow prior to the entry into the annular test section. Measurements were made both with a cylindrical three-hole pitot probe and hot films. The major characteristics noted in the decay of tangential velocity was the change from a free-vortex nature in the inlet to that of a forced-vortex nature at the outlet. Axial and tangential shear stress profiles were computed from integral-differential forms of conservation equations using the measured velocity profiles in the integrals. Turbulence intensity terms are not measured and are excluded. Axial and tangential diffusivities are computed from the appropriate shear profiles. It turns out that axial diffusivities are weakly influenced by swirl. Large spikes in the tangential viscosities occur in regions where the character of the tangential velocity profile is changing from free to forced vortex.

Scott and Bartlett [46] studied annular swirl flow with the initial swirl profile of the forced-vortex type. Swirl was generated by passing air through a rotating honeycomb-like bundle of tubes. Measurements are made with a cylindrical pitot tube similar to [45]. The major goal of these experiments was to obtain experimental data on the axial decay of angular momentum and inferring values of effective turbulent tangential viscosity. Their results show a uniform axial decay of angular momentum and a profile

shape independent of axial location. The tangential profile shape and tangential viscosity distribution and magnitude do not depend on the initial rate of swirl.

In order to achieve flame stabilization and better control of mixing process, multiple coaxial swirling streams can be introduced into the swirl combustor. Therefore, the characteristics of coannular and coaxial swirling flows are now reviewed. Mattingly and Oats [47] made an experimental investigation of the mixing characteristics of coannular swirling flows. In this investigation, swirl is generated by a row of stationary vanes in the inner stream only, thereby leading to flow conditions unstable in the sense of Rayleigh's criterion of stability [48]; i.e., flows with positive radial angular momentum gradients are stable, while flows with negative gradients are unstable. The swirling inner stream and the axially directed outer stream are exhausted into a confined constant area test section. A five-hole pitot probe is used to measure static and total pressures as well as three mean velocity components. It is noticed that an enhanced radial mixing is created which they claim is as a result of the Rayleigh instability.

A series of experiments have been carried out to study the turbulent momentum transfer in coaxial jets with and without swirl. References [49] - [52] are among the recent studies in homogeneous flows under noncombusting conditions.

Habib and Whitelaw [49] started their investigation of coaxial jets by making measurements in a turbulent confined coaxial jet without swirl with hot-wire anemometry. Flows from axisymmetric coaxial jets were issued into a large circular tube. The area ratio of the tube to the outer jet was eight. The measurements included distributions of the axial mean velocity and the components of the Reynolds stress tensor. Two cases were studied with the ratio of maximum annulus to pipe velocity of one and three. They show, for example, that the larger velocity ratio results in a larger region of recirculation, larger velocity gradients, and larger turbulence intensities in the mixing region and downstream of the region of reverse flow. Later, they incorporated a swirl generator in the annular section and made measurements in the resultant flow with and without swirl [50]. The swirl generator was similar to the one used in Reference [21]. A combination of laser Doppler anemometry, hot wire, and a three-hole pitot tube was used to make measurements. The data allow comparison between the results of the above three techniques in regions of recirculation. The influence of swirl and confinement is shown to be the increased tendency towards centerline recirculation. The results are compared with calculations based on the solutions of finite-difference forms of the steady Navier-Stokes equations and an effective viscosity hypothesis. They concluded that the two-equation model, although able to represent the nonswirling flow, is less appropriate for the swirling flow.

The study of Vu and Gouldin [51] is carried out in a circular tube with a coaxial jet located at the entrance to the tube. The area ratio of the tube to the jet is about 18. Detailed time mean and fluctuating flow measurements are obtained for a coswirl and a counterswirl condition with a five-hole pitot probe and hot-wire anemometer. Swirl for inner and outer jets is generated by fixed and adjustable vanes, respectively. A recirculation zone occurs only for counterswirl case. As the outer swirl magnitude is decreased from maximum counterswirl to zero and then increased again to give coswirl, the size and the reverse flow velocities in the recirculation bubble diminish. Tangential velocities inside the bubble are low. More turbulence is generated in the interjet shear layer under counterswirl than for coswirl.

Roback and Johnson [52] studied mass and momentum transfer in a test facility similar to Reference [51], but the area ratio of the tube to the outer jet was 4.3. Swirl is imparted to the external stream. A combination of laser velocimeter (LV) and laser induced fluorescence (LIF) techniques is employed to obtain mean and fluctuating velocity and concentration distribution, which were used to derive mass and momentum turbulent transport parameters currently incorporated into various combustor flow models. The results of these measurements indicate that the largest momentum turbulent transport is in the r - z plane. Mixing for swirling flow is completed in one-third the length required for nonswirling flow.

So, Ahmed, and Mongia made an experimental investigation of gas jets in confined swirling air flows [53, 54]. The swirling flow is generated in a tube by a vane type swirler. The jet is located centrally in the swirler, and the diameter ratio of the tube to jet is 14. Both the jet and the swirling flow are fully turbulent. Velocity measurements are taken with a laser Doppler anemometer. Their results show that jets in confined flow with and without external swirl are highly dissipative. This is because the jet momentum has to work against large resistance in the fluid due to confinement. As a result, external swirl has little or no effect on the jet behavior. On the other hand, the jet even with a small amount of axial momentum is enough to completely eliminate the recirculation region in the swirling flow. The jet augments the turbulence field only in a small region surrounding the jet, beyond which the turbulence field is essentially the same as that of confined swirling flows.

A large body of literature exists for swirling flows with combustion and flame and some of these are reviewed in References [26, 27]. As mentioned earlier, many problems encountered by the use of water-cooled pressure probes and hot-wire anemometers, for measurements in complex turbulent swirling flows with combustion and flame, are overcome by the advent of laser Doppler velocimetry. One of the unique advantages which makes this technique desirable for use in swirling flows is that it is truly directional; i.e., both the direction and magnitude of velocity are determined. Also by

this method, the measurement can be made without disturbing the flow and in situations where there is no dominant flow direction. References [55-58] have made use of laser velocimetry in studying confined swirling flows with combustion.

Baker et al. [55, 56] measured values of three components of mean velocity and corresponding normal turbulent stresses in the flow within an enclosure which is a representative of a small-scale furnace with an axisymmetric, swirling flow configuration. The measurements are obtained in isothermal air flow and in a combustion mixture of air and natural gas. Exit swirl numbers of zero and 0.52 are investigated. A laser anemometer with light frequency shifting is used to obtain measurements. They demonstrate that the regions of recirculation are generally longer with combustion and that the turbulence is far from isotropic over most of the flow field. As expected, the swirl substantially reduced the length of the flame but also tended to increase the nonisotropic region of the flow.

Laser velocimeter measurements in the initial mixing region of a confined turbulent diffusion flame burner were made by Owen [57]. The experimental facility consists of an axisymmetric combustor in which a central gaseous fuel stream is mixed with a coaxial annular air stream. To impart swirl to the airflow, straight swirl vanes are inserted into the annular passage of the injector. Mean and rms turbulent velocity levels are measured for axial and tangential components of the reacting flow field. He measured four different swirl strengths near the exit of the burner

and found there was no significant variation on the time-mean profiles for increasing swirl. He also found high turbulence levels with significant deviation from isotropy over the initial mixing region of the jet. In this area large-scale fluctuations decrease for increase in swirl strength.

Gouldin et al. [58] have investigated the flow configuration of two confined concentric coswirling and counterswirling jets in a cylindrical combustor with and without combustion. The central jet flow was premixed methane/air, and the annular jet flow was air. Swirl was generated in the inner and outer jets by tangential slots and adjustable vanes, respectively. The data for reacting and nonreacting flows are obtained by laser anemometry. A closed central recirculation zone is observed in both swirl conditions for reacting flow but only in counterswirl for nonreacting flow. Large anisotropic velocity fluctuations are observed in high shear regions and in the vicinity of the recirculation zone.

2.3 THEORETICAL STUDIES OF SWIRLING FLOWS

A number of theoretical studies covering laminar, turbulent, weak and strong swirling jets have been carried out in the past. Loitsyanski [59] studied the axisymmetrical laminar swirling jet. His analysis was based on the simplified forms of the equations of motion obtained by invoking the boundary-layer approximation. He retained both axial and radial pressure gradient terms and obtained series solutions for the velocity components. He also extended the

analysis to the turbulent case by the use of Prandtl's mixing length and momentum transfer theory. His results are mainly applicable in the fully developed region of the jet at some distance downstream of the nozzle exit. Loitsyanski's solution requires also that the flow not reverse in direction at any point (weak swirl). At large axial distances from the origin, his laminar solution predicts the same asymptotic state as the classical free jet solution obtained by Schlichting [60].

Görtler [61] performed analytical studies of an incompressible laminar jet in the limit of very weak swirl. In this limit, the radial pressure gradient may be ignored, i.e. $p = p(x)$ only; and moreover a linearization of the momentum equations in swirl velocity is admissible. Based on these and the boundary-layer approximation of the Navier-Stokes equations, Görtler reduces the evolution of a weakly swirling laminar jet problem to an eigenvalue problem of an ordinary, second-order differential equation. Furthermore, upon finding a suitable transformation for the dependent and independent variables, the governing differential equation is transformed into a Legendre type, for which exact solutions are derived. By replacing the kinematic viscosity with an effective constant eddy viscosity, Görtler generalizes his theory to include turbulent, weakly swirling free jets as well.

A theory is proposed by Steiger and Bloom [62] in which incompressible and compressible, axially symmetric laminar free mixing: e.g., wakes and jets, with small, moderate, and large swirl

can be examined. The tangential and axial velocity components and the stagnation enthalpy are assumed to have polynomial profiles in the radial direction. The assumption of very small radial velocity allowed the use of boundary-layer type formulation in the analysis. The Karman integral method is then applied to the viscous layer, i.e. the wake, of a rotating axisymmetric body with no comparison to experimental data.

Shao-Lin Lee [63] has obtained closed-form solutions for an axisymmetric turbulent swirling jet using similarity assumptions for the axial and the tangential velocities. The radial and axial velocities are linked via an entrainment assumption, after G. I. Taylor [64]. The theoretical predictions are compared to the experimental data of Rose [10], where close agreement, in the case of weak swirl, is demonstrated. Lee's assumptions of the Gaussian axial velocity distribution and the corresponding similar tangential velocity profile were directly deduced from Rose's experiment, where similarity conditions were observed for $x/D > 1.5$.

Chigier and Chervinsky [12, 13] have performed theoretical and experimental studies of turbulent swirling jets issuing from a round orifice. They used boundary layer-approximations and assumptions of similar profiles to integrate the equations of motion for incompressible turbulent flows. The similarity assumption was experimentally demonstrated to hold in a swirling jet, for weak and moderate swirls, for $x/D > 4$. For strongly swirling flows, where the mean axial velocity distribution shows a central trough, or what

is also known as a double hump profile, the similarity was not observed until 10 diameters. For $x/D > 10$, the location of the maximum mean axial velocity shifted back to the jet centerline, from which point the similarity was observed. The measured mean axial velocity and static pressure profiles were described by Gaussian error curves, and the mean tangential velocity profile was expressed in terms of third-order polynomials. The empirical constants in the data-fit expressions of Chigier and Chervinsky are functions of the degree of swirl in the jet defined as

$$G \equiv w_{120} / u_{120} \quad (4)$$

the ratio of maximum mean tangential-to-axial velocity at the nozzle exit.

In recent years, there has been considerable progress in the swirling flow field predictions using finite difference numerical techniques. The flow of an incompressible viscous fluid is most often treated by the stream function-vorticity ($\psi - \Omega$) formulation [65]. The advantages of this technique in reducing the number of partial differential equations is outweighed by its problems regarding the implementation of boundary conditions and treating strongly swirling flow fields.

To overcome the problems associated with ($\psi - \Omega$) formulation, most recent emphasis is being placed on direct solution for primitive variables P, U, V, W instead of ψ and Ω [66-69]. This method is based on the numerical solution of a finite difference representation of the Navier-Stokes equations in primitive variable

form. Reference [66] is actually a computer code for swirling turbulent axisymmetric recirculating flows in practical isothermal combustor geometries. A two-equation ($K - \epsilon$) turbulence model and a stair-step boundary representation of the sloping sidewalls are implemented in this code. References [67] and [68] have extended the code applications and compared the predictions with experimental data. Due to the limitations of ($K - \epsilon$) models, Reynolds stress closure models have also been considered in numerical predictions of swirling and nonswirling jets [69]. Problems associated with this technique are discussed in this reference. For a review of flow field modeling techniques in practical combustor geometries, Reference [70] can be consulted.

2.4 VORTEX BREAKDOWN

Vortex breakdown phenomenon is an abrupt structural change which can occur along the axis of swirling flows or the leading edge vortex formed above delta wings at high angles of attack. It has been recognized for a long time that local flow reversal can be produced in a circular duct flow by introducing sufficiently high degree of swirl into the flow field. Such a swirl induced zone of recirculation is the basis for one of the classical techniques for flame stabilization in combustion chambers and furnaces. In the study of swirling flows, the term "vortex breakdown" refers to the formation of a free stagnation point or recirculation zone on the axis of flows with significant streamwise vorticity.

Gouldin and Depsky [58] have classified the mean flow field of swirling flows, depending on the presence or absence of mean flow reversal as follows:

- (1) No flow reversal
- (2) A central recirculation zone
- (3) A toroidal recirculation zone.
- (4) A long backflow region or columnar flow.

Class 2 includes flows with vortex breakdown. Increasing swirl strength will cause transition from class 1 to class 2 or class 3; and with further increase in swirl, it may transit to class 4. They concluded that, in addition to swirl number, Reynolds number, initial velocity profiles, and flow geometry have a significant influence on swirling flows and most likely on the class of recirculation zone they generate. Syred and Beer [26], Lilley [27], Gore and Ranz [44], and Vu et al. [51] among others have suggested that the flow recirculation produced in swirl-stabilized combustion chambers is related to vortex breakdown. They did not, however, offer any fundamental arguments about the nature of this phenomenon. According to References [26] and [27], the usual point of onset of flow reversal occurs at swirl number of about 0.6, which is called the "critical swirl number." They reached the conclusion that the precise effect of swirl on the flow field is found to depend upon many other factors as well as swirl number: for example, nozzle geometry. The presence of a central hub or the addition of a divergent nozzle encourages a larger recirculation

zone and reduces substantially the critical swirl number. It is also observed that recirculation zones tend to be larger when the flow is produced by swirl vanes as opposed to an axial-plus-tangential entry swirl generator, and they are much more pronounced in confined swirling flows than the ones generated in free swirling jets.

References [71-74] are among the literature dealing with the fundamental nature of vortex breakdown. Squire [71] suggests that breakdown might occur when the flow can sustain infinitesimal standing waves. His idea is that, if such waves exist, disturbances which are present far downstream might spread along the vortex and hence disrupt the flow nearer the start. Since the standing waves of indefinitely great length are the first to become possible as the swirl velocity is gradually increased, he proposed the limiting condition for the existence of such waves to be the inceptive state for vortex breakdown.

The most satisfactory explanation for vortex breakdown thus far proposed is that of Benjamin [72]. He associates vortex breakdown with a transition between an upstream supercritical region into which axisymmetric waves cannot propagate and a downstream subcritical region through which axisymmetric waves can propagate. In the transition or transcritical region, waves propagating from downstream accumulate to form a vortex breakdown. In other words, he considers vortex breakdown as fundamentally a transition similar to hydraulic jump in open channel flow, from a uniform state of

swirling flow (supercritical) to another state (subcritical) featuring axisymmetric waves of finite amplitude.

Sarpkaya [73, 74] made some experiments in swirling flows in a diverging cylindrical tube in which various types of vortex breakdown were observed. The swirling water was generated by adjustable swirl vanes. Basically three types of vortex breakdown were observed, viz. double helix breakdown, spiral breakdown (followed by turbulent mixing), and axisymmetric breakdown (followed by a thicker vortex core than the spiral breakdown and finally by turbulent mixing). The first mode is observed only in the divergent tube experiments, and the spiral mode is more commonly observed over a delta wing at high angles of attack, while the axisymmetric mode generally appears in axisymmetric swirling flows. The axisymmetric breakdown may also evolve from double helix or spiral modes. For an exhaustive list of references and critical evaluation of the proposed theories of vortex breakdown, References [75-77] can be consulted.

2.5 AERODYNAMIC EXCITATION OF FREE SHEAR FLOWS

Aerodynamic excitation of axisymmetric jets has been under extensive theoretical and experimental investigation over the past decade. It is already understood that acoustic excitation at the "right" Strouhal number ($\frac{f \cdot D}{U}$) has a significant effect on the mixing characteristics of shear layers, provided that the excitation amplitude is beyond a certain minimum "threshold" level.

The idea of a preferred mode of jet instability was first introduced by Crow and Champagne [78]. They showed that the entrainment volume flow, in an axisymmetric jet, could be increased by about 32 percent by acoustic excitation at Strouhal number of 0.3 based on nozzle exit diameter. Later Zaman and Hussain [79, 80] showed that turbulent mixing, in a free circular jet, is enhanced at Strouhal numbers between 0.2 and 0.8 and is suppressed between 2 and 4. They also concluded that enhancement or suppression of turbulent mixing not only depends on the Strouhal number but also is affected by the nature of the nozzle boundary layer (i.e. laminar, transitional, or turbulent).

Moore [81] and Ahuja [82] showed that the threshold level of the excitation acoustic pressure for effective turbulent mixing and a consequential jet noise amplification can be taken to be 0.8% of the jet dynamic head at the "correct" Strouhal number. For an excellent review and bibliography in the area of aerodynamic excitation, References [5] and [83] can be consulted.

The objective of the present investigation is to obtain a basic understanding of the response of cold swirling turbulent free jets to acoustic excitation. To our knowledge, this is the first attempt to study the effect of excitation on a swirling jet. As a first step, a free swirling turbulent jet with a swirl number of 0.35 is excited internally by plane acoustic waves, and the results are compared with a similar jet without swirl. The mass flux is kept constant in the two cases. Only experimental results are presented

in this report and further studies are needed to understand the mechanism of interaction.

2.6 MEASUREMENT TECHNIQUES IN SWIRLING FLOWS

Experimental observations in swirling flow fields have been conducted for a number of years. Measurement techniques developed for these three-dimensional flow experiments are as follows:

- (1) Multihole-probe techniques
- (2) Hot-wire anemometry
- (3) Laser-Doppler velocimetry.

As the present experiments involved development of a five-hole probe measurement technique; and as the turbulence field was qualitatively measured with constant temperature hot-wire anemometry, only the literature regarding these techniques is reviewed in this report.

2.6.1 Multihole-Probe Techniques

A variety of multihole probes, having three, five, or seven holes with different tip shapes, have been designed and fabricated in the past for measurement of velocity vector magnitude and direction, as well as static and total pressure. Several combination probes, mainly of the nulling type, are experimentally evaluated in Reference [84]. In the nulling method, probes are usually rotated in the flow field until the direction-sensing pressures are nulled, meaning the probe is aligned with the flow.

The probe may also be set fixed in the flow field (non-nulling method) and flow direction determined from a correlation based on the relationship between the probe pressures and flow direction. Measurements with fixed-position probes in subsonic flow over a range of Reynolds numbers is presented by Krause and Dudzinski [85]. Design and calibration procedure of a three-hole probe (used for 2-D flow measurements) and a five-hole probe (used for 3-D flow measurements) is studied in this paper.

Multihole probes have been designed with a variety of measuring tip shapes. Spherical probes have been developed by Lee and Ash [86] for three-dimensional flow measurements. Static pressure and magnitude and direction of velocity vector for any arbitrary flow angle can be measured with this probe without nulling. Satisfactory measurements are obtained within a rotating blade cascade with three percent accuracy. Hale and Norrie [87] have also studied the theory of the five-hole spherical pitot probe technique and improved the calibration procedure for measurements in a flow whose direction is approximately known. The results of their calibration can be put in a form suitable for reduction of the test data by digital computers.

Bryer and Pankhurst [88] have carried out an extensive study of multihole pressure probes having a variety of tip designs like spherical, conical, or pyramidal heads. Details of the design and construction steps of various probes are given as well as their general principles of operation and practical performance. Combination probes which are capable of simultaneous measurement of

many quantities including temperature are also discussed. The application of several types of pressure probes for measurement of static and total pressure, velocity vector magnitude and direction, and skin friction are also discussed by Chue [89]. This reference can serve as a useful supplement to Reference [88] by adding further details on topics discussed in it and topics not already included.

References [90, 91] deal with measurements in separated flows. Yajnik and Gupta [90] mounted a modified basic three-hole probe on a pitching mechanism and aligned it with the local flow direction such that the pressure difference between the two outer tubes was equal to zero. Local velocity and the flow direction in one plane can thus be determined. This design and set-up appears attractive; but the system is not versatile, since it cannot measure the local sidewash angle of the flow. In order to overcome the above limitation, a rather small five-hole probe was selected by Seetharam et al. [91]. This probe was ideally suited for separated flow measurements due to its capability to provide pitch and yaw angle information as well as static and total pressures. They provided a means for nulling the probe in one axis only and to utilize nonlinear calibration relations to determine flow direction with respect to the second axis. They realized that for probe positions within five probe diameters of the wall, proximity of the wall influences the probe readings and results in an error in the indicated local pitch angle of the velocity vector. The maximum error is reported to be about four degrees when the probe is in contact with the surface.

A fast method for accurate mechanical design and minimum effort manufacturing procedure of miniature conical five-hole probes is presented by Gallington and Hollenbaugh [92]. The smallest probe that they constructed had an outside diameter of 2.7 mm, and they claim that their technique can probably be applied to fabricate probes as small as 1 mm outer diameter. Detailed procedure of calibration of miniature five-hole probes for on-line data reduction is reported by Barker et al. [93]. A computer-aided technique to find the three components of velocity and the static and total pressures is presented. The four pressure coefficients, defined in terms of the pressures measured from each of the five holes or pressure ports, are calculated using matrix manipulation.

Samet and Einav [94] present the results of their study to construct, calibrate, and employ a special type of directional pressure probe which they call the "five-tube pressure probe" or "5TPP." Topics such as calibration techniques, various sources of error, and correction procedures are discussed in detail. This type of probe has an outside diameter of 4.2 mm and is robust and easy to manufacture. The tubes are made of 0.9 mm i.d. stainless steel hypodermic tubing and are bonded together with epoxy glue. They have described a calibration procedure for using the probe in non-nulling method of measurement in large and small flow angles. The procedure of Reference [91] is recommended by them for null-reading method. Measurements were performed in an axisymmetric turbulent jet with a coflowing uniform stream. Within the potential core the

results of STPP were in good agreement with those obtained by hot-wire anemometry. Further downstream errors of not more than 4% are observed.

The effect of a nearby solid surface which was noticed in Reference [91] is also addressed by Tamigniaux and Oats [95]. They also observed that overreading angle of attack increased with increased approach to the wall. This is because the wall interference causes an increased pressure at the port closest to the wall. They concluded that the validity of the probe readings can be extended to an area close to the wall by including the effect of wall interaction in the calibration procedure. Generally speaking, there are not yet reliable methods for calibrating multi-hole probes for the effects of large shear rates or of nearby solid surfaces. As a result, measurements taken near the solid boundaries, or within the early developing shear layer between streams, can only be interpreted qualitatively at best.

Due to flow separation at the probe tip, if five-hole probes are not nulled in flow direction, they are unsatisfactory for flow measurements at angles larger than about 20 degrees [90]. A new method is recommended for calibrating five-hole probes for extending their useful measurement range up to flow angles of about 85 degrees [96]. The calibration technique involves adjustment of the calibration coefficients to allow valid calibration at larger flow angles without additional cost of a seven-hole probe. The coefficients are adjusted by replacing the center port pressure with

the upwind port pressure as the reference pressure, and replacing the stalled downwind port pressure with center-port pressure. This extended range is valid in pitch only when the yaw ports are nulled.

As discussed by Yajnik and Gupta [90], the five-hole probes could not be calibrated to give useful flow information beyond flow angles of about 20 degrees measured from the flow direction to the probe axis. This is because at high flow angles one of the side ports in the five-hole probe becomes almost a stagnation point while the opposite port measures in the separated wake [93]. Neither of these pressures is sensitive to small changes in flow angle. Of course nulling the probe can improve this problem. Some special calibration techniques have also increased this limit [96]. The seven-hole probe is a desirable choice for measurements in flows at high angles [97]. This reference describes the fabrication, calibration, and use of a non-nulling seven-hole probe that permits accurate measurement of all steady-flow properties, provided that the local flow makes an angle of no more than 80 degrees with respect to the probe axis. The determination method comprises explicit polynomial relationships for all the desired output quantities in terms of pressures measured by the probe. This method can be easily programmed in matrix notation on a data acquisition system. Representative flow angle accuracies are 0.4 degrees at low flow angles and one degree at high flow angles.

The calibration technique developed in Reference [97] for incompressible flows is further extended to subsonic compressible

flows by Everett et al. [98]. They observed that the maximum flow angle at which valid measurements can be obtained varies inversely with Mach number. This limit ranges from about 65 degrees at Mach 0.88 to nearly 85 degrees at Mach 0.2. Their data reveal no significant influence of Reynolds number on the results within the range of values tested.

2.6.2 Hot-Wire Techniques

Turbulence measurements in a complex flow field have always been a complicated problem encountered by researchers. One of the most widely used instruments to obtain turbulence quantities as well as mean velocity components is the hot-wire technique. Methods of measuring swirling flow fields using hot-wire anemometry are briefly reviewed here. There are essentially two methods available for measurement of three-dimensional flows using hot-wire probes. The first technique is the use of multi-orientation of a single hot wire. The second method is the application of a three-sensor probe. Of course, single inclined and cross-wires have also been applied for three-dimensional flow measurements.

Multi-orientation of a single hot wire is a method devised originally by Dvorak and Syred [99]. They used a single normal hot wire oriented at three different positions so that the center one was separated by 45 degrees from the other two. A crossed-wire probe was additionally used to measure correlation coefficients. King [100] modified the above technique. His method called for a

normal wire to be oriented through six different positions, each orientation separated by 30 degrees from the adjacent one. Mean and root mean square voltages were measured at each orientation. The data reduction was performed using some assumptions regarding the statistical nature of the turbulence, making it possible to solve for three time-mean velocities, the three normal turbulence stresses, and the three turbulence shear stresses.

At Oklahoma State University, Janjua et al. [37, 101] studied the six-orientation hot-wire probe techniques, developed a suitable data reduction code, and presented results of its application in nonswirling free and confined jet flows. Jackson and Lilley [38] extended the above technique to investigate nonswirling and swirling nonreacting turbulent confined flows. They also studied the accuracy and directional sensitivity of the six-orientation single normal hot-wire technique [39]. They performed an uncertainty analysis on the data reduction procedure by changing the individual input parameters and noting their effect on the deduced property of the flow. It is concluded that the least accurate output quantities are the shear stresses, in particular the $x\theta$ component. A directional sensitivity analysis is also presented by them, that assesses the relative value of the deduced flow properties to local time mean velocity orientation relative to the probe. It is also concluded that the technique adequately measures the properties of the flow field independent of the dominant flow direction except when the flow is predominantly in the direction of the probe holder.

The influence of wall proximity on hot-wire velocity measurement is experimentally investigated by Oka and Kostic [102]. Their measurements are carried out with a DISA constant temperature hot-wire anemometer, using a standard miniature probe. They showed that the increased cooling of the hot wire in the vicinity of a colder wall gives rise to higher apparent velocities at the measuring points. They observed that the wall influence could be detected at the same dimensionless distance, a fact which may serve as an indication of whether wall influence is present in a certain measurement in turbulent flows.

Application of multi-orientation of a slanted wire in flow measurements is reported in References [103-105].

Moussa and Eskinazi [103] tried to measure the mean flow velocity and direction in a three-dimensional flow field by using a rotatable 45 degree slanted wire. Making use of the directional properties of hot wires, they calibrated the probe for all possible angles and prepared detailed charts which included the flow angles as function of four mean voltages obtained at different stations. Hoffmeister [104, 105] applied similar technique for determining three components of mean velocity and six Reynolds stresses in a 3-D turbulent flow. His procedure is restricted to a stationary turbulent field in a homogeneous, incompressible, and isothermal fluid. The use of multi-orientation of a single slanted wire in turbulent flows is not yet fully established.

Although the rotated-wire technique is simple in both concept and application, the technique can be very time consuming, especially where measurements are required at a large number of data points in a 3-D flow. Further, the technique is not particularly suitable for accurate measurements of very small flow angles. The cooling effects of intense velocity fluctuations, when these are present, also offer another criticism of the technique. The method, being basically a statistical technique, is applicable only to stationary turbulent flows. Considering the above problems, the three-sensor probe will be another alternative which enables measurements of the three components of mean velocity and six components of Reynolds stresses simultaneously [106, 107, 41].

A real-time hot-wire method has been developed to make measurements in 3-D turbulent flow fields where fluctuations are high and the flow direction is unknown (within limits) [106]. A DISA triaxial-wire probe is used for this investigation. The wires are mutually orthogonal, forming a right-angled coordinate system. The resultant mean velocity could be measured with good accuracy within a cone of 30 degrees half apex angle around the probe axis. Turbulent kinetic energy could also be measured with 10-15% accuracy within a cone of half apex angle of 12 degrees.

Extensive research has been performed on the applicability of three-sensor hot-wire probe techniques for 3-D mean and turbulence flow measurements at Pennsylvania State University [107]. Hot-wire equations, data processing procedure, calibration techniques, and a

discussion of various errors in the measurements are presented in this reference. Some improvements that can be made to improve the accuracy of this technique are also discussed.

Application of the triple hot-wire probe for turbulence measurements in swirling confined flows is reported by Janjua and McLaughlin [41]. The probe was operated by three separate but closely matched anemometers. Calibration of the probe was performed by orientation of the probe axis colinear with the calibration jet and resolving the velocity components in directions normal to the three wires to obtain voltage versus normal component of velocity for the three respective wires. This method is also recommended and used by Yavauzkurt et al. [106]. It is concluded that the mean velocities measured by the triple-wire probe are in good agreement with five-hole probe results. The turbulent normal and shear stresses measured by this method are also in general agreement with the corresponding results obtained from the six-orientation single-hot-wire technique.

3. EXPERIMENTAL FACILITIES AND INSTRUMENTATION

3.1 JET FACILITY

The jet facility consists of a 30-inch diameter cylindrical plenum tank, swirl generator, air supply and control system, excitation section, and a convergent nozzle exhausted to the test cell. A schematic diagram of the jet facility is shown in Figure 1.

3.1.1 Swirl Generator

One of the major objectives of the present investigation was to study the effect of initial tangential velocity distribution on the mean evolution of a swirling turbulent free jet. To achieve that, a swirl generator capable of producing swirling flows at a constant swirl number but at different initial swirl distributions was required. The design of swirl generators in practice today is generally based upon the following principles of swirl production [8]:

- a) Fixed or adjustable vanes
- b) Axial-plus-tangential entry
- c) Spinning, fully developed pipe flow
- d) Flow through a rotating perforated plate

A common problem associated with all of the above techniques of swirl generation is the fact that there is no control over the shape of the initial swirl distribution generated by them. To solve this problem, a unique swirl generator capable of generating swirling

flows at a constant swirl number but at a variety of initial swirl profiles is designed and fabricated. The principle of axial-plus-tangential entry is applied for swirl generation. It consists of 54 elbow-shaped nozzles mounted on three concentric circular manifolds (Fig. 2) which are in turn mounted inside a 76.2 cm (30 in.) diameter cylindrical casing (Fig. 3). Tangential air entering into the swirl generator through the elbow-shaped nozzles is mixed with the axial air passing through the casing and generates a swirling flow. By individual control of the air flow through the concentric manifold rings, flows having various initial swirl profiles at a constant swirl number can be generated. Swirl strength can be controlled by varying the proportion of axial and tangential air supply. The components of the swirl generator are described as follows:

a) Manifold Rings

These circular rings have diameters of 57.2, 38.1, and 19.1 cm (22.5, 15.0, and 7.5 in.) and are called manifolds A, B, and C, respectively. Manifold A is located upstream, B is in the middle, C is mounted in the downstream part of the cylindrical casing, and they are concentric. They are formed from stainless steel piping and incorporate welded mounting pads on their upstream and downstream faces for the attachment of elbow-shaped nozzles. Blueprints of these manifolds are included in Appendix D.

b) Elbow-Shaped Nozzles

Tangential air enters into the swirl generator through 54 nozzles mounted on the manifold rings. Manifolds A, B, and C are equipped with a total of 24, 18, and 12 nozzles, respectively, half of which are mounted on the upstream and the other half on the downstream face of the manifolds. Among the requirements in selecting and modifying these nozzles were maximum mass flow rate capacity with minimum blockage to the casing and minimum noise generation. Initially three sizes of elbows were selected, and different shapes and sizes of inlet restrictors and outlets were mounted in them [108]. The mass flow rates of the above combinations were experimentally measured in a flow laboratory, and the results are shown in Figure 4. It was concluded that a 1.91 cm (.75 in.) pipe elbow with a .64 cm (.25 in.) size inlet restrictor meets the mass flow rate requirement. Next, the overall sound pressure level (OASPL) of the air passing through this elbow was measured with a microphone; and it was concluded that the screech which was present in the spectra disappeared and the OASPL was reduced from 106 to 92.5 dB when three 30-mesh screens were inserted into the elbow and a multi-hole piece was placed at its outlet. The schematic of the multi-hole piece is illustrated in Figure 5. The mass flow rate of the final nozzle assembly was measured and found to be acceptable.

The elbows are screwed into their mounting pads located on front and rear faces of manifold rings, and their angles were set so

that the outlet flow from each elbow just touches the outlet of the neighboring elbow and so on. This way a well-developed stream tube of swirling flow is generated by the flow from each manifold. The swirl generator is bolted to the plenum tank as shown in Figure 6.

3.1.2 Air Supply and Control System

A schematic diagram illustrating the complete air supply and control system components is shown in Figure 7. The 40 psig axial air is supplied to the plenum tank through an eight-inch pipe. An eight-inch butterfly valve bypassed by a 1.5 inch gate valve allowed the regulation and control of the axial air. The axial air system and controls are shown in Figure 8.

The 125 psig tangential air is supplied by a six-inch pipe, through an air filter and manual shut-off valve to a small size plenum chamber, as shown in Figure 9. From there, the high pressure air is passed through three separate orifice plates and flow control valves to the three swirl-generating manifolds. A schematic diagram of the orifice runs is included in Appendix D. The variation of mass flow rate through each orifice plate versus the pressure drop across them is measured and used in the calibration procedure for total mass flow measurements. The calibration curves for the orifice plates are shown in Figures 10-12. A differential pressure transducer is hooked up across each orifice plate to measure pressure drop.

3.1.3 Excitation Section

A cylindrical section, which is installed downstream of the swirl generator, houses four acoustic drivers and microphones which are equally spaced around the circumference. Each driver is enclosed in a sealed can and is vented to the nozzle to equalize pressure across the speaker diaphragm. The drivers have a rated power of 40 w with a flat response over a frequency range of 500 Hz - 13 KHz. Each driver is connected to a dual channel Altec Lansing 100 w power amplifier. Amplitude and frequency of the input signal to the four drivers could be selected by a variphase tone generator.

3.1.4 Exit Nozzle

Two convergent nozzles with exit diameters of 11.43 cm (4.5 in.) and 8.89 cm (3.5 in.) were used for mean flow experiments and excitability tests, respectively. The nozzle was located downstream of the excitation section and was exhausted to the test cell. A photograph of the complete jet facility is illustrated in Figure 13.

3.2 INSTRUMENTATION

3.2.1 Five-Hole Pitot Probe

A five-hole pitot probe is designed and fabricated to measure three components of time mean velocity, mean flow angles, and static

and total pressures. The probe has a diameter of 0.318 cm (0.125 in.) at the sensing tip and is hook-shaped to allow probe shaft rotation without altering the probe tip location. The probe has a 45 degree cone angle, and the pressure ports are located at the midspan of the conical surface. Dimensions of the probe are shown in Figure 14. It is carefully calibrated in a calibration facility where precise measurements of the five port pressures at a range of known flow angles are made and converted to nondimensional parameters. The calibration procedure is discussed in Appendix A.

The probe was mounted on an L. C. Smith actuator which allowed probe shaft rotation about its axis for nulling in the yaw direction. This was performed automatically by commands from a Validyne demodulator which tries to equalize pressures at port numbers 2 and 4 of the probe. Port pressures were measured from the signals sent by a two-pound pressure transducer to a Fluke voltmeter. The data acquisition system and the operating procedure are described in Sections 3.2.5 and 4.1, respectively.

3.2.2 Hot-Wire Anemometry

A limited qualitative turbulence data is obtained along the jet centerline by standard hot-wire techniques employing linearized constant temperature anemometers. Only the streamwise mean and turbulence intensity are measured. Along the jet axis, the tangential and radial components of mean velocity are assumed negligible compared to the streamwise component; and therefore, the

results from a single element hot-film probe are assumed to represent the actual streamwise components. The mean data obtained by the hot-film probe are in reasonable agreement with the five-hole probe results.

3.2.3 Microphone

Considering the same assumptions mentioned in Section 3.2.2, the overall sound pressure level was also qualitatively measured along the jet centerline by means of a (B & K) condenser microphone. The microphone had an outside diameter of 0.635 cm (0.25 in.) and was fitted with a nose cone. The sound pressure levels in the power spectrum were measured relative to 20 μ pa.

3.2.4 Probe Positioning

As mentioned in Section 3.2.1, the five-hole probe could be rotated around its own shaft axis (yaw direction) by an L. C. Smith actuator. This rotation could be performed by commands from the yaw-nulling mechanism as well as manually by the keyboard control switches.

The above-mentioned actuator, hot-films, and microphones were mounted on a traversing mechanism made by Klinger. The unit allows simultaneous traverses in x, y, and z directions with .003 cm (.001 in.) accuracy. The direction and step size were programmed in the computer and could also be performed manually by means of control

switches of the stepper motor controller. The traverser can be seen in Figure 13.

3.2.5 Data Acquisition System

The schematic diagrams of the data acquisition set-up for the five-hole pitot probe measurements and hot-wire anemometry are shown in Figures 15 and 16, respectively. The central controller for the whole system was an HP-9836 computer, which was programmed to access digital voltmeters, relay switches, scanivalve, signal analyzer, and traversing mechanism.

For the five-hole probe measurements, at each measuring point, the probe was allowed to be nulled in yaw the direction. The yaw angle was then recorded by averaging the readout of the L. C. Smith controller meter which indicates the angular rotation of the probe about its own shaft axis. The five ports of the probe were then scanned by the scanivalve, and the time-averaged pressures were also recorded. Finally, the above recorded data were used by the computer to calculate the mean flow parameters by application of the calibration curves. The calibration procedure and computer programs are included in Appendices A and C, respectively.

For hot-film and microphone measurements, as well as excitation experiments, the data acquisition system was identical to Reference [109]. The HP computer could read the signals from a DISA constant-temperature anemometer through Fluke digital voltmeters. The data could be stored and plotted as mean velocities and turbulent

intensities. Hot-wire calibration procedure is discussed in Appendix B. Basic signal processing functions could be performed by a Wavetek model 804A signal processor. It could calculate, plot, and store power spectra, cross spectra, and other correlation functions. Layout of the data acquisition system and instrumentation in the control room is shown in Figure 17.

4. EXPERIMENTAL PROCEDURE

4.1 MEAN FLOW MEASUREMENTS

Mean flow measurements were made by means of a five-hole pitot probe as described in Section 3.2.1. Before each test, all signal conditioners and the Validyne demodulator were adjusted for no-flow condition. The air control valves of the swirl generator were then opened enough so that the differential pressure transducers across the orifice plates indicated the desired pressure drop corresponding to a known mass flow rate. The computer was programmed to move the probe to the desired measuring point by means of a traversing mechanism. At each point, the probe was allowed a period of 10 seconds to be nulled automatically in yaw direction. Then the time averaged yaw angle was recorded by the computer from the output of a voltmeter which was hooked up in series with the L. C. Smith actuator controller. The scanivalve was then activated through a relay actuator to scan through the five ports of the probe outlet. The time-averaged differential pressures were recorded from the signals of a two-pound pressure transducer. The above information was used by the computer to calculate the mean flow characteristics using calibration information. Calibration curves and computer programs are included in Appendices A and C, respectively.

4.2 FLUCTUATING FLOW MEASUREMENTS

As pointed out in Section 3.2.2, limited qualitative turbulence data were obtained along the jet centerline using standard hot-wire techniques. Only the streamwise turbulence intensity was measured by a single-element constant-temperature hot-film probe. It was assumed that along the jet axis, the tangential and radial velocity components were negligible compared to the streamwise component.

Each day before the test, the TSI hot-film probe, the DISA constant-temperature anemometer, the DISA linearizer, and the rest of the circuit were checked for calibration. The calibration procedure details are specified in Appendix B.

In a typical test run involving single hot-film measurements of turbulence intensities and mean velocities, the following procedure was followed. The control valves of the swirl generator manifolds were opened enough so that the differential pressure transducers across the orifice plates indicated the desired pressure drop corresponding to a known mass flow rate.

The hot-film probe was then mounted on the traverser and moved to the desired location. The HP computer then read a Fluke voltmeter to determine the dc and ac anemometer output voltages. It then time averaged the dc and ac signals separately and converted them to mean and fluctuating velocities, respectively. Simultaneously a Wavetek model 804A signal analyzer could average and store the spectra if needed.

4.3 OVERALL SOUND PRESSURE LEVEL MEASUREMENTS

Before each test run, the microphone was calibrated using a (B&K) pistonphone so that the sound pressure levels in the power spectrum were relative to 20 μ pa. The pistonphone generated a frequency of 250 Hz at 124 dB. The microphone was then mounted on the traversing mechanism and moved along the jet axis. The output from the microphone was fed to the signal analyzer through a B&K amplifier.

4.4 EXCITABILITY EXPERIMENTS

For excitation experiments, procedures similar to those of Reference [109] were followed. A Wavetek model 152 programmable variphase tone generator was used as a source of selectable wave forms. It could generate sine, cosine, triangle, and square wave forms of frequencies between one Hz and 100 KHz and amplitudes from 10 mv peak to 9.99 v peak. Amplitude, phase, and waveform for each channel could be independently programmed. Frequency could also be programmed and applied to all channels.

At the beginning of each test, the Altec-Lansing power amplifiers were adjusted manually to provide the desired voltage input to the acoustic drivers, and the amplitude and frequency were set on the tone generator. Basic signal processing functions could be performed by a Wavetek model 804A signal processor receiving signals from hot film and microphone. Excitability experiments were

conducted at constant sound pressure level of 126 dB as measured by a microphone at the nozzle exit.

4.5 SUMMARY OF THE TESTS

The following measurements were made for two flow conditions having equal swirl numbers of 0.48 but with different initial tangential velocity distributions:

- 1) Mean flow measurements along the jet axis with the five-hole probe
- 2) Radial traverses with the five-hole probe at the following downstream stations:
 $x/D = 0.06, 0.5, 1.0, 1.5, 2.0, 2.5, 3.0, 3.5, 4.0,$
 $5.0, 6.0, 9.0, 10.5, 12.0$
- 3) Single-wire hot-film measurements along the jet axis
- 4) Overall sound pressure level measurements along the jet axis
- 5) Excitability experiments along the jet axis for flows with swirl numbers of 0.35 and zero (no swirl case)
- 6) Investigation of the effect of screens on mean characteristics of swirling flows at swirl numbers of 0.52 and 0.34.

5. RESULTS AND DISCUSSION

Figure 17 is a definition sketch showing the coordinates used in this report. For a complete list of subscripts, superscripts, and abbreviations, the list of symbols should be consulted.

5.1 SYSTEM EVALUATION

5.1.1 Instrumentation

The multihole-probe technique has already been proved by many investigators to be an inexpensive and reliable method for swirling flow measurements. References [1, 12, 35, and 47] are among the numerous studies which have used this method of measurement extensively both in confined and free swirling flow fields. To check the accuracy of the five-hole probe technique, measurements are made in an axisymmetric nonswirling free jet, and the results are compared with those of the hot-wire anemometry in Figures 18 and 19. Excellent agreement between these results is observed up to a downstream distance of about four nozzle diameters. Further downstream, less than five percent error is noticed in the five-hole probe results. This is the nature of all pressure probes which lose their sensitivity in flow regions with low dynamic pressure.

5.1.2 Swirl Generator

Capability of the jet facility to generate swirling flows at a wide range of swirl numbers was checked by making measurements with the five-hole pitot probe. Figure 20 illustrates the downstream development of the mean centerline axial velocity at various swirl numbers. Radial distribution of the mean axial velocity at $x \approx 0.06D$ at the same swirl numbers is plotted in Figure 21. These plots illustrate the flows with swirl numbers ranging from zero (no swirl) to in excess of critical swirl number ($S_{crit} = 0.6$). As the pressure probe technique is not suitable for reversed flow measurements, the negative velocities are recorded as zero by the computer and plotted accordingly. For the same reason, the calculation of the swirl number in the presence of reversed flow was not possible. From Figure 20 it is clear that for a flow with a swirl number beyond the critical swirl number ($S > 0.6$), a vortex breakdown region is developed from a downstream distance of $x \approx 2.0D$ to $x \approx 3.0D$. Further increase in swirl number enlarges the size of the reversed flow bubble and moves the forward stagnation point further upstream and eventually inside the nozzle as illustrated in Figures 22 and 23. As will be discussed in Section 5.2, the shape of initial tangential velocity distribution has a significant effect on the value of critical swirl number. As the initial swirl profile changes from a forced vortex type towards free vortex distribution, the critical swirl number gradually reduces. Due to the importance of vortex breakdown phenomenon in combustion

research, further experiments are scheduled to be made using laser Doppler velocimetry (LDV) measurements. The effects of acoustic excitation on the vortex breakdown will also be investigated.

As mentioned before, one of the major objectives of this investigation was to study the effect of initial tangential velocity distribution on the mean evolution of free swirling turbulent jets. To do that, flows with identical swirl numbers but having different initial swirl profiles should be generated. This was the idea behind the design and fabrication of our unique swirl generator. Figure 24 illustrates two distinct tangential velocity distributions at swirl number of 0.48 generated in our facility. Both profiles represent Rankine type (combination free and forced) vortices. The flow generated by manifold A is dominated by the forced vortex part, while the one generated by manifold C is dominated by its free vortex part.

5.2 EFFECT OF INITIAL MEAN TANGENTIAL VELOCITY DISTRIBUTION ON THE EVOLUTION OF FREE SWIRLING TURBULENT JETS

5.2.1 Mean Flow Field

The experimental results presented in this section are time-averaged data gathered from two swirling jets generated separately by manifolds A and C. The swirl number in both jets was held constant at 0.48; and the mass-averaged, mean axial Mach number at the nozzle exit was ≈ 0.14 . The Reynolds number based on the mean axial velocity and the nozzle diameter was, in both cases, 375,000.

The two extreme tangential velocity distributions investigated in our facility are plotted in Figure 24. The vortex core size generated by manifold C, at $x/D = 0.06$, is about a quarter of the nozzle exit diameter, while that of manifold A spans the full exit plane. It is also noted that the center of the smaller vortex is displaced from the nozzle geometric center by nearly $0.1 D$, at $x/D = 0.06$, thereby leading to nonaxisymmetric flow conditions. This puzzling behavior was further investigated by allowing the vortical flow to emerge from the nozzles of various lengths. It was noted that the vortex core center described a "helical path" as evidenced by the appearance of the vortex center above, below, and to the side of the nozzle axis. A plausible explanation of this behavior may be found in the inviscid flow theory (see for example, Batchelor, Reference [110]), which predicts a spiral motion for an off-centered vortex filament as it passes through a contraction. Figure 25 schematically shows this phenomenon. In our case, it seems that manifold C is mounted slightly off center, causing this kind of behavior. The condition of axisymmetry for the swirling jet generated by manifold C is achieved at $x/D \approx 1.0$, as will be discussed later in this section. The forced vortex, i.e. the solid body rotation flow, produced by manifold A is axisymmetric as it emerges from the nozzle.

The radial distribution of mean axial velocity at the nozzle exit is shown in Figure 26. It is the nature of vortical flows, in general, which would not allow flat-top axial velocity profiles to

be generated. The differences in the axial flow distributions at the nozzle exit produced by manifolds A and C, as shown in Figure 26, could be directly related to the size of the vortex cores generated by these manifolds. Furthermore, the condition of near axisymmetry is observed for the swirling jet generated by manifold A, while that of manifold C is still asymmetric.

An evidence of a very strong inward (i.e. negative) radial flow is revealed in Figure 27 for the manifold-C-generated swirling flow. Further, the magnitudes of the radial and axial velocity components are comparable in this case in the near field. Hence, widely accepted boundary-layer-type approximation, i.e. $V/U \sim 0(\epsilon)$, made in the theoretical analysis of rotating jets is invalid in the near field of even moderately swirling jets (e.g. with $S = 0.48$). A manifestation of this assumption, i.e. $V/U \sim 0(\epsilon)$, on the radial momentum equation leads to the radial equilibrium condition, i.e.

$$-\frac{1}{\rho} \frac{\partial p}{\partial r} = \frac{V^2}{r} \quad (5)$$

which is also invalid for the rotating free jets of the type generated by manifold C and depicted in Figure 27. The driving force behind such a large radial inflow is the radial static pressure gradient associated with the core of such concentrated vortex filaments indentifying this as a pressure-driven phenomenon. The axial velocity peak observed in the jet center (see Figure 26) is the continuity-consequence of this radial inflow. The flow generated by the largest manifold, i.e. A, experiences mild

radial inflow and is axisymmetric. The rotating flow produced by the smallest manifold, i.e. C, is asymmetric and, as shown in the latter parts of this section, will remain asymmetric up to $x/D \approx 1$.

Figure 28 reveals a static pressure deficit in the core of the swirling jets, produced by manifolds A and C, $x/D \sim 0.06$. The depth of the pressure trough for the concentrated vortex flow, i.e. the one generated by manifold C, is nearly 2.5 times that of the large core vortex, i.e. due to manifold A. We also note the similarity between the radial velocity and the static pressure profiles as plotted in Figures 27 and 28. Again, the symmetry and lack of it could be seen in the A- and C-generated flows, respectively.

The axial evolution of the mean tangential velocity is plotted in Figure 29 (a) and (b). In part (a), the manifold-A-generated swirling flow is clearly axisymmetric and shows a rapid decay with axial distance. Beyond four diameters, the mean tangential velocity in the jet is so small as to make an accurate measurement with the five-hole probes questionable. The initial offset between the jet and the nozzle geometric center is clearly visible, in Figure 9 (b), for $x/D < 1.0$. Beyond one nozzle diameter, the two centers coincide. Moving towards the condition of axisymmetry, i.e. the self-centering action of the jet, is a natural tendency we observed in our experiments. Comparison of parts (a) and (b) of Figure 29 also reveals that the concentrated vortex, i.e. due to manifold C, decays at a slower rate than the solid-body rotation flow induced by manifold A, up to four nozzle diameters.

Widely different axial evolution of the mean axial velocity profiles, for the two swirling jets generated by manifolds A and C, is noted from Figure 30 (a) and (b), respectively. The large core-vortex flow, i.e. (a), shows a continuous gradual decay of the mean axial velocity component along the jet. The small core-vortex flow, i.e. (b), demonstrates a central trough or a double-hump profile associated with the swirl numbers higher than 0.48 (namely 0.6). The mean centerline velocity on the jet axis, i.e. $r/D = 0$, in part (b) shows a rapid initial deceleration followed by an acceleration period which has never been reported for $S = 0.48$ jets. Upon further examination of the mean axial velocity between three and four diameters, we observed that the small-core-vortex jet with $S = 0.48$ was on the verge of vortex breakdown, as shown in Figure 31. The forward and rear stagnation points, both very close to the jet axis, exhibited an unsteady behavior, as had been noted in the earlier vortex breakdown experiments. The fact that a swirling jet has been brought to the point of breakdown at a swirl number (i.e. 0.48) significantly lower than the critical value was assumed to be (i.e. $S_{crit} \gtrsim 0.6$) is the most remarkable result of our mean-flow investigation.

Downstream development of the mean radial velocity is shown in Figure 32. In part (a), a very minor radial inflow is measured which quickly disappears as the jet evolves in the axial direction. The small core-vortex flow, i.e. (b), due to larger inflow radial velocities, persists longer than (a) and, as shown,

decays to nearly zero radial velocity in about five diameters. The mean static pressure deficit in the swirling jet within the first three diameters of the jet evolution is plotted in Figure 33. The strong adverse pressure gradient along the jet axis, measured for the small core-vortex flow, i.e. part (b), is recognized as the principal contributor to the onset of the vortex breakdown, as noted in Figure 31. The mean flow data for 10 radial stations in the near field of both flows ($x < 5D$) are tabulated in Tables 1 through 20. The decay of the mean tangential velocity maximum with axial distance is shown for the jets generated by manifolds A and C in Figure 34. The forced-vortex case, i.e. the one produced by manifold A, exhibits continuous decay along the jet while the small-core vortex initially develops in an irregular manner, at least for $x/D < 1.5$, then follows the same trend as the forced-vortex flow. Up to four diameters, the mean tangential velocity maximum of the manifold-C-generated flow decays at a slower rate than the manifold-A-produced swirling jet. Beyond four diameters, the tangential speeds are very small, and identical behavior is measured for the two jets.

Figure 35 shows the continuous decay of the mean axial velocity maximum along the jet axis for a downstream distance of twelve nozzle-exit diameters. The two jets behave in a very similar manner; however, the small-core-vortex jet decays faster than the forced-vortex flow. Finally, the decay of the mean axial velocity along the jet axis is presented in Figure 36. The swirling jet

produced by manifold C is on the verge of breakdown, while that of manifold A exhibits classical behavior for this level of swirl number, i.e. 0.48. Mean flow data along the jet centerline are tabulated in Tables 21 and 22.

5.2.2 Fluctuating Flow Field

As mentioned in Sections 3.2.2 and 3.2.3, streamwise turbulence intensity and overall sound pressure level were measured along the jet centerline with a single-element hot-film probe and a B&K microphone, respectively. Along the jet axis, the tangential and radial components of mean velocity are negligible compared to the streamwise component; and therefore the results from a single-element hot-film probe are assumed to represent the actual streamwise values. The validity of the above assumption is shown in Figure 37 where the results of the hot-film and five-hole probe measurements along the jet centerline are compared and observed to be in excellent agreement in the near field ($x < 4D$).

Streamwise turbulence intensities and overall sound pressure levels are tabulated in Tables 23-25 and are compared for the two cases in Figures 38 and 39, respectively. As can be seen from these figures, the flow generated by manifold C has much larger turbulence intensities and higher OASPL than the flow generated by manifold A in the near field.

5.3 EXCITABILITY EXPERIMENTS

One of the objectives of the present investigation was to obtain a basic understanding of the response of cold swirling turbulent free jets to acoustic excitation. To our knowledge, this is the first attempt to study the effect of excitation on a swirling jet. As a first step, a free swirling turbulent jet, with a swirl number of 0.35, is excited internally by plane acoustic waves; and the results are compared with a similar jet without swirl. Only experimental results are presented in this paper, and further studies are needed to understand the mechanism of interaction.

For both the swirling and nonswirling jets under investigation, the mass flow rate is held approximately constant at about 0.64 kg/sec (1.4 lbs/sec). The swirling jet mass flow rate was measured with an orifice meter, while that of the nonswirling jet was based on the area integral of the axial velocity profile at the nozzle exit. The Mach and Reynolds numbers based on mass-averaged axial velocity at the nozzle exit are 0.26 and 5.8×10^5 , respectively. The swirling jet has a swirl number of 0.35.

The radial distributions of the time-mean axial velocity, measured at $x = 0.06D$, for the swirling and nonswirling jets is plotted in Figure 40. The form of the profile for the swirling jet deviates from the flat-top shape of the nonswirling jet as expected. The rapid expansion of the swirling jet is also noticeable in this figure. The time-mean tangential velocity distribution at $x = 0.06D$ for the swirling jet is shown in Figure

41. The distribution is in the form of a Rankine-type vortex (combined free and forced vortex). The geometrical and the jet axis coincide from $x/D \approx 1.0$. The decay of time-mean axial velocity component along the jet centerline for both flows is plotted in Figure 42. The length of potential core is about four diameters for the nonswirling jet. In the case of the swirling jet, the decay of the time-mean axial velocity starts from the nozzle exit.

To examine the effect of excitation on the swirling jet and compare with the excited nonswirling jet, both flows are excited internally by plane acoustic waves upstream of the nozzle inlet. To isolate the effect of excitation frequency, the sound pressure level is kept constant at 126 dB for both jets at all excitation frequencies, measured at the center of the nozzle exit.

Figures 43 and 44 illustrate the growth of the instability waves triggered at different excitation frequencies for the nonswirling and swirling jets, respectively. It is observed that the swirling jet under investigation, as well as the nonswirling jet, is excitable by plane acoustic waves. At equal excitation frequencies, the instability waves grow about 50 percent less in peak rms amplitude in the swirling jet, as compared to the nonswirling jet. This difference is not unexpected, as linear instability theory states that the stability of the free shear layers depends upon the detailed velocity distributions. Here we are dealing with two jets which are entirely different as far as velocity and pressure distributions are concerned. It is also

expected that the growth of the instability waves should also depend upon the swirl number which affects the velocity and pressure distributions.

For the nonswirling jet, the location of the maximum growth of the instability waves is approximately at the end of the potential core ($x = 4.0D$). This is in agreement with the observation in the literature that the axisymmetric disturbances achieve their peak amplitude near the end of the potential core (e.g. Ref. [111]). For the swirling jet, the potential core does not exist and the maximum growth occurs at about $x = 2.5D$. This location should also depend on swirl number.

The variation of the peak rms amplitude of the axial velocity fluctuations on the jet axis versus the Strouhal number ($St = \frac{f \cdot D}{U_a}$) is plotted in Figure 45. From this figure it is observed that the maximum growth of the instability wave is measured at a Strouhal number of 0.4, based on mass-averaged axial velocity at the nozzle exit for both cases. This is in agreement with the results quoted in the literature for the nonswirling axisymmetric jets (Ref. [79]). For the swirling jets, the effect of swirl strength on the preferred Strouhal number requires further investigation.

Even though significant improvement in jet mixing, as a result of excitation, is measured in our facility for nonswirling jets (Ref. [109]), no change is observed in the mean velocity components of the swirling jet due to excitation. Two plausible explanations may be forwarded, namely: a) The presence of strong static pressure

gradients in the near field of a swirling jet (with moderate to strong swirl) overwhelms the turbulence-induced shear layer growth, and b) higher initial turbulence level of the swirling jet as compared to its nonswirling counterpart dampens the growth of the shear layer instability wave. The effect of core turbulence intensity on the mixing and excitability of an axisymmetric, nonswirling cold free jet is examined by Raman et al. (Ref. [112]), which supports our argument. External excitation by helical waves with a more powerful excitation device may be beneficial.

It should be noted that as the swirl number exceeds the critical value of 0.60, or as the initial tangential velocity distribution approaches a free-vortex profile, a recirculating zone starts to develop and therefore drastic changes in the response due to excitation are expected.

5.4 EFFECT OF SCREEN

The effect of screen on the swirling flow is investigated by placing different screens upstream from an 8.89 cm (3.5 in) diameter exit nozzle. Two flows were compared for the effect of screen as follows:

- a) A flow with swirl number of 0.52 and having an initial swirl profile of Rankine-type vortex dominated in the free vortex part (having small vortex core) generated by manifold C.

b) A flow with swirl number of 0.34 and having an initial swirl profile of Rankine-type vortex dominated in the forced vortex part (having large vortex core) generated by manifold A.

The screens tested were 50 x 50, 30 x 30, 6 x 6, and 4 x 4 mesh standard screens. The percent reduction in swirl number is tabulated in the following table:

Screen Mesh Size	Swirl Number	Percent Reduction in Swirl Number
50 x 50	0.52	46%
	0.34	53%
30 x 30	0.52	27%
	0.34	38%
6 x 6	0.52	0%
	0.34	18%
4 x 4	0.52	0%
	0.34	6%

From these results it is observed that the effect of screens is more pronounced on the flow with lower swirl number in all cases. This can be as a result of the initial swirl distributions of the flows under investigation. It seems that the swirling jet with smaller size vortex core can penetrate through the screens with less reduction of its swirl number.

6. SUMMARY AND CONCLUSIONS

The following summarizes the major conclusions of our experimental investigation:

- a. Initial development of a subsonic swirling free jet is dominated by the nozzle exit tangential velocity distribution.
- b. Vortex breakdown in swirling jets may occur at significantly lower swirl numbers than have previously been reported, i.e. $S_{crit} < 0.6$.
- c. Large radial inflows will make a boundary-layer-type approximation, i.e. $V/U \sim O(\epsilon)$, and its subsequent radial equilibrium condition invalid in the near field of the jets with moderate to strong swirls.
- d. Reducing the size of the vortex core in a swirling jet creates a higher swirl-number effect on the mean flow.
- e. Reducing the size of the vortex core in a swirling jet creates higher streamwise turbulence intensities and higher overall sound pressure levels along the jet axis in the near field ($x < 4D$). It also causes the swirling jet to penetrate screens with less reduction of its swirl number.
- f. The cold turbulent swirling free jet under investigation ($S = 0.35$) is found to be excitable by plane acoustic waves. At a constant excitation sound pressure level of 126 dB, the growth of the shear layer instability waves

depends on the excitation frequency. These waves grow about 50 percent less in peak rms-amplitude; and the downstream location of their maximum growth is further upstream for the swirling jet under investigation, compared to a nonswirling jet with the same axial mass flux. Maximum growth of instability waves is observed at Strouhal number of 0.4 for both swirling and nonswirling jets (based on mass-averaged axial velocity). In spite of the growth of instability waves, so far no change in the mixing of the swirling jet, as a result of excitation, has been observed.

7. RECOMMENDATIONS FOR FUTURE WORK

7.1 SWIRLING FLOW INVESTIGATION

1. A complete set of turbulence data to supplement the existing mean data will give more insight into the observed phenomenon.
2. Application of the nonintrusive laser anemometry is ideal for this complicated flow field and permits making measurements in areas with reversed flows. Vortex breakdown phenomena can also be studied.
3. Some sort of flow visualization will give visual ideas of exactly what is happening in the flow field, what to expect from the data, and where to concentrate most of the measurements.
4. Comparison of measured jet evolution with the predictions of a reliable computer code permits parametric study of the flow and helps analyzing the observed phenomenon.

7.2 ACOUSTIC EXCITATION

From the results of this experiment, it seems that even though the instability waves grow in the swirling jet under investigation, no effect on jet mixing is noticed. The following improvements in the experimental facility may be beneficial.

- 1) Moving the location of the acoustic drivers to the downstream of the nozzle exit (external excitation) which results in higher excitation amplitude and also allows helical mode of excitation.

- 2) Using more powerful excitation devices.
- 3) Installation of an acoustic treatment section in the plenum tank upstream of the swirl generator.

The above improvements are being implemented in our jet facility, and another series of excitation experiments will be conducted shortly.

We also intend to implement the following measurements in order to assess the swirling jet excitability more thoroughly:

- 1) rms amplitude based on total fluctuating velocity will be measured.
- 2) Hot-wire or laser spectra to indicate the effect of excitation on broadband turbulence will be studied.

Of course, high initial turbulence levels, in the case of swirling jet, is another factor which reduces the effectiveness of excitation in improving the mixing rate. This problem remains unsolved because any attempt to reduce the turbulence level automatically reduces the swirl number as well.

8. REFERENCES

- [1] Chigier, N. A.; Beer, J. M. "Velocity and Static Pressure Distributions in Swirling Air Jets Issuing from Annular and Divergent Nozzles." Transactions of the ASME, Journal of Basic Engineering, December 1964, pp. 788-796.
- [2] Pratte, B. D.; Keffer, J. F. "The Swirling Turbulent Jet." Journal of Basic Engineering, Vol. 93, December 1972, pp. 639-748.
- [3] Young, A. D.; Rao, K. N. "Some Low Speed Experimental Results on the Effects of Swirl and Velocity Distribution on an Axisymmetric Jet." Aeronautical Quarterly, Vol. 29, November 1978, pp. 270-284.
- [4] Hallett, W. L. H. "Swirl Generator for Independent Variation of Swirl and Velocity Profiles." AIAA Journal, Vol. 24, No. 7, 1986, pp. 1212-1213.
- [5] Rice, E. J.; Zaman, K. B. M. Q. Control of Shear Flows by Artificial Excitation. AIAA Paper No. 87-2722, 11th Aeroacoustics Conference, Sunnyvale, CA, Oct. 19-21, 1987.
- [6] Ahuja, K. K.; Burrin, R. H. Control of Flow Separation by Sound. AIAA Paper No. 84-2298, Williamsburg, Virginia, Oct. 15-17, 1984.
- [7] Zaman, K. B. M. Q.; Bar-Sever, A.; Mangalam, S. M. "Effect of Acoustic Excitation on the Flow over a Low-Re Airfoil." Journal of Fluid Mechanics, Vol. 182, 1987, pp. 127-148.

- [8] Gupta, A. K.; Lilley, D. G.; Syred, N. Swirl Flows. Abacus Press, Tunbridge Wells, England, 1984.
- [9] Beer, J. M.; Chigier, N. A. Combustion Aerodynamics. Halsted Press Division, John Willey & Sons, Inc., New York, 1972.
- [10] Rose, W. G. "A Swirling Round Turbulent Jet, Part 1: Mean Flow Measurements." Journal of Applied Mechanics, Dec. 1962, pp. 615-625.
- [11] Pratte, B. D.; Keffer, J. F. "A Counter-rotating Pair of Turbulent Jets." Journal of Fluid Engineering, June 1973, pp. 207-213.
- [12] Chigier, N. A.; Chervinsky, A. "Experimental and Theoretical Study of Turbulent Swirling Jets Issuing from a Round Orifice." Israel Journal of Technology, Vol. 4, No. 1, 1966, pp. 44-54.
- [13] Chigier, N. A.; Chervinsky, A. "Experimental Investigation of Swirling Vortex Motion in Jets." Journal of Applied Mechanics, June 1967, pp. 443-445.
- [14] Kerr, N. M.; Fraser, D. "Swirl, Part 1: Effect on Axisymmetrical Turbulent Jets." Journal of the Institute of Fuel, Vol. 38, December 1965, pp. 519-526.
- [15] Hiatt, G. F.; Powell, G. E. "Three-Dimensional Probe for Investigation of Flow Patterns." The Engineer, Vol. 213, 1962, pp. 165-170.

- [16] Mathur, M. L.; MacCallum, N. R. L. "Swirling Air Jets Issuing from Vane Swirlers." Journal of the Institute of Fuel, May 1967, pp. 214-225.
- [17] Miller, D. R.; Comings, E. W. "Static Pressure Distribution in the Free Turbulent Jet." Journal of Fluid Mechanics, Vol. 3, Oct. 1957, pp. 1-16.
- [18] Elsner, J. W.; Drobniak, S. "Turbulence Structure in Swirling Jets." Structure of Complex Turbulent Shear Flow, IUTAM Symposium, Marseille, 1982, pp. 219-228.
- [19] Syred, N.; Beer, J. M.; Chigier, N. A. "Turbulence Measurements in Swirling Recirculating Flows." Proceedings, Salford Symposium on Internal Flows, 1971, pp. B27-B36.
- [20] Sislian, J. P.; Cuswort, R. A. "Measurements of Mean Velocity and Turbulence Intensities in a Free Isothermal Swirling Jet." AIAA Journal, Vol. 24, No. 2, February 1986, pp. 303-309.
- [21] Riberio, M. M.; Whitelaw, J. H. "Coaxial Jets with and without Swirl." Journal of Fluid Mechanics, Vol. 96, Part 4, 1980, pp. 769-795.
- [22] Chigier, N. A.; Chervinsky, A. "Aerodynamic Study of Turbulent Burning Free Jets with Swirl." 11th Symposium on Combustion, The Combustion Institute, Pittsburgh, PA, 1967, pp. 489-499.

- [23] Chigier, N. A.; Dvorak, K. "Laser Anemometer Measurements in Flames with Swirl." 15th International Symposium on Combustion, Tokyo, Japan, Aug. 1974, pp. 573-582.
- [24] Fujii, S.; Eguchi, K.; Gomi, M. "Swirling Jets with and without Combustion." AIAA Journal, Vol. 19, No. 11, November 1981, pp. 1438-1442.
- [25] Claypole, T. C.; Syred, N. "The Effect of Combustion on the Aerodynamics of Swirling Jets." Fluid Mechanics of Combustion Systems, the Fluids Engineering Conference (ASME), Boulder, Colorado, June 22-23, 1981.
- [26] Syred, N.; Beer, J. M. "Combustion in Swirling Flows: A Review." Combustion and Flame, Vol. 23, 1974, pp. 143-201.
- [27] Lilley, D. G. "Swirl Flows in Combustion: A Review." AIAA Journal, August 1977, pp.1063-1078.
- [28] Hartnett, J. P.; Eckert, E. R. G. "Experimental Study of the Velocity and Temperature Distribution in a High Velocity Vortex-Type Flow." Transactions of the ASME, Vol. 79, May 1957, pp. 751-757.
- [29] King, M. K.; Rothfus, R. R.; Kermod, R. I. "Static Pressure and Velocity Profiles in Swirling Incompressible Tube Flow." A. I. Ch. E. Journal, Vol. 15, No. 6, Nov. 1969, pp. 837-842.
- [30] Yajnik, K. S.; Subbalaah, M. V. "Experiments on Swirling Turbulent Flows, Part I: Similarity in Swirling Flows." Journal of Fluid Mechanics, Vol. 60, Part 4, 1973, pp. 665-687.

- [31] Weske, D. R.; Sturov, G. YE. "Experimental Study of Turbulent Swirled Flows in a Cylindrical Tube." Fluid Mechanics--Soviet Research, Vol. 3, No. 1, Jan.-Feb. 1974, pp. 77-82.
- [32] Sukhovich, YE. P. "Experimental Investigation of Local Properties of Swirled Turbulent Flow in Cylindrical Channels." Fluid Mechanics--Soviet Research, Vol. 7, No. 3, May-June 1978, pp. 74-84.
- [33] Mathur, M. L.; MacCallum, N. R. L. "Swirling Air Jets Issuing from Vane Swirlers, Part 2: Enclosed Jets." Journal of the Institute of Fuel, Vol. 40, June 1967, pp. 238-245.
- [34] Sander, G. F.; Lilley, D. G. The Performance of an Annular Vane Swirler. AIAA Paper No. 83-1326, Seattle, Washington, June 27-29, 1983.
- [35] Rhode, D. L.; Lilley, D. G.; McLaughlin, D. K. Mean Flow Fields in Axisymmetric Combustor Geometries with Swirl, AIAA Paper No. 82-0177, Orlando, Florida, January 11-14, 1982.
- [36] Yoon, H. K.; Lilley, D. G. Five-Hole Pitot Probe Time-Mean Velocity Measurements in Confined Swirling Flows, AIAA Paper No. 83-0315, Reno, Nevada, January 10-13, 1983.
- [37] Janjua, S. I.; McLaughlin, D. K.; Jackson, T. W.; Lilley, D. G. "Turbulence Measurements in a Confined Jet Using a Rotating Single-Wire Probe Technique." AIAA Journal, Vol. 21, No. 12, Dec. 1983, pp. 1609-1610.
- [38] Jackson, T. W.; Lilley, D. G. Turbulence Characteristics of Swirling Flowfields. NASA CR-174918, May 1985.

- [39] Jackson, T. W.; Lilley, D. G. "Accuracy and Directional Sensitivity of a Single-Wire Technique." AIAA Journal, Vol. 24, No. 3, March 1986, pp. 451-458.
- [40] McKillop, B. E.; Lilley, D. G. Turbulence Measurements in a Complex Flow Field Using a Crossed Hot-Wire. AIAA Paper No. 84-1604, Snowmass, Colorado, June 25-27, 1984.
- [41] Janjua, S. I.; McLaughlin, D. K. Turbulence Measurements in a Swirling Confined Jet Flowfield Using a Triple Hot Wire Probe. NASA CR-169668, Nov. 1982.
- [42] Lilley, D. G. "Swirling Flows in Typical Combustor Geometries." Journal of Propulsion, Jan.-Feb. 1986, pp. 64-72.
- [43] Lilley, D. G. Investigation of Flowfields Found in Typical Combustor Geometries. NASA CR-3869, Feb. 1985.
- [44] Gore, R. W.; Ranz, W. E. "Backflows in Rotating Fluids Moving Axially through Expanding Cross Sections." A. I. Ch. E. Journal, Vol. 10, No. 1, Jan. 1974, pp. 83-88.
- [45] Scott, C. J.; Rask, D. R. "Turbulent Viscosities for Swirling Flow in a Stationary Annulus." Journal of Basic Engineering, Dec. 1973, pp. 557-566.
- [46] Scott, C. J.; Bartlet, K. W. "Decaying Annular Swirl Flow with Inlet Solid Body Rotation." Journal of Fluid Engineering, March 1976, pp. 33-40.

- [47] Mattingly, J. D.; Oates, G. C. "An Experimental Investigation of the Mixing of Coannular Swirling Flows." AIAA Journal, Vol. 24, No. 5, May 1986, pp. 785-792.
- [48] Rayleigh, J. W. S. "On the Dynamics of Revolving Fluids." Proceedings of the Royal Society, Vol. 6A, 1916, pp. 148-154.
- [49] Habib, M. A.; Whitelaw, J. H. "Velocity Characteristics of a Confined Coaxial Jet." Journal of Fluid Engineering, Vol. 101, Dec. 1979, pp. 521-529.
- [50] Habib, M. A.; Whitelaw, J. H. "Velocity Characteristics of Confined Coaxial Jets with and without Swirl." Journal of Fluid Engineering, Vol. 102, March 1980, pp. 47-53.
- [51] Vu, B. T.; Gouldin, F. C. "Flow Measurements in a Model Swirl Combustor." AIAA Journal, Vol. 20, No. 5, May 1982, pp. 642-651.
- [52] Roback, R.; Johnson, B. V. Mass and Momentum Turbulent Transport Experiments with Confined Swirling Coaxial Jets. NASA CR-168252, Aug. 1983.
- [53] So, R. M. C.; Ahmed, S. A.; Mongia, H. C. An Experimental Investigation of Gas Jets in Confined Swirling Air Flow. NASA CR-3832, Sept. 1984.
- [54] So, R. M. C.; Ahmed, S. A.; Mongia, H. C. "Jet Characteristics in Confined Swirling Flow." Experiments in Fluids, No. 3, Springer-Verlag, 1985, pp. 221-230.

- [55] Baker, R. J.; Hutchinson, P.; Whitelaw, J. H. "Velocity Measurements in the Recirculation Region of an Industrial Burner Flame by Laser Anemometry with Light Frequency Shifting." Combustion and Flame, Vol. 23, 1974, pp. 57-71.
- [56] Baker, R. J.; Hutchinson, P.; Khalil, E. E.; Whitelaw, J. H. "Measurements of Three Velocity Components in a Model Furnace with and without Combustion." 15th Symposium on Combustion, the Combustion Institute, Pittsburgh, PA, 1975, pp. 553-559.
- [57] Owen, F. K. Laser Velocimeter Measurements of a Confined Turbulent Diffusion Flame Burner. AIAA Paper No. 76-33, Washington, D.C., January 26-27, 1976.
- [58] Gouldin, F. C.; Depsky, J. S.; Lee, S. L. "Velocity Flowfield Characteristics of a Swirling Flow Combustor." AIAA Journal, Vol. 23, No. 1, Jan. 1985, pp. 95-102.
- [59] Loitsyanski, L. G. "The Propagation of a Twisted Jet in an Unbounded Space Filled with the Same Fluid." Prikladnaya Matematika I Mekhanika, Vol. 17, 1953, pp. 3-16.
- [60] Schlichting, H. Boundary Layer Theory, 6th ed., McGraw-Hill Book Company, Inc., New York, N.Y. 1968, p. 218.
- [61] Görtler, H. "Decay of Swirl in an Axially Symmetrical Jet, Far from the Orifice." Revista, Matemática Hispanoamericana, Vol. 14, 1954, pp. 143-178.
- [62] Steiger, M. H.; Bloom, M. H. "Axially Symmetric Laminar Free Mixing with Large Swirl." Journal of Heat Transfer, Vol. 84-85, November 1962, pp. 370-374.

- [63] Lee, S. L. "Axisymmetrical Turbulent Swirling Jet." Journal of Applied Mechanics, Vo. 32, 1965, pp. 258-262.
- [64] Taylor, G. I. Dynamics of a Mass of Hot Gas Rising in Air. U.S. Atomic Energy Commission, MDDC-919, LADC-276, 1945.
- [65] Kubo, I.; Gouldin, F. C. "Numerical Calculations of Turbulent Swirling Flow." Fluid Mechanics of Combustion, Fluids Engineering Conference, Montreal, Quebec, May 12- 15, 1974, pp. 61-74.
- [66] Lilley, D. G.; Rhode, D. L. A Computer Code for Swirling Turbulent Axisymmetric Recirculating Flows in Practical Isothermal Combustor Geometries. NASA CR-3442, Feb. 1982.
- [67] Rhode, D. L.; Lilley, D. G. Predictions and Measurements of Isothermal Flowfields in Axisymmetric Combustor Geometries. NASA CR-174916, May 1985.
- [68] Abujelala, M. T.; Lilley, D. G. Confined Turbulent Swirling Recirculating Flow Predictions. NASA CR-174917, May 1985.
- [69] Launder, B. E.; Morse, A. "Numerical Prediction of Axisymmetric Free Shear Flows with a Reynolds Stress Closure." Symposium on Turbulent Shear Flows, Penn. State University, 1977, pp. 279-294.
- [70] Lilley, D. G. "Flowfield Modeling in Practical Combustors: A Review." Journal of Energy, Vol. 3, No. 4, July-Aug. 1979, pp. 193-210.

- [71] Squire, H. B. Analysis of Vortex Breakdown Phenomenon,
Part 1. Rept. 102, Aeronautics Department, Imperial College,
London, 1960.
- [72] Benjamin, T. B. "Significance of the Vortex Breakdown
Phenomena." Journal of Basic Engineering, June 1965, pp. 519-
524.
- [73] Sarpkaya, T. "On Stationary and Travelling Vortex
Breakdowns." Journal of Fluid Mechanics, Vol. 45, Part 3,
1971, pp. 545-559.
- [74] Sarpkaya, T. "Vortex Breakdown in Swirling Conical Flows."
AIAA Journal, Vol. 9, No. 9, September 1971, pp. 1792-1799.
- [75] Hall, M. G. "Vortex Breakdown." Annual Review of Fluid
Mechanics, Vol. 4, 1972, pp. 195-218.
- [76] Leibovich, S. "The Structure of Vortex Breakdown." Annual
Review of Fluid Mechanics, Vol. 10, 1978, pp. 221-246.
- [77] Leibovich, S. "Vortex Stability and Breakdown: Survey and
Extension." AIAA Journal, Vol. 22, No. 9, 1984, pp. 1192-
1206.
- [78] Crow, S. C.; and Champagne, F. H. "Orderly Structure in Jet
Turbulence." Journal of Fluid Mechanics, Vol. 48, Part 3,
1971, pp. 547-591
- [79] Zaman, K. B. M. Q.; Hussain, A. K. M. F. "Vortex Pairing in a
Circular Jet Under Controlled Excitation, General Jet
Response." Journal of Fluid Mechanics, Vol. 101, 1980, pp.
449-491.

- [80] Zaman, K. B. M. Q.; Hussain, A. K. M. F. "Turbulence Suppression in Free Shear Flows by Controlled Excitation." Journal of Fluid Mechanics, Vol. 103, 1981, pp. 133-159.
- [81] Moore, C. J. "The Role of Shear-Layer Instability Waves in Jet Exhaust Noise." Journal of Fluid Mechanics, Vol. 80, Part 2, 1977, pp. 321-367.
- [82] Ahuja, K. K.; Lepicovsky, J.; Tam, C. K. W.; Morris, P. J.; Burrin, R. H. Tone Excited Jet, Theory and Experiments. NASA CR-3538, November 1982.
- [83] Stone, J. R.; McKinzie, D. J. Acoustic Excitation--A Promising New Means of Controlling Shear Layers. NASA TM-83772, June 1984.
- [84] Schulze, W. M.; Ashby, G. C.; Erwin, J. Several Combination Probes for Surveying Static and Total Pressure and Flow Direction. NASA TN-2830, Nov. 1952.
- [85] Krause, L. N.; Dudzinski, T. J. Flow Direction Measurement with Fixed-Position Probes in Subsonic Flow over a Range of Reynolds Numbers. NASA TM-52576, 1969.
- [86] Lee, J. C.; Ash, J. E. "A Three Dimensional Spherical Pitot Probe." Transactions of the ASME, April 1956, pp. 603-608.
- [87] Hale, M. R.; Norri, D. H. The Analysis and Calibration of the Five-Hole Spherical Pitot. ASME, 67-WA/FE-24, November 1967.
- [88] Bryer, D. W.; Pankhurst, R. C. Pressure Probe Methods for Determining Wind Speed and Flow Direction. Her Majesty's Stationery Office, London, 1971.

- [89] Chue, S. H. "Pressure Probes for Fluid Measurement." Prog. Aerospace Sci., Vol. 16, No. 2, 1975, pp. 147-223.
- [90] Yajnik, K. S.; Gupta, R. P. "A New Probe for Measurement of Velocity and Flow Direction." Journal of Physics E: Scientific Instruments, Vol. 6, 1973, pp. 82-86.
- [91] Seetharam, H. C.; Wentz, W. H.; Walker, J. K. "Measurement of the Post Separated Flowfields on Airfoils." Journal of Aircraft, Vol. 14, No. 1, January 1977, pp. 95-96.
- [92] Gallington, R. W.; Hollenbaugh, C. F. A Fast Method for Accurate Manufacture of Small Five-Hole Probes. USAFA-TR-79-7, July 1979, pp. 114-119.
- [93] Barker, K. W.; Gallington, R. W.; Minster, S. N. "Calibration of Five Hole Probes for On-Line Data Reduction." Aeronautics Digest, Spring 1979; USAFA-TR-79-7, USAF Academy, Co., July 1979, pp. 101-113.
- [94] Samet, M.; Einav, S. "Directional Pressure Probe." Rev. Sci. Instrum., Vol. 55, No. 4, April 1984, pp. 582-588.
- [95] Tamigniaux, T. L. B.; Oates, G. C. "Effect of a Nearby Solid Surface on a Five-Hole Pressure Probe." AIAA Journal, Vol. 2, No. 2, 1986, pp. 335-336.
- [96] Ostowari, C.; Wentz, W. H. "Modified Calibration Technique of a Five-Hole Probe for High Flow Angles." Experiments in Fluids, 1983, pp. 166-168.

- [97] Gallington, R. W. Measurement of Very Large Flow Angles with Non-Nulling Seven-Hole Probes. USAFA-TN-81-1, February 1981, USAF Academy, Co.
- [98] Everett, K. N.; Gerner, A. A.; Durston, D. A. "Seven Hole Cone Probes for High Angle Flow Measurement: Theory and Calibration." AIAA Journal, Vol. 21, No. 7, July 1982, pp. 992-998.
- [99] Dvorak, K.; Syred, N. "The Statistical Analysis of Hot Wire Anemometer Signals in Complex Flowfields." Paper presented at DISA conference, University of Leicester, England, 1972.
- [100] King, C. F. "Some Studies of Vortex Devices--Vortex Amplifier Performance Behavior." PhD Thesis, University College of Wales, Cardiff, 1978.
- [101] Janjua, S. I. Turbulence Measurements in a Complex Flowfield Using a Six-orientation Hot-wire Probe Technique. M.S. Thesis, Oklahoma State University, Stillwater, Dec. 1981.
- [102] Oka, S.; Kostic, Z. "Influence of Wall Proximity on Hot-Wire Velocity Measurements." DISA Information, No. 13, May 1972, pp. 29-33.
- [103] Moussa, Z. M.; Eskinazi, S. "Directional Mean Flow Measurements Using a Single Inclined Hot Wire." The Physics of Fluids, Vol. 18, No. 3, March 1975, pp. 298-305.
- [104] Hoffmeister, M. "Using a Single Hot-Wire Probe in Three-Dimensional Turbulent Flow Fields." DISA Information, No. 13, May 1972, pp. 26-28.

- [105] Hoffmeister, M.; Helmstadter, E.; Graichen, K. "The Application of a Single Hot-Wire Measuring Technique to Three-Dimensional Turbulent Flows in Mixing Vessels." Proceedings of Symposium on Turbulence in Liquids, Rolla, Missouri, 1977, pp. 295-302.
- [106] Yavauzkurt, S.; Crawford, M. E.; Moffat, R. J. "Real Time Hot-Wire Measurements in Three Dimensional flows." Symposium on Turbulence, University of Missouri Rolla, 1977, pp. 265-275.
- [107] Lakshminarayana, B. "Three Sensor Hot Wire/Film Techniques for Three Dimensional Mean and Turbulence Flow Field Measurement." TSI Quarterly, Vol. 8, Issue 1, January-March 1982, pp. 3-13.
- [108] Rice, E. J. Private communications.
- [109] Raman, G.; Ghorashi, B. Enhanced Mixing of an Axi-Symmetric Jet by Aerodynamic Excitation. NASA CR-175059, March 1986.
- [110] Batchelor, G. K. An Introduction to Fluid Dynamics. Cambridge University Press, Cambridge, 1967.
- [111] Petersen, R. A.; and Samet, M. M. "On the Preferred Mode of Jet Instability." To appear in Journal of Fluid Mechanics.
- [112] Raman, G.; Zaman, K. B. M. Q.; and Rice, E. J. Initial Turbulence Effect on Jet Evolution with and without Tonal Excitation. AIAA Paper No. 87-2725, 11th Aeroacoustics Conference, Palo Alto, CA, Oct. 19-21, 1987.

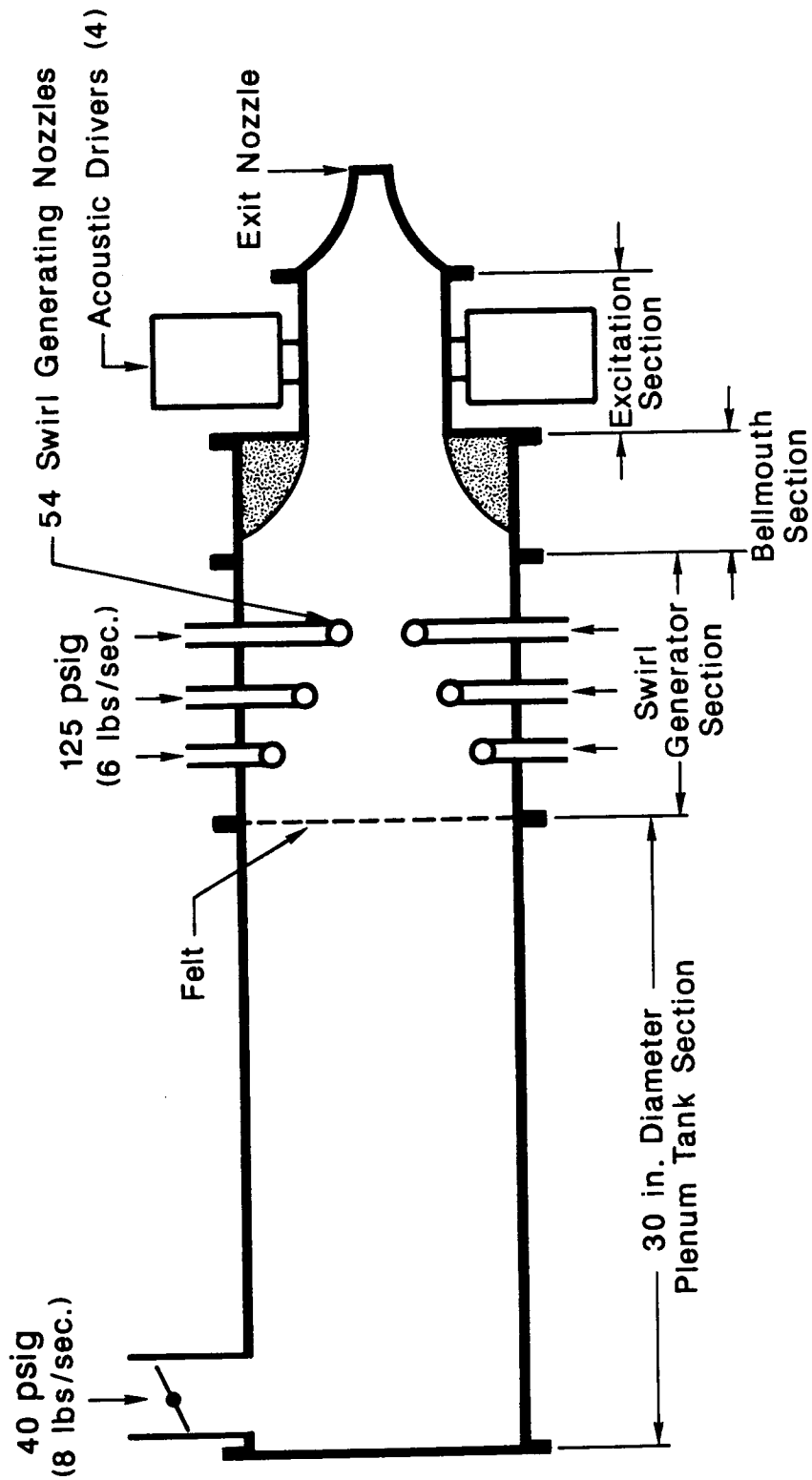


Figure 1. Schematic diagram of the jet facility

ORIGINAL PAGE
BLACK AND WHITE PHOTOGRAPH

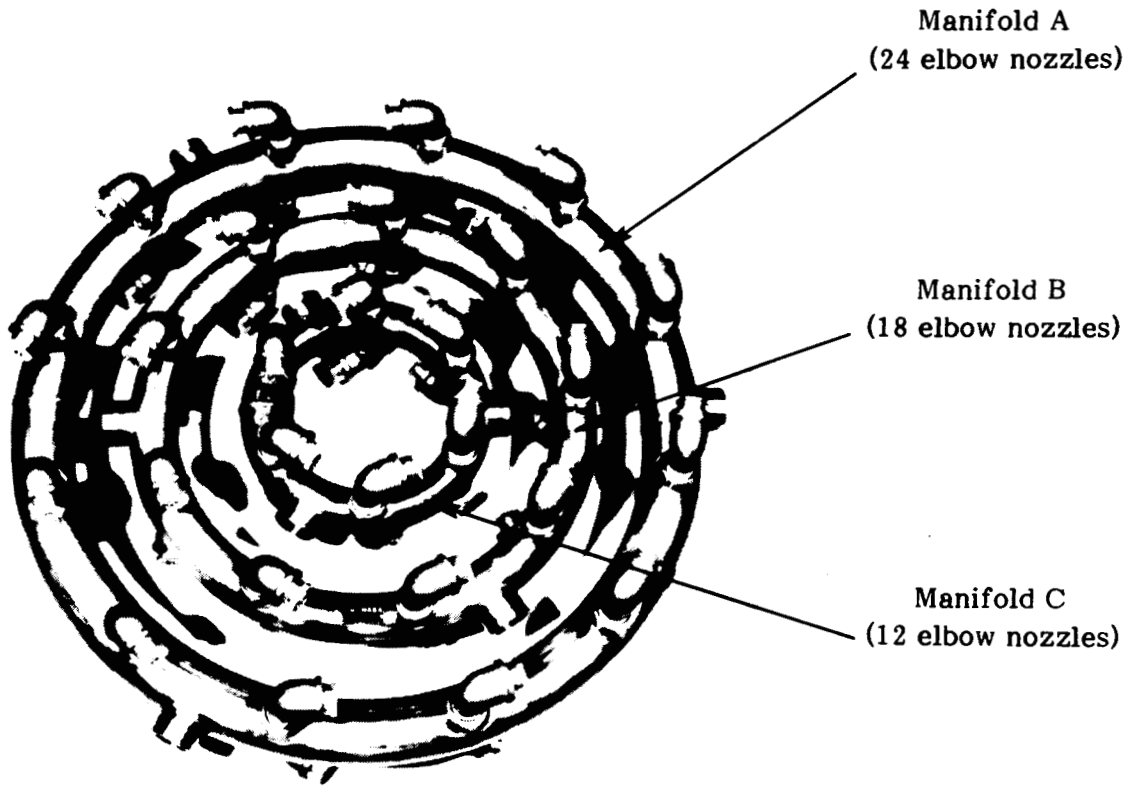
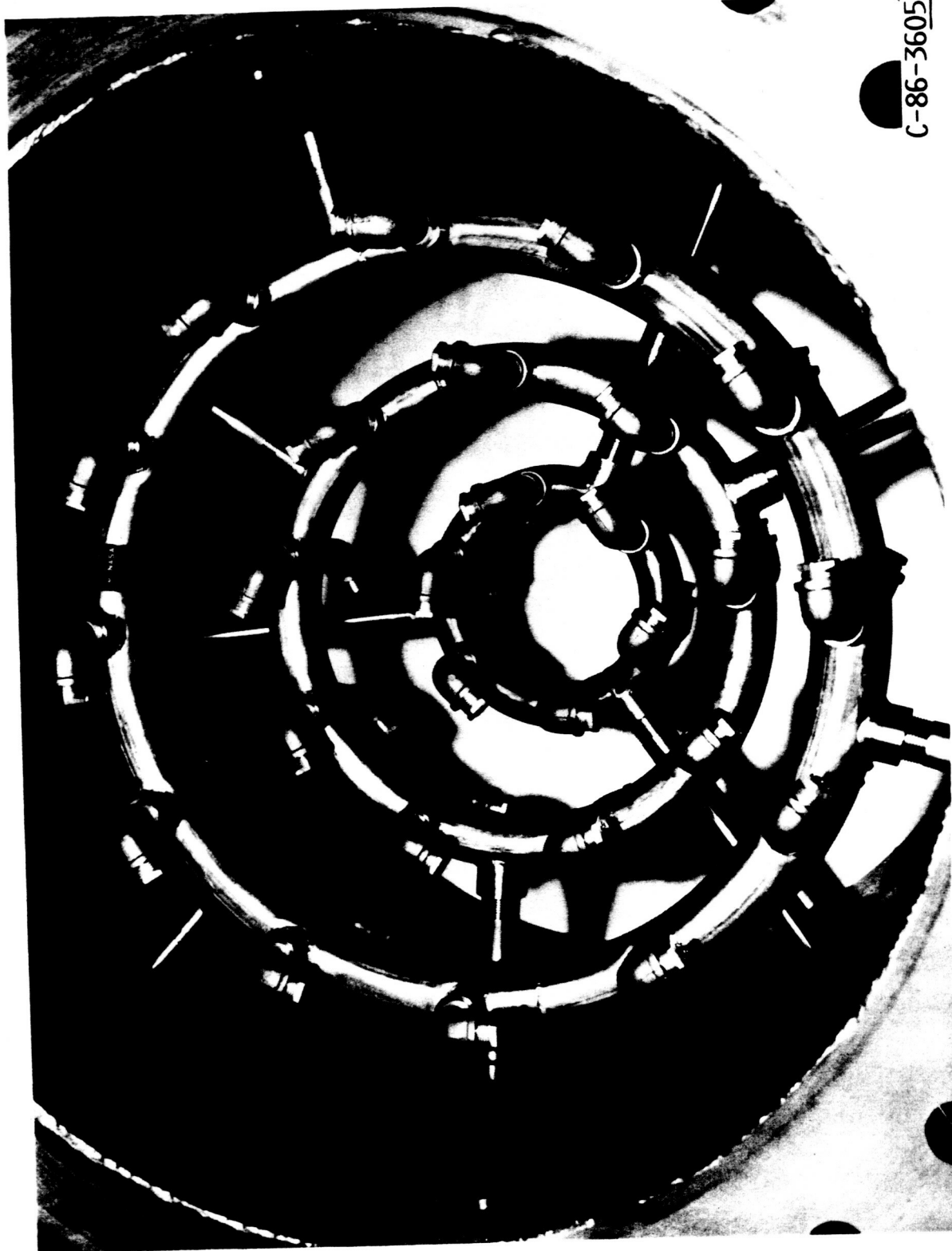


Figure 2: Swirl-Generating Unit: Manifold Rings and Elbow Nozzles (Unassembled)

ORIGINAL PAGE
BLACK AND WHITE PHOTOGRAPH



C-86-3605]

Figure 3: Location of Manifolds Inside the Spool Piece.

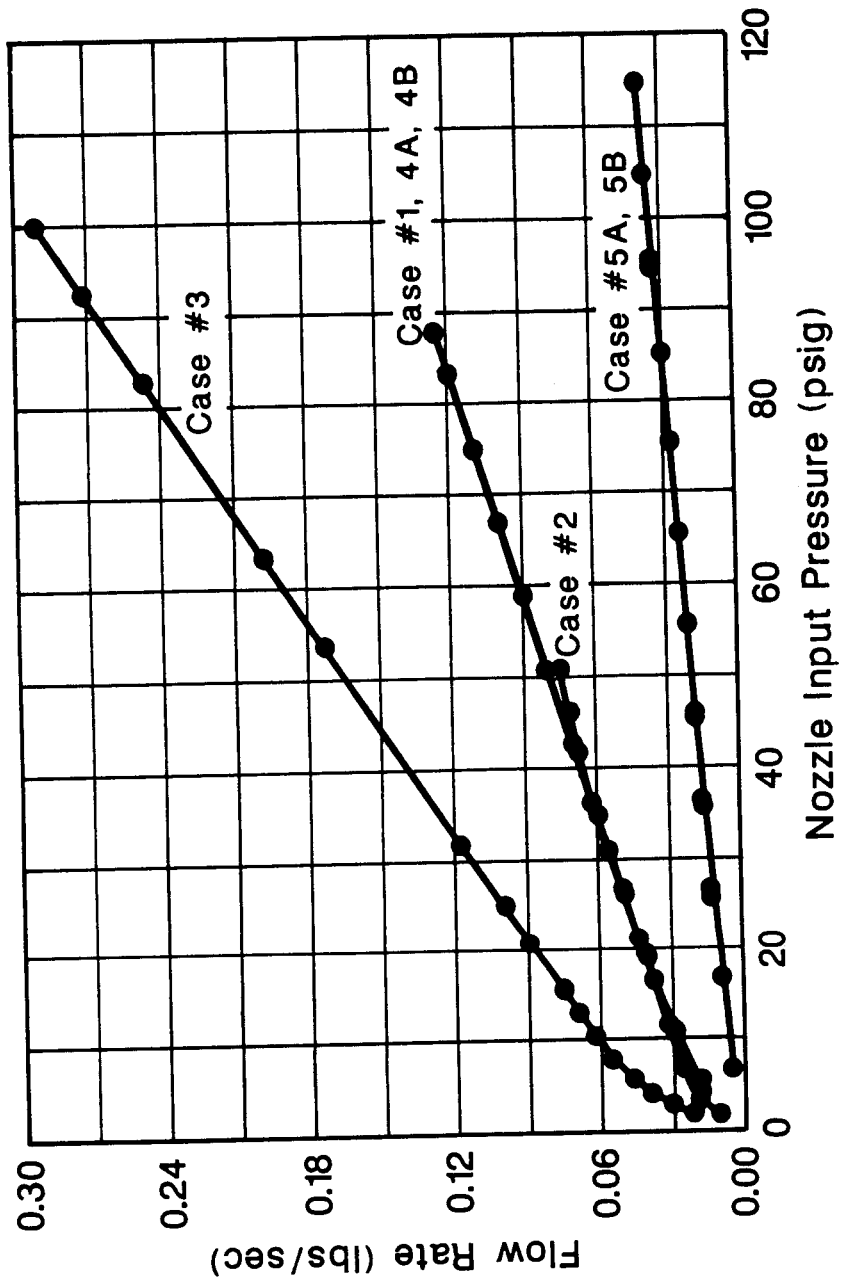


Figure 4: Variation of Elbow Nozzle Mass Flow Rate with Inlet Air Pressure

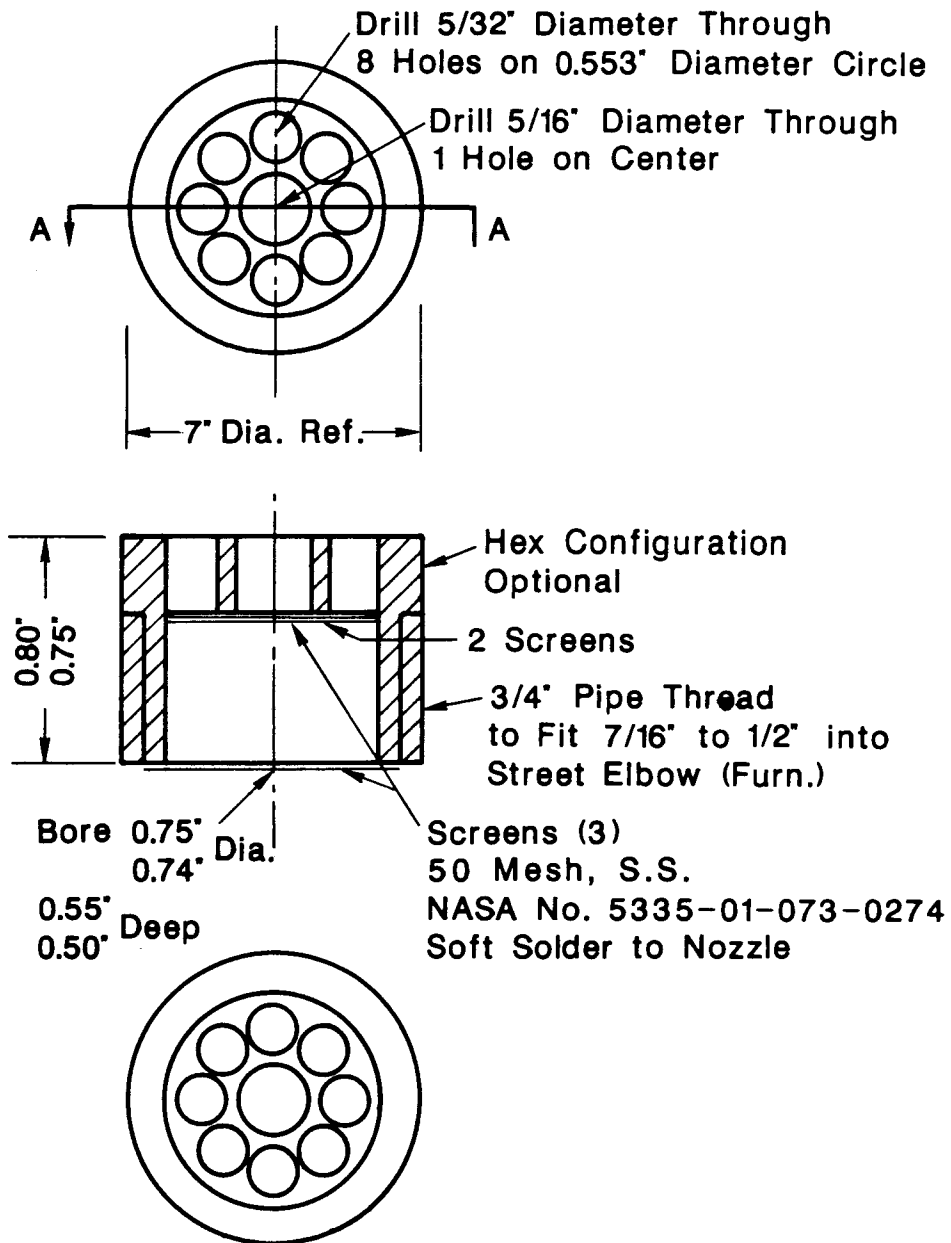


Figure 5: Elbow-Nozzle Outlet Multi-Hole Piece

ORIGINAL PAGE
BLACK AND WHITE PHOTOGRAPH

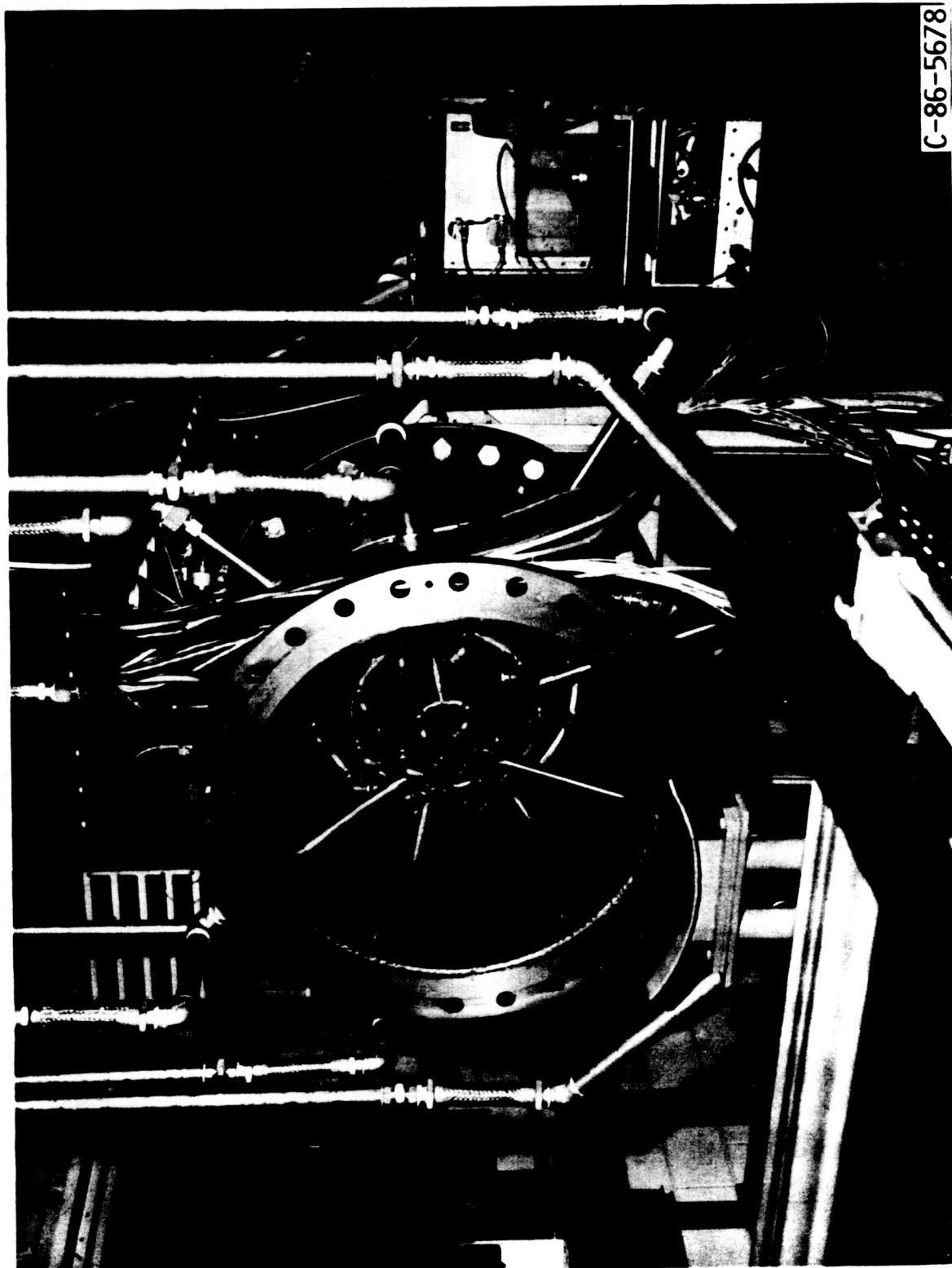


Figure 6: Swirl Generator and Plenum Tank.

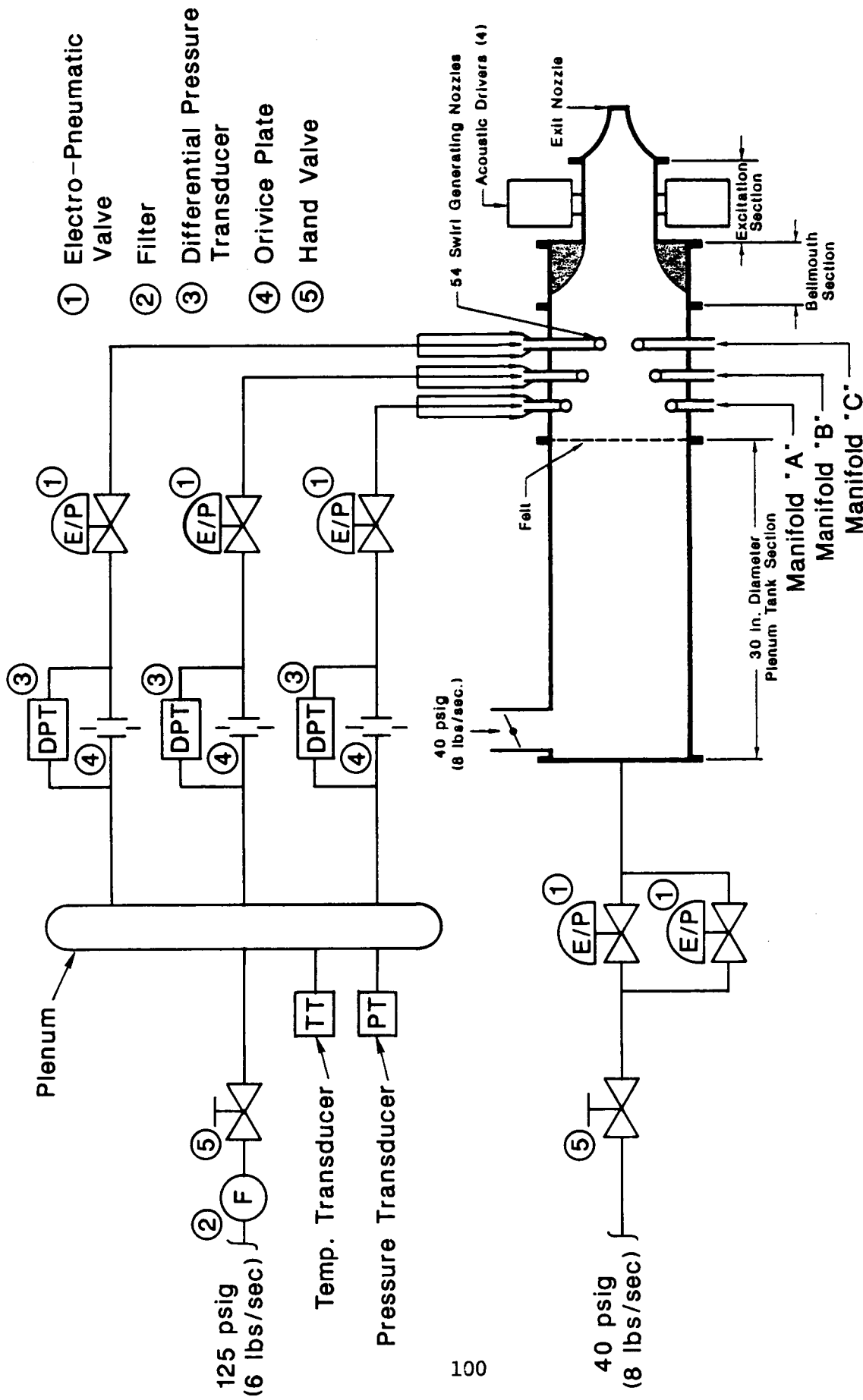


Figure 7: Schematic Diagram of the Air System Components

ORIGINAL PAGE
BLACK AND WHITE PHOTOGRAPH

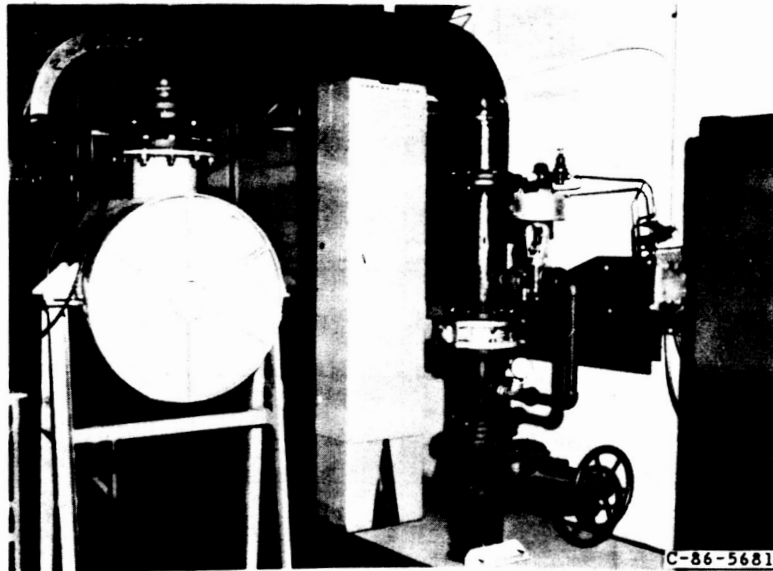


Figure 8: Axial Air Pipes and Controls.

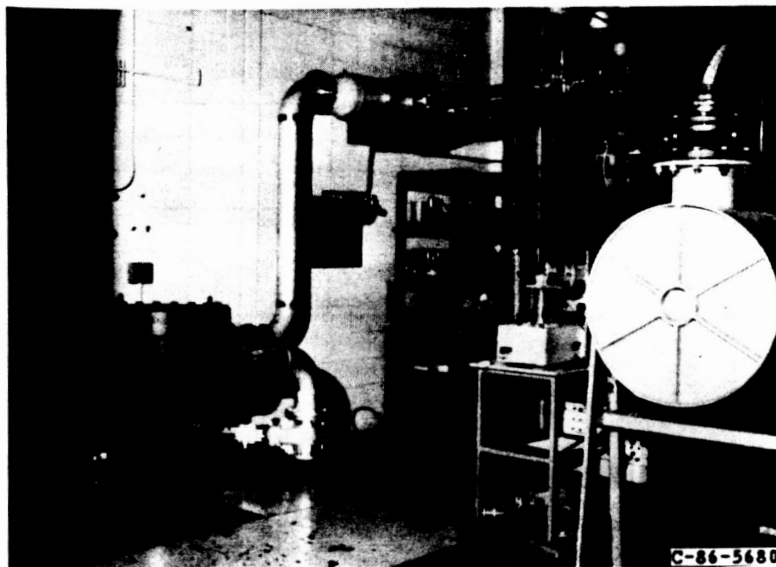


Figure 9: Tangential Air Pipes and Controls.

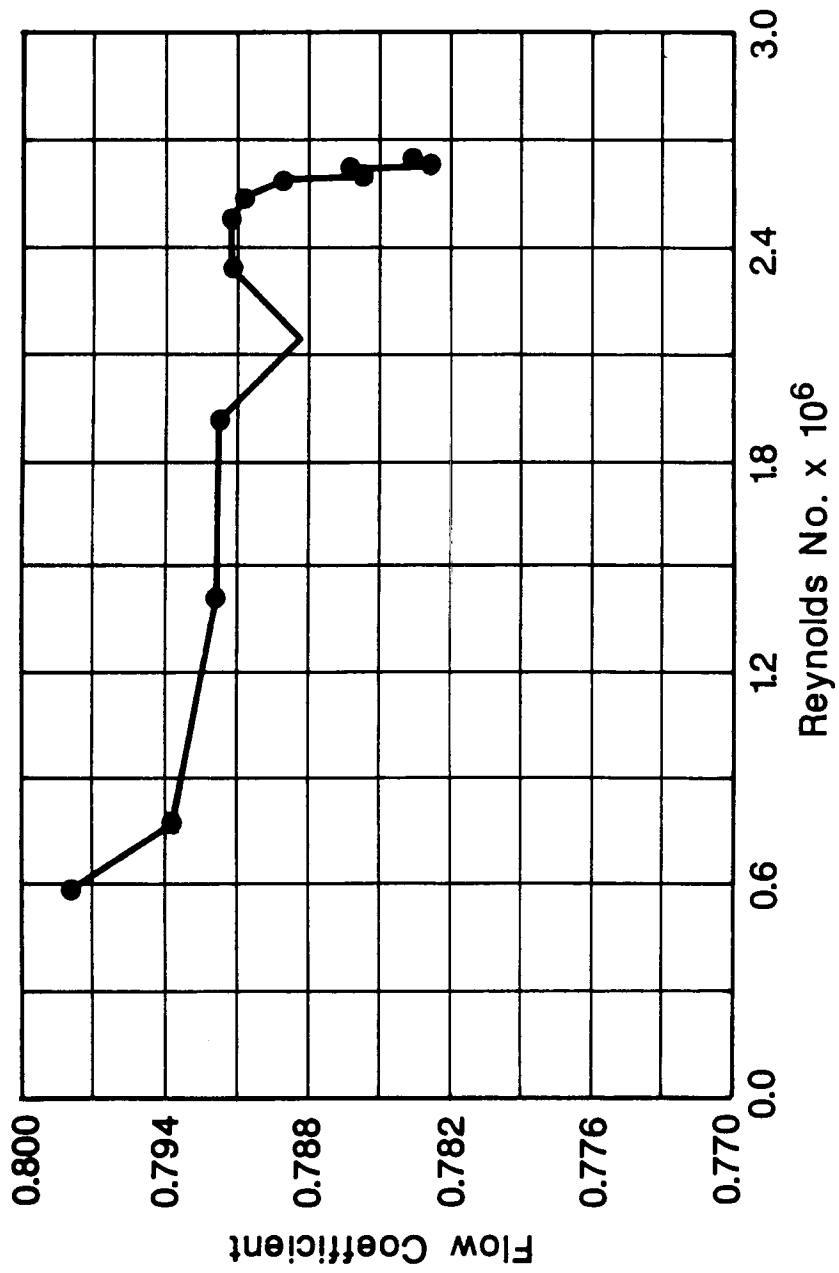


Figure 10: Calibration Curve for Orifice Plate #1

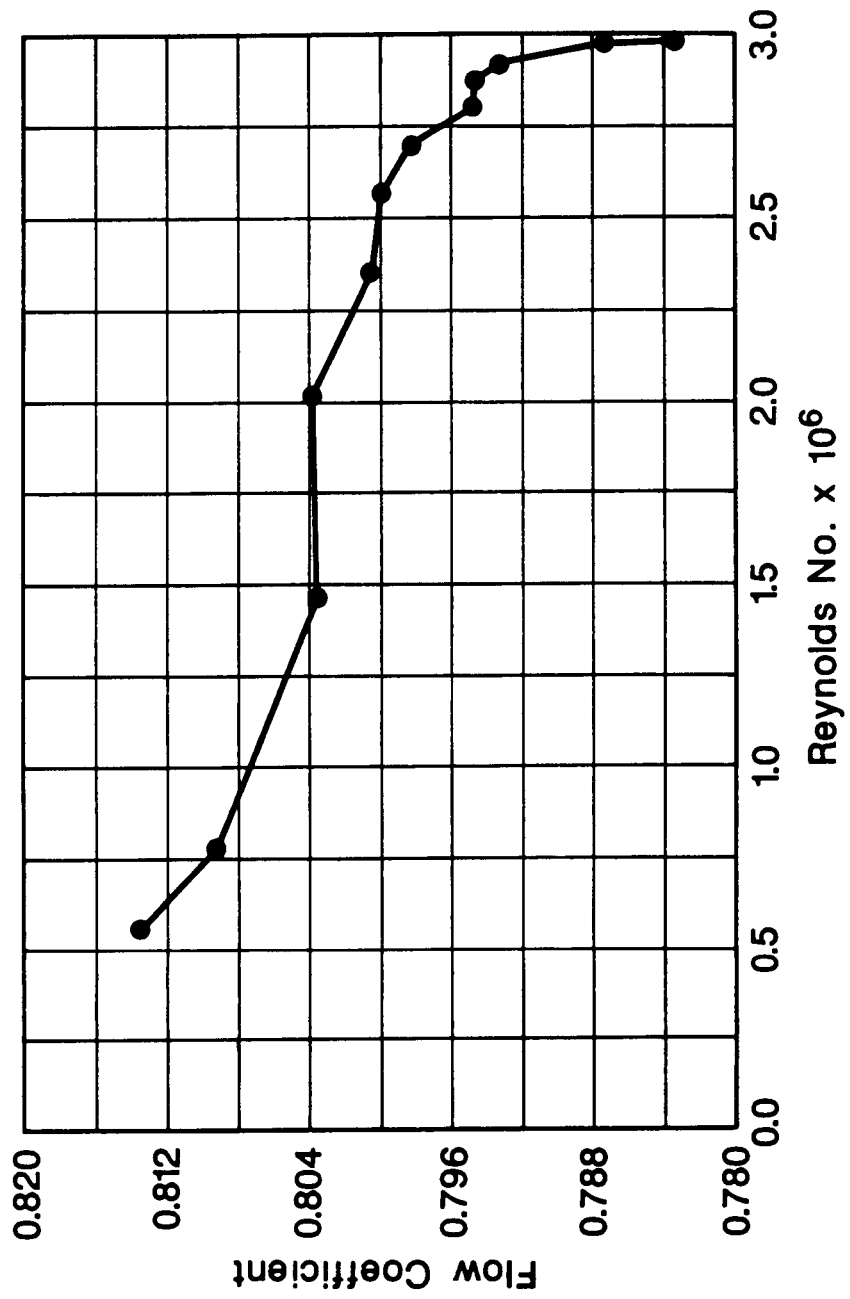


Figure 11: Calibration Curve for Orifice Plate #2

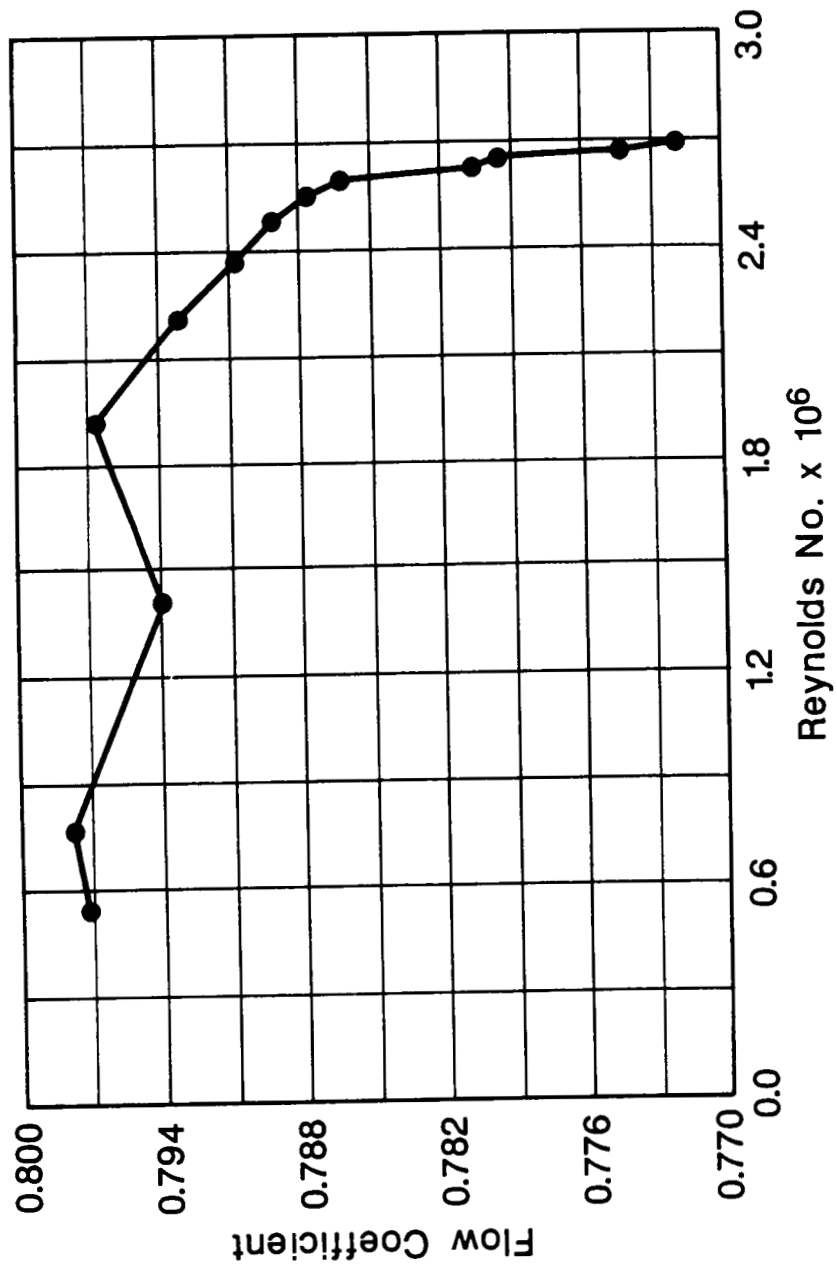


Figure 12: Calibration Curve for Orifice Plate #3

ORIGINAL PAGE
BLACK AND WHITE PHOTOGRAPH



Figure 13: Jet Facility and Traversing Mechanism.

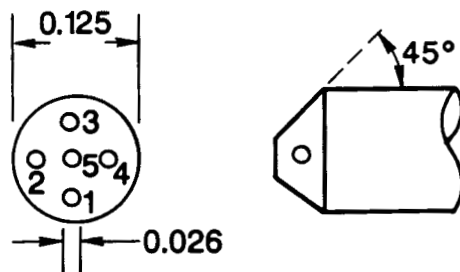
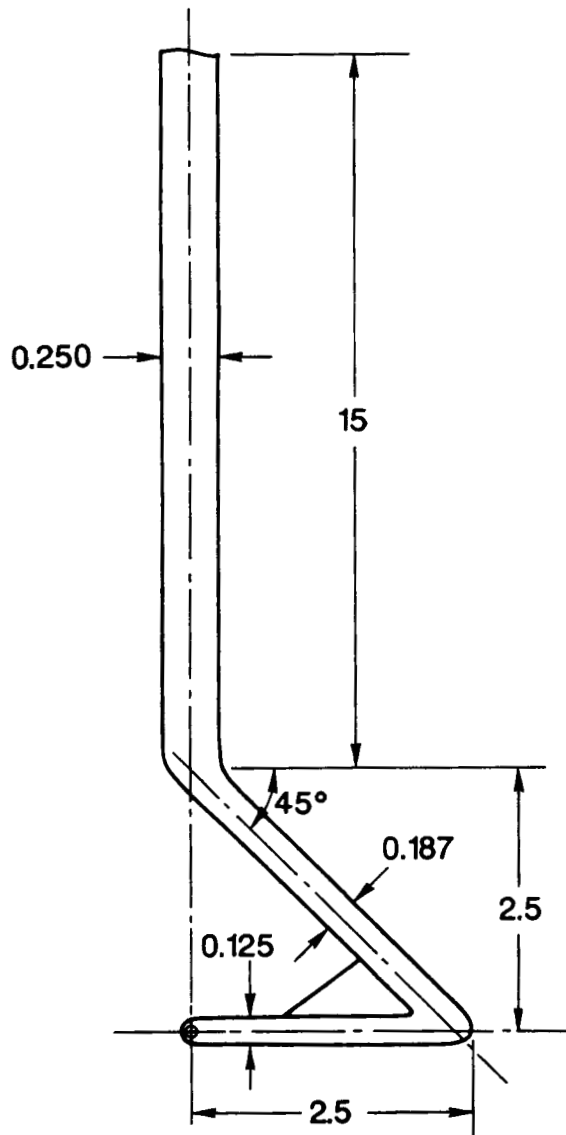


Figure 14: Dimensions of Probe in Inches

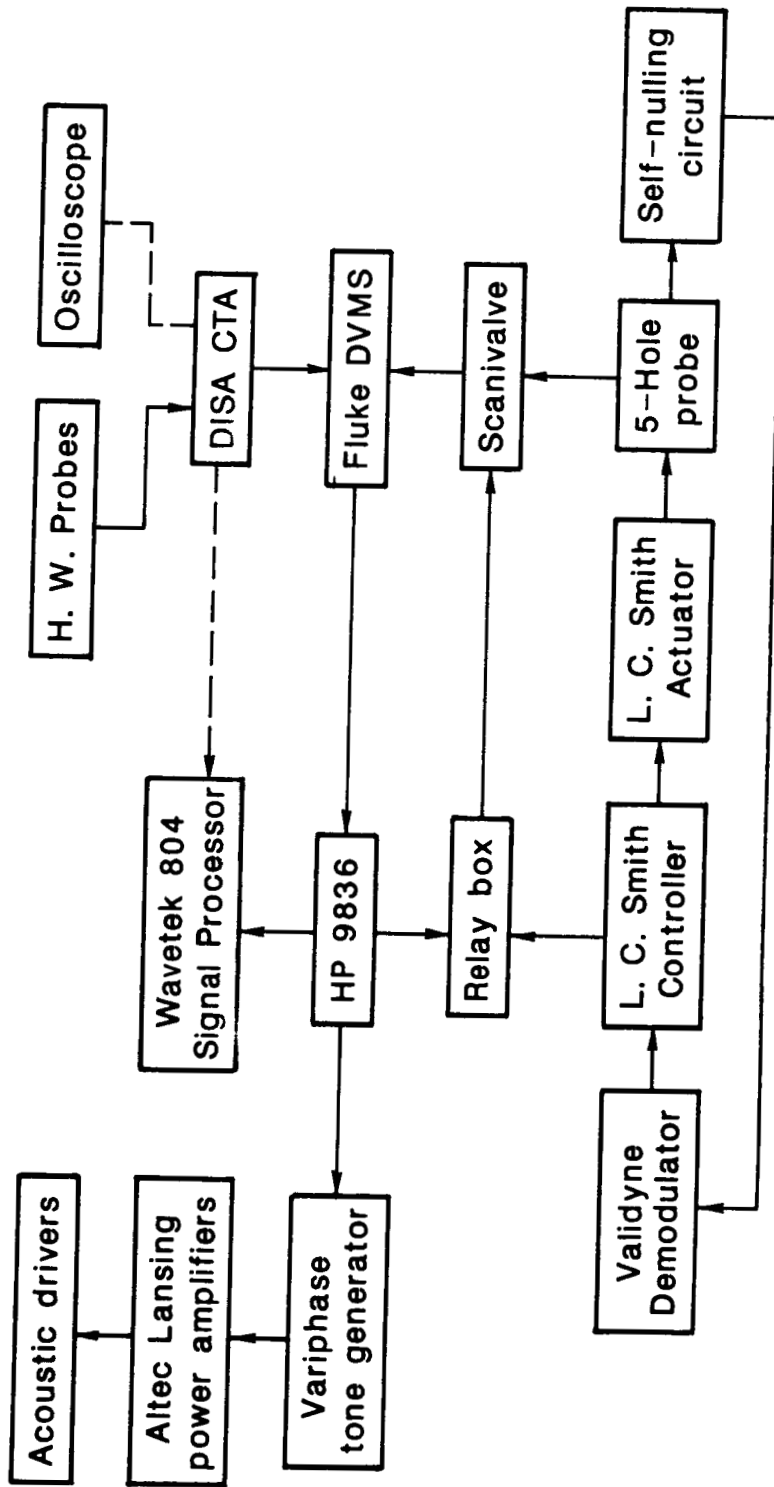
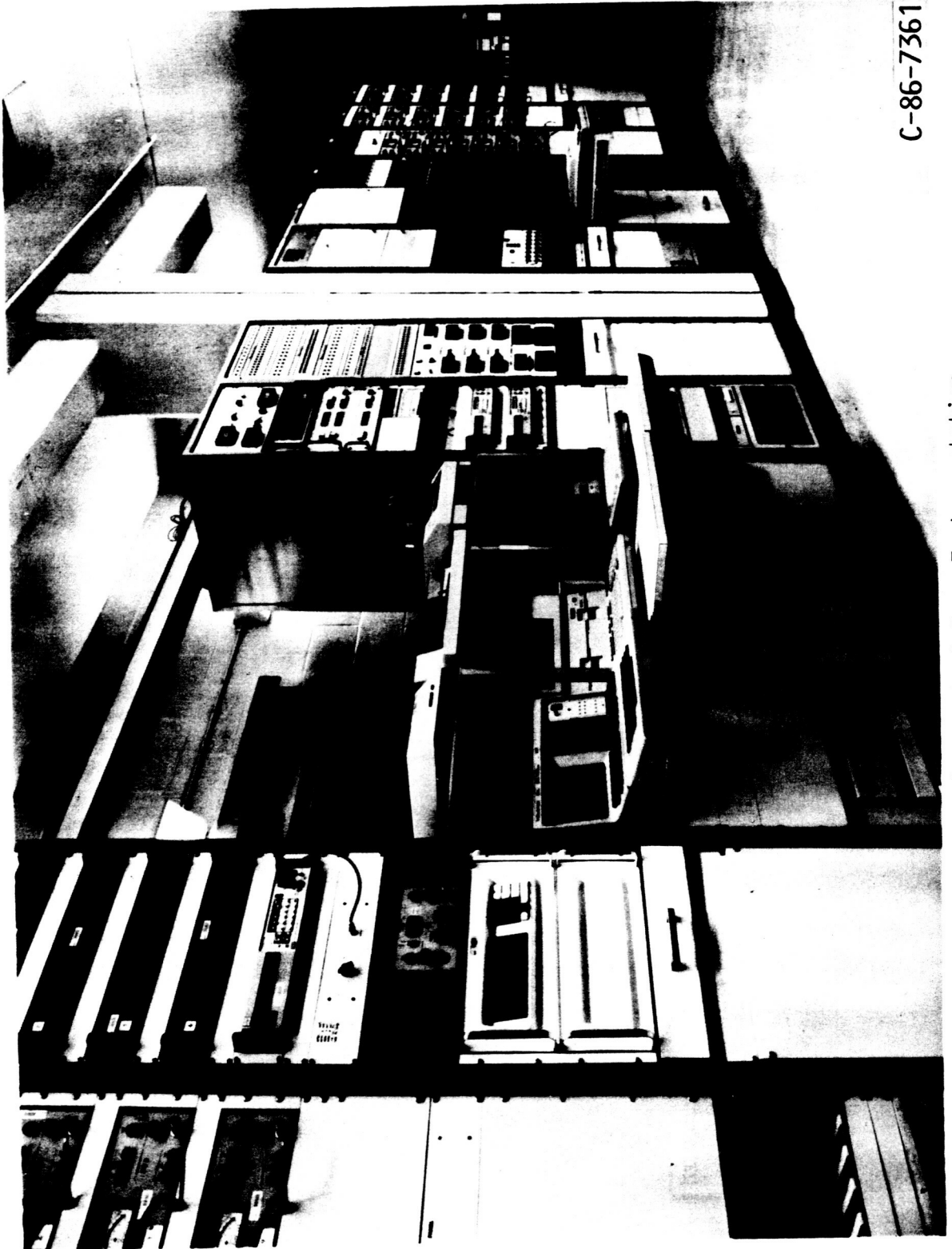


Figure 15: Schematic Diagram of Data Acquisition System

ORIGINAL PAGE
BLACK AND WHITE PHOTOGRAPH



C-86-7361

Figure 16: Control Room Instrumentation.

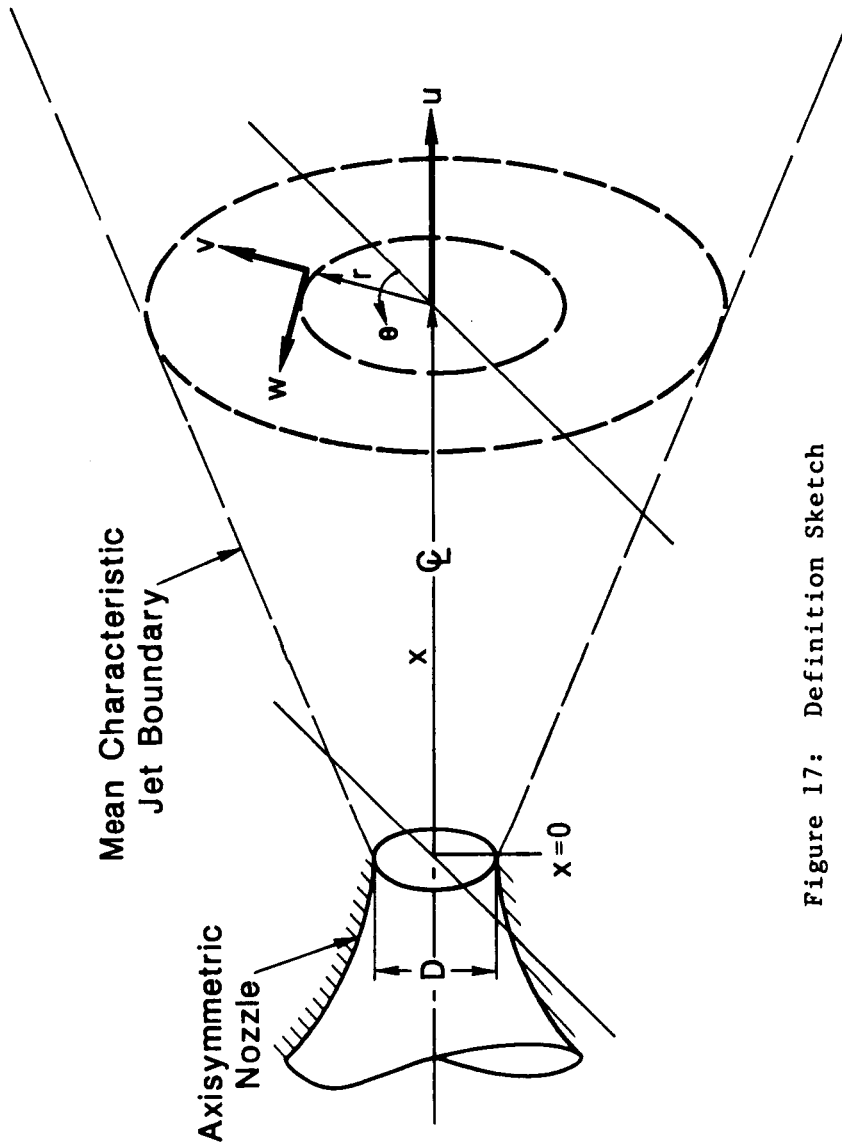


Figure 17: Definition Sketch

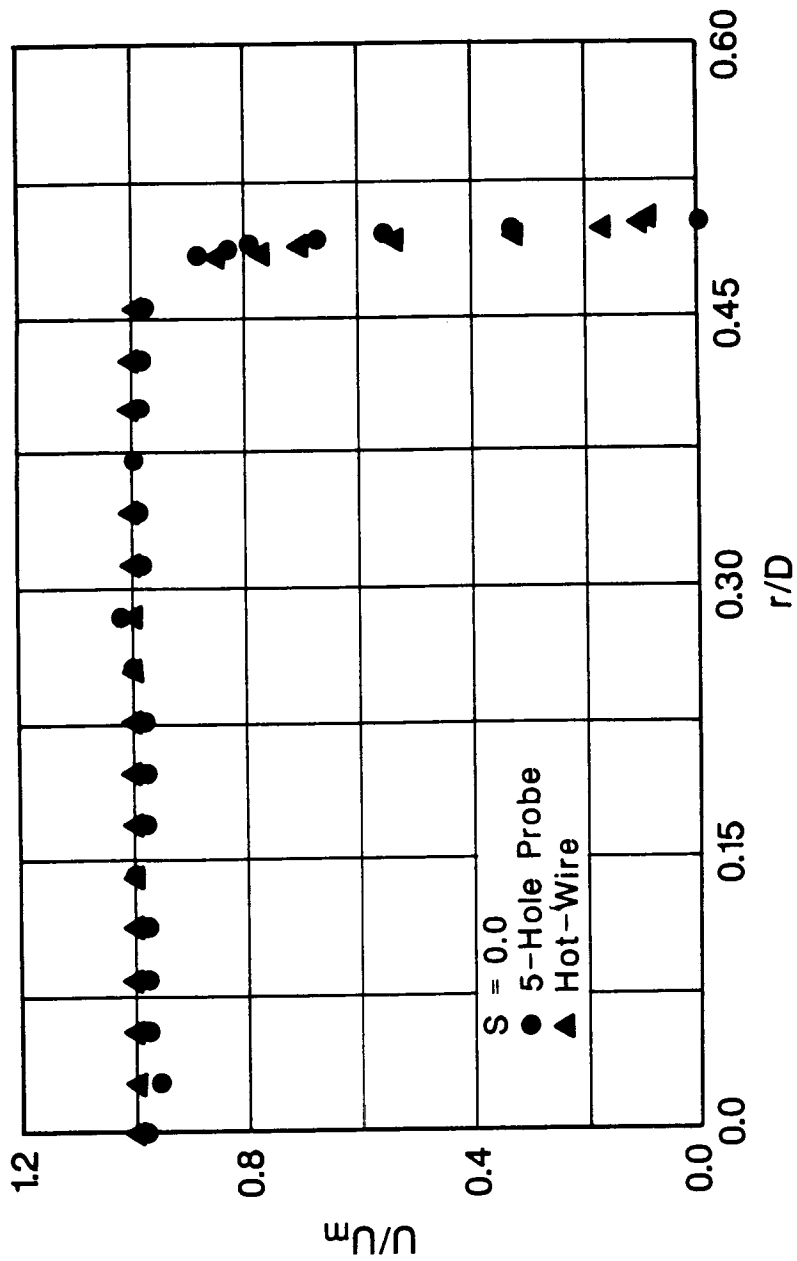


Figure 18: Comparison Between Hot-Wire and 5-Hole Probe Data at the Nozzle Exit

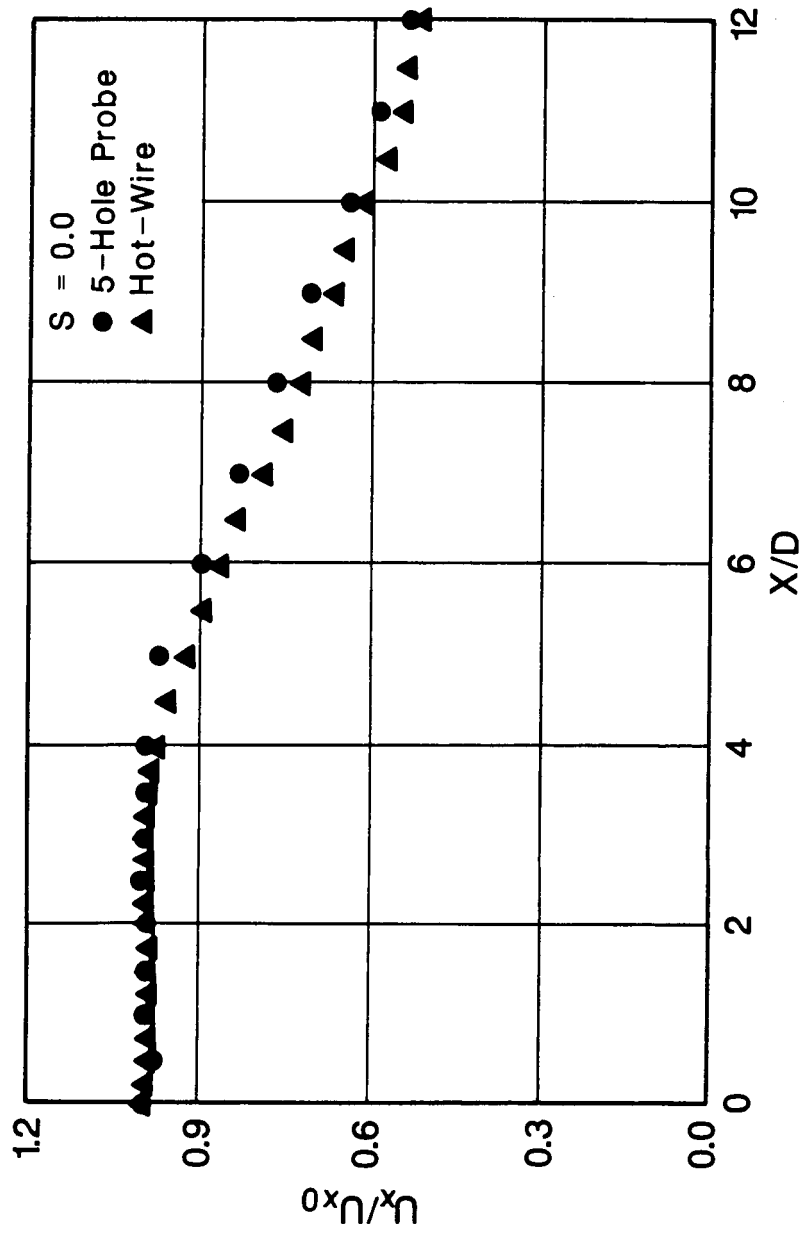


Figure 19: Comparison Between Hot-Wire and 5-Hole Probe Data along the Jet Axis

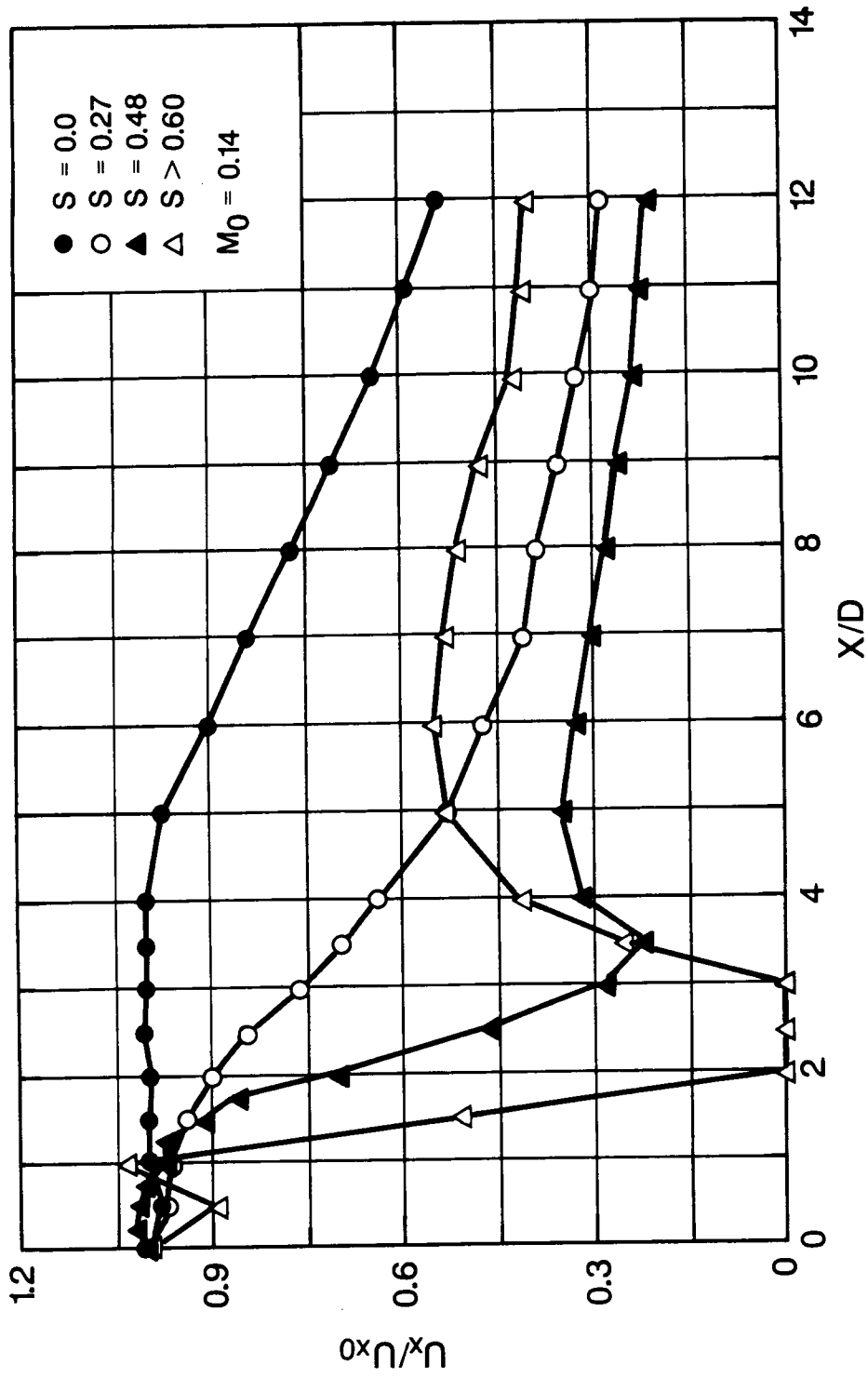


Figure 20: Downstream Development of Centerline Axial Velocity for Different Swirl Numbers

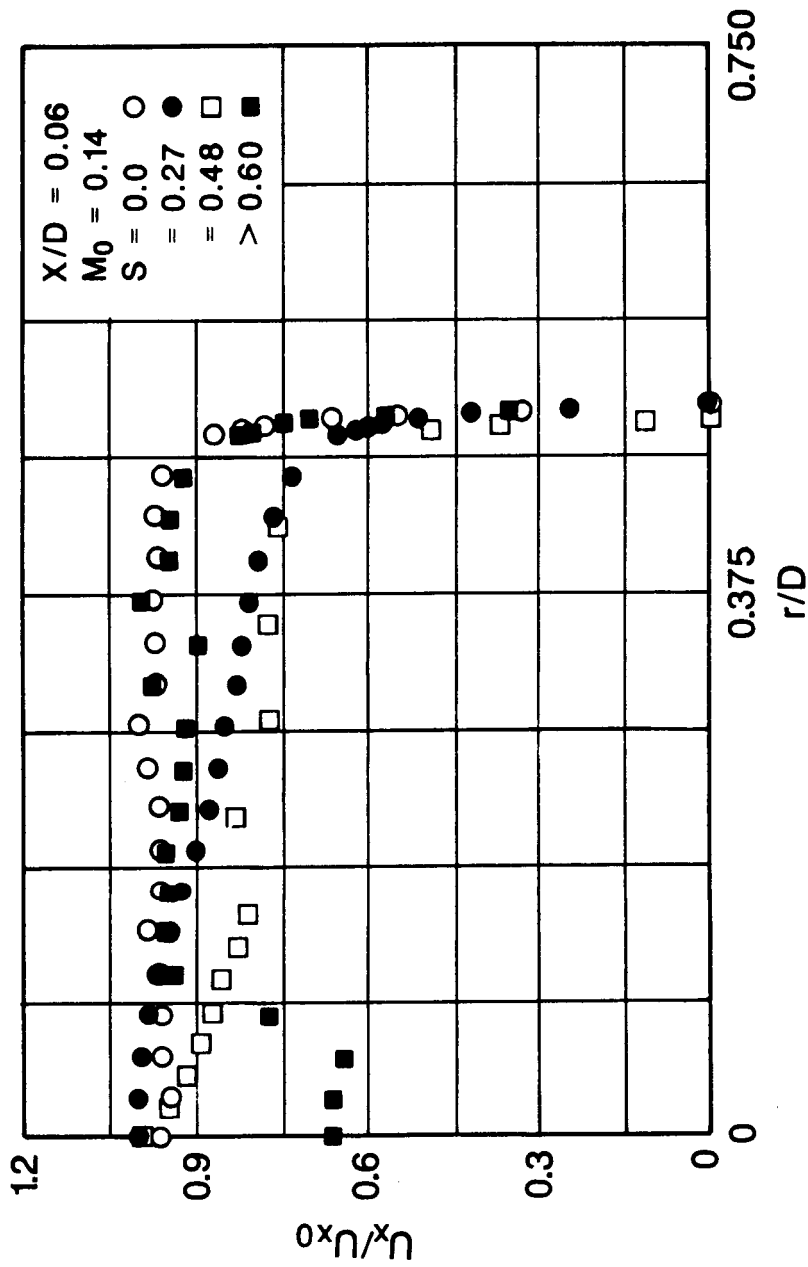


Figure 21: Radial Distribution of Mean Axial Velocity for Different Swirl Numbers

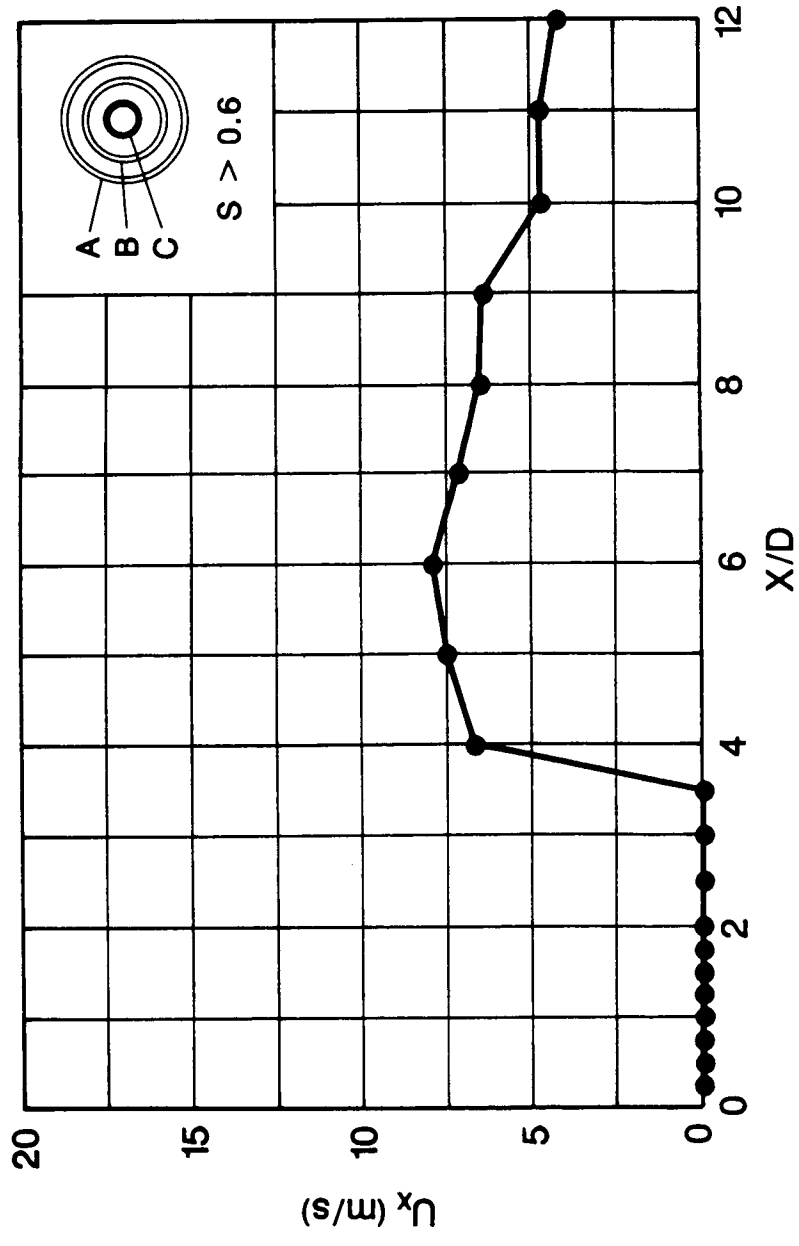


Figure 22: Vortex Breakdown Along the Jet Axis at High Swirl Numbers

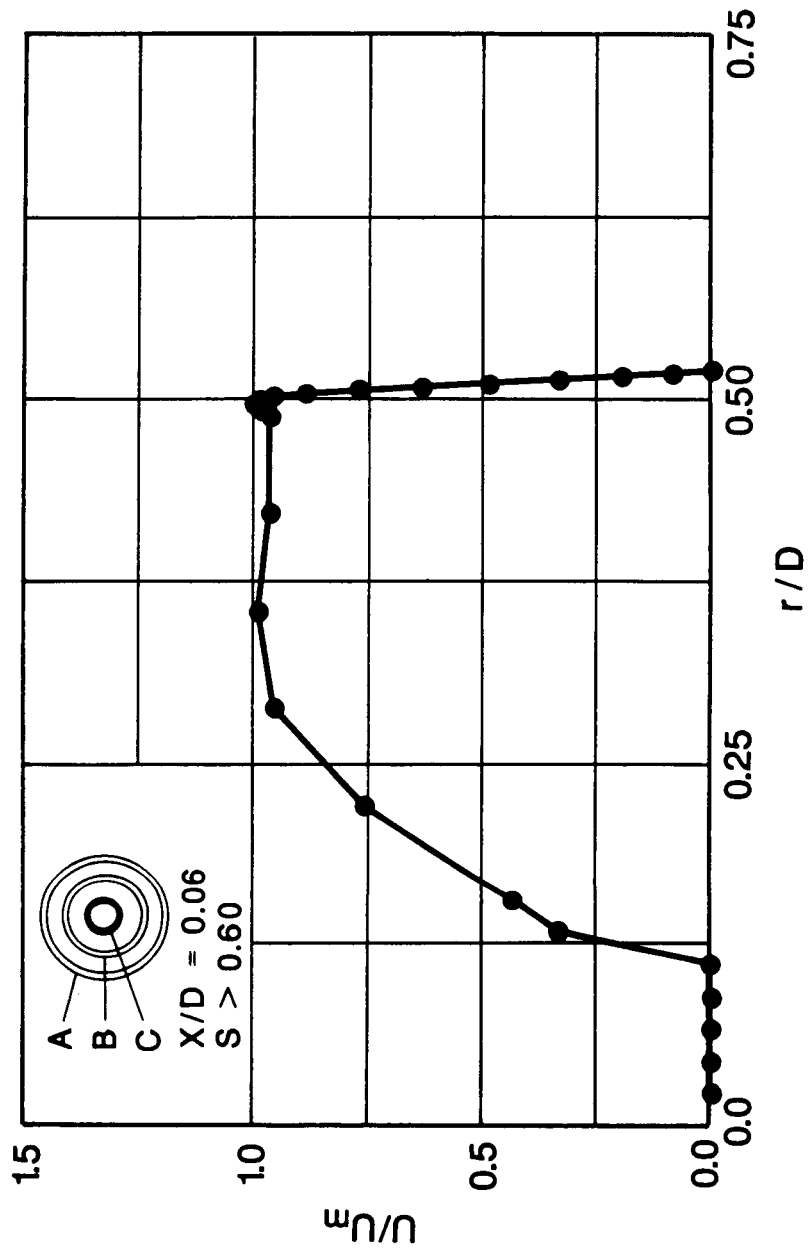


Figure 23: Vortex Breakdown at the Nozzle Exit at High Swirl Numbers

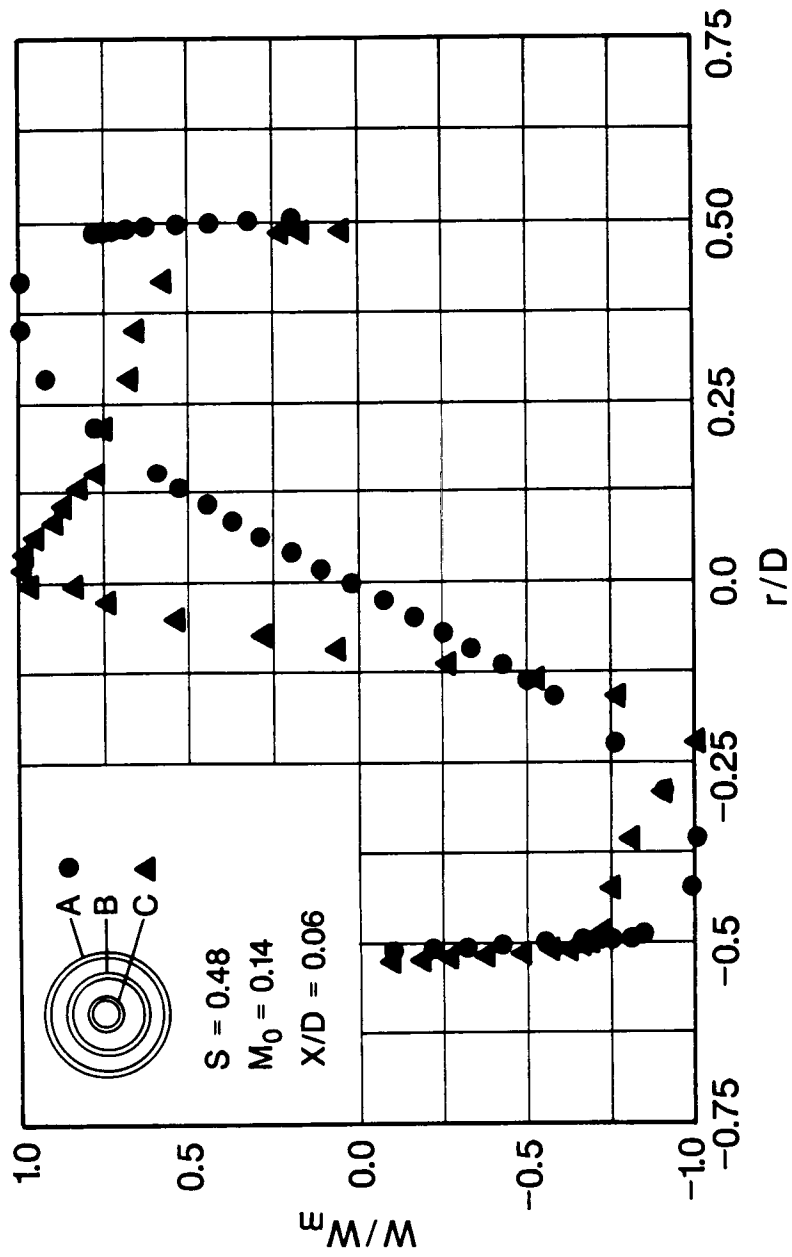


Figure 24: Radial Distribution of the Mean Tangential Velocity

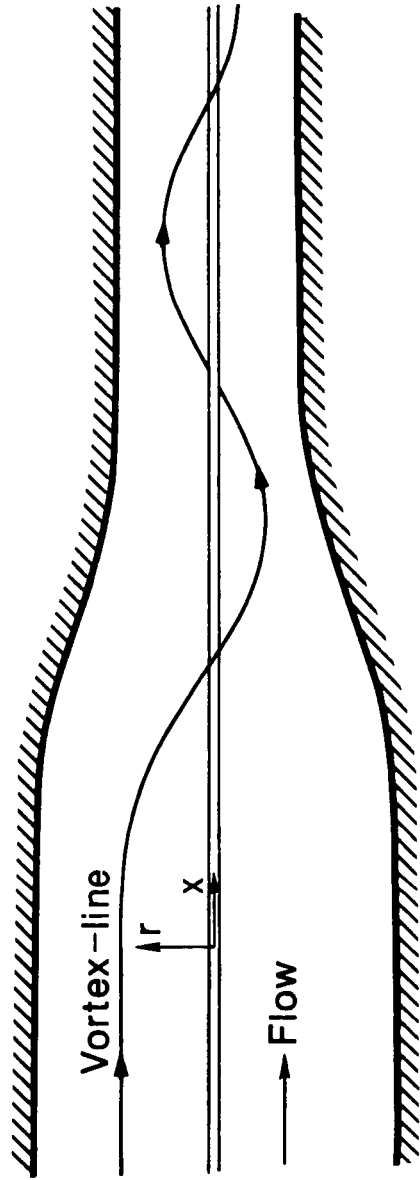


Figure 25: Conversion of a Straight Vortex-Line into a Helix on Passage through a Contraction

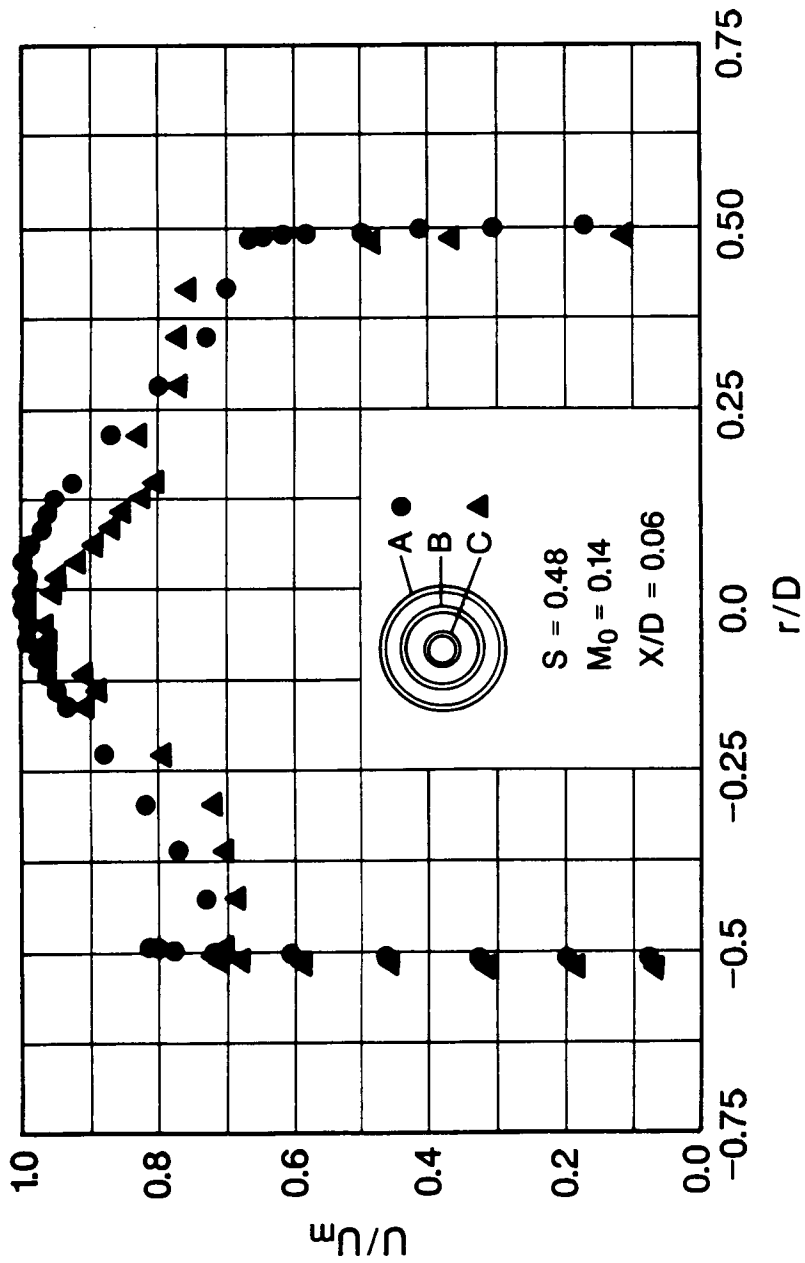


Figure 26: Radial Distribution of the Mean Axial Velocity

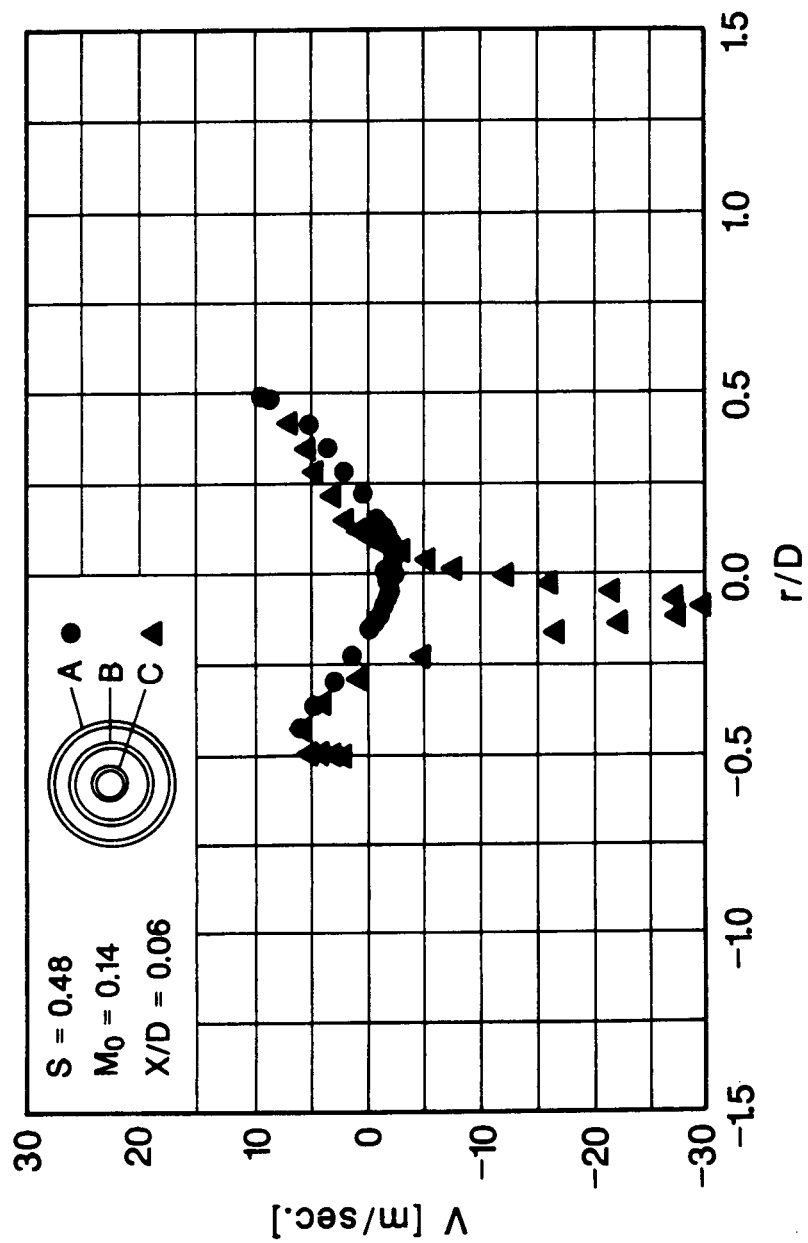


Figure 27: Radial Distribution of the Mean Radial Velocity

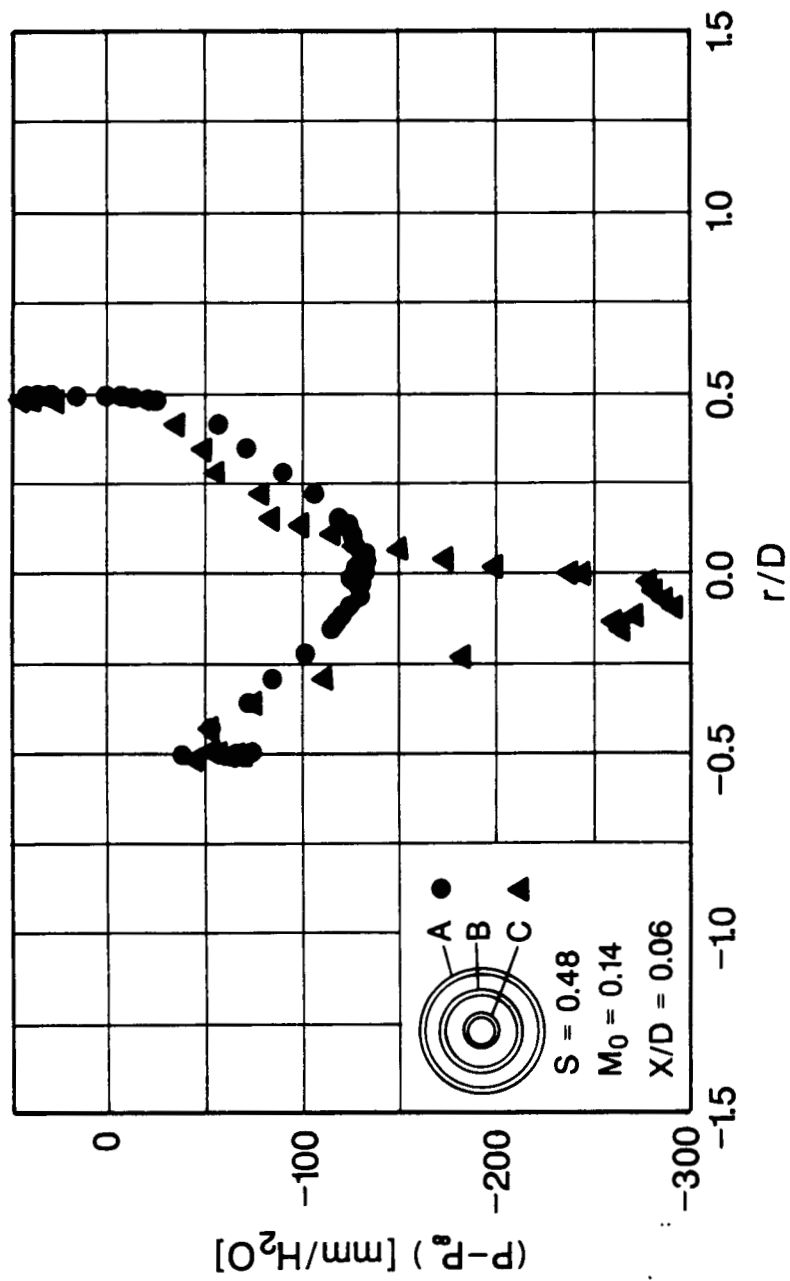
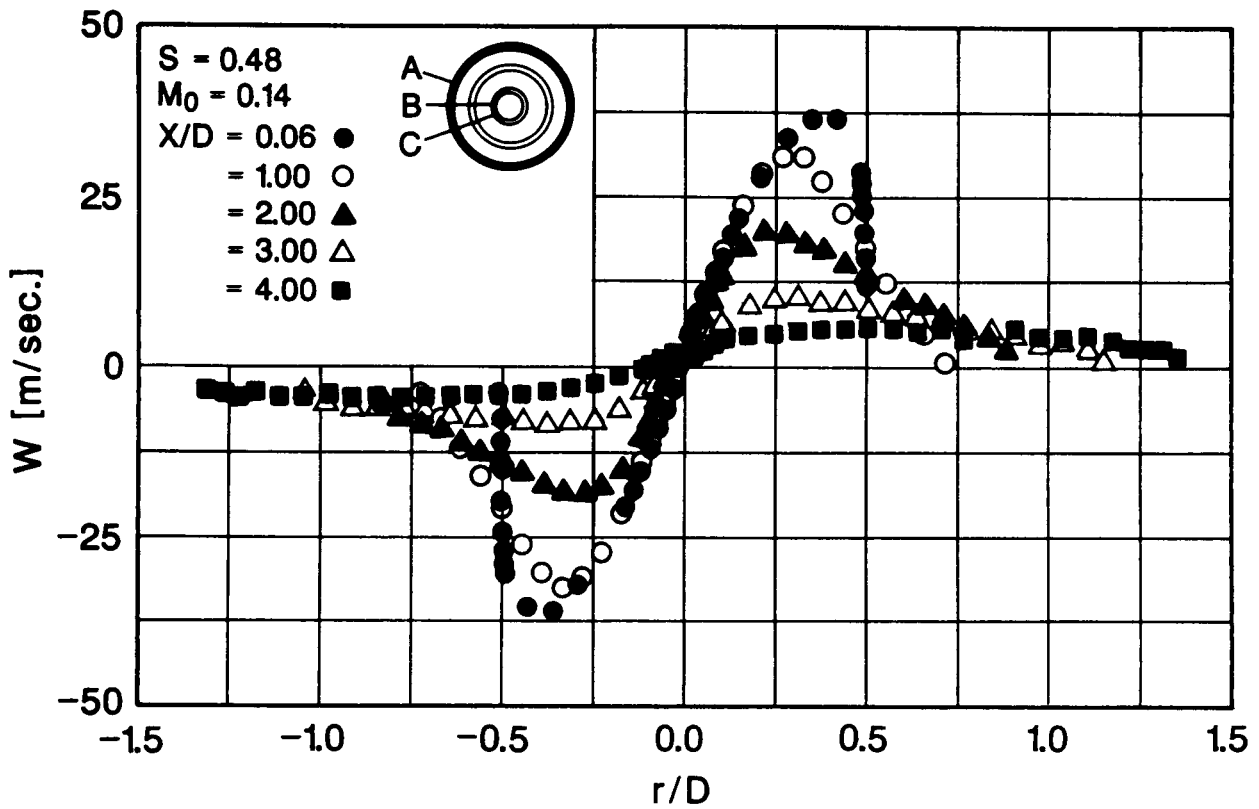
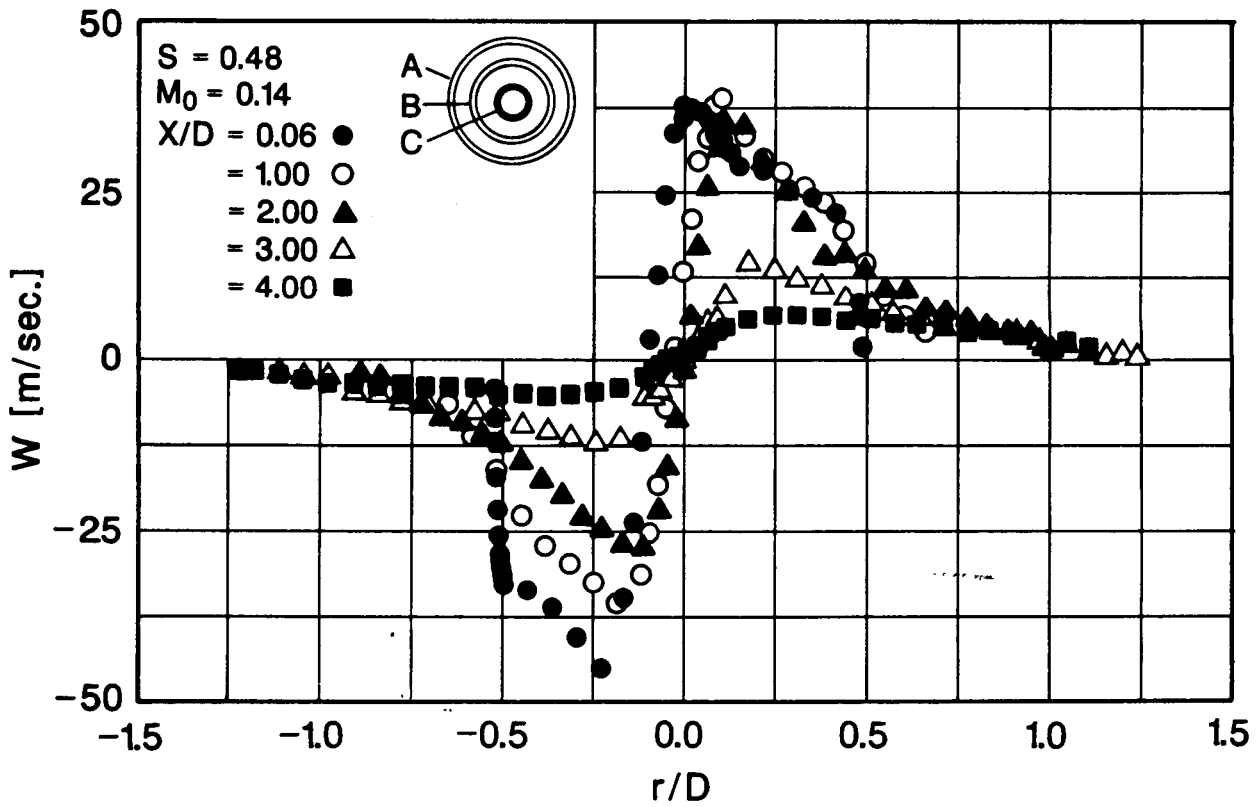


Figure 28: Radial Distribution of the Mean Static Pressure Deficit

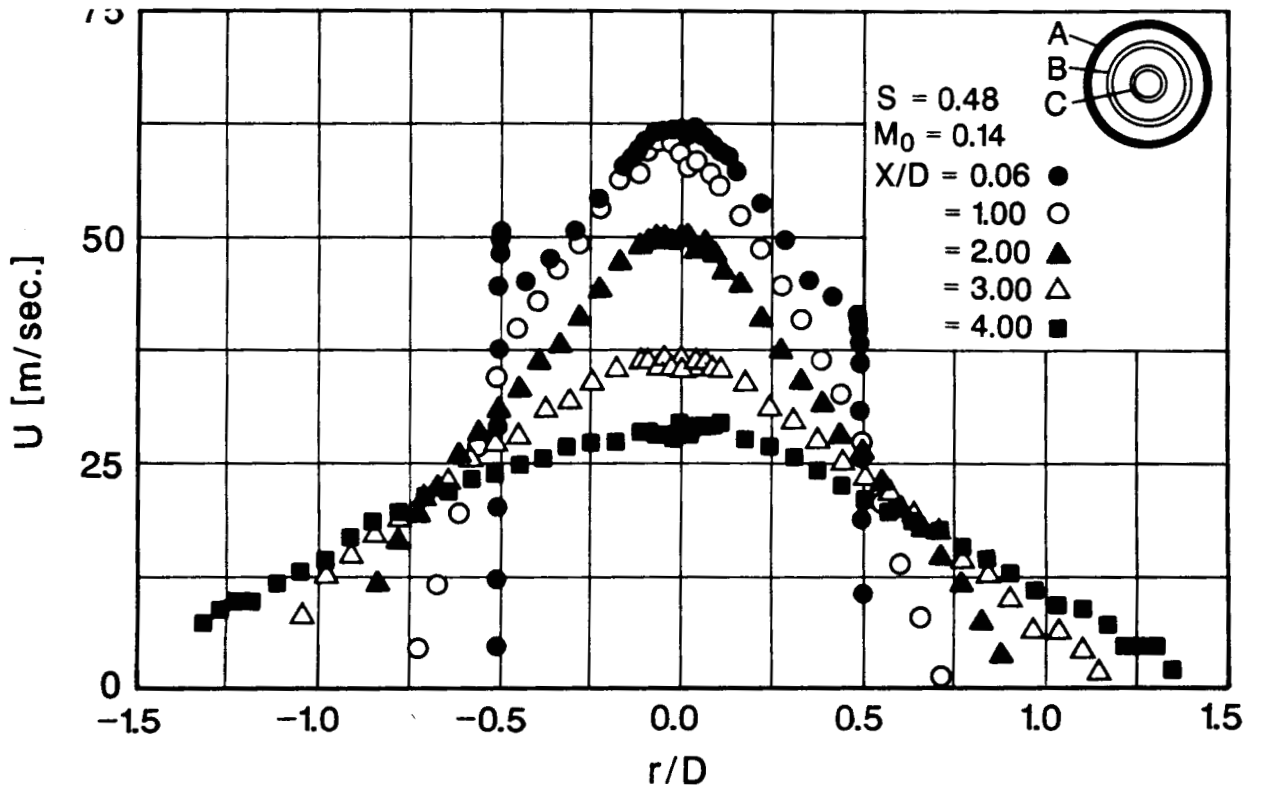


(a) Manifold A

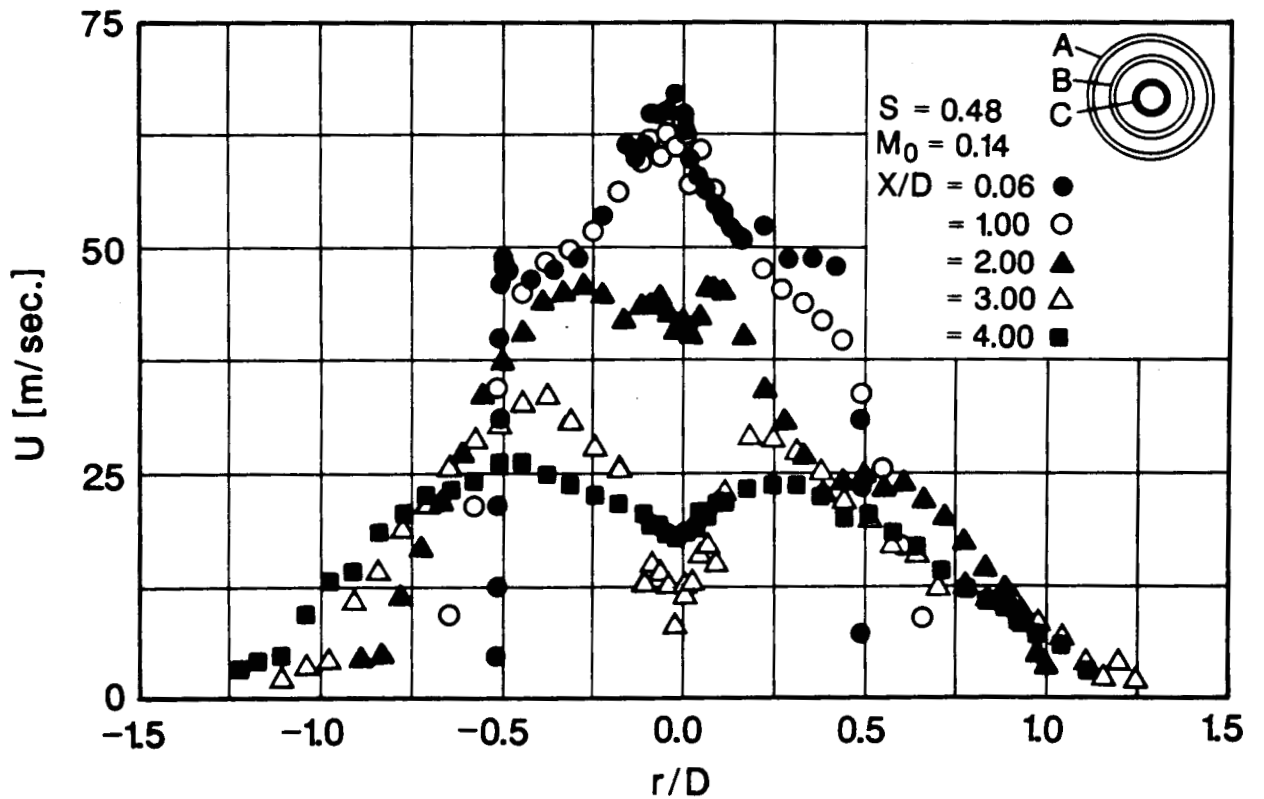


(b) Manifold C

Figure 29: Downstream Development of the Mean Tangential Velocity



(a) Manifold A



(b) Manifold C

Figure 30: Downstream Development of the Mean Axial Velocity

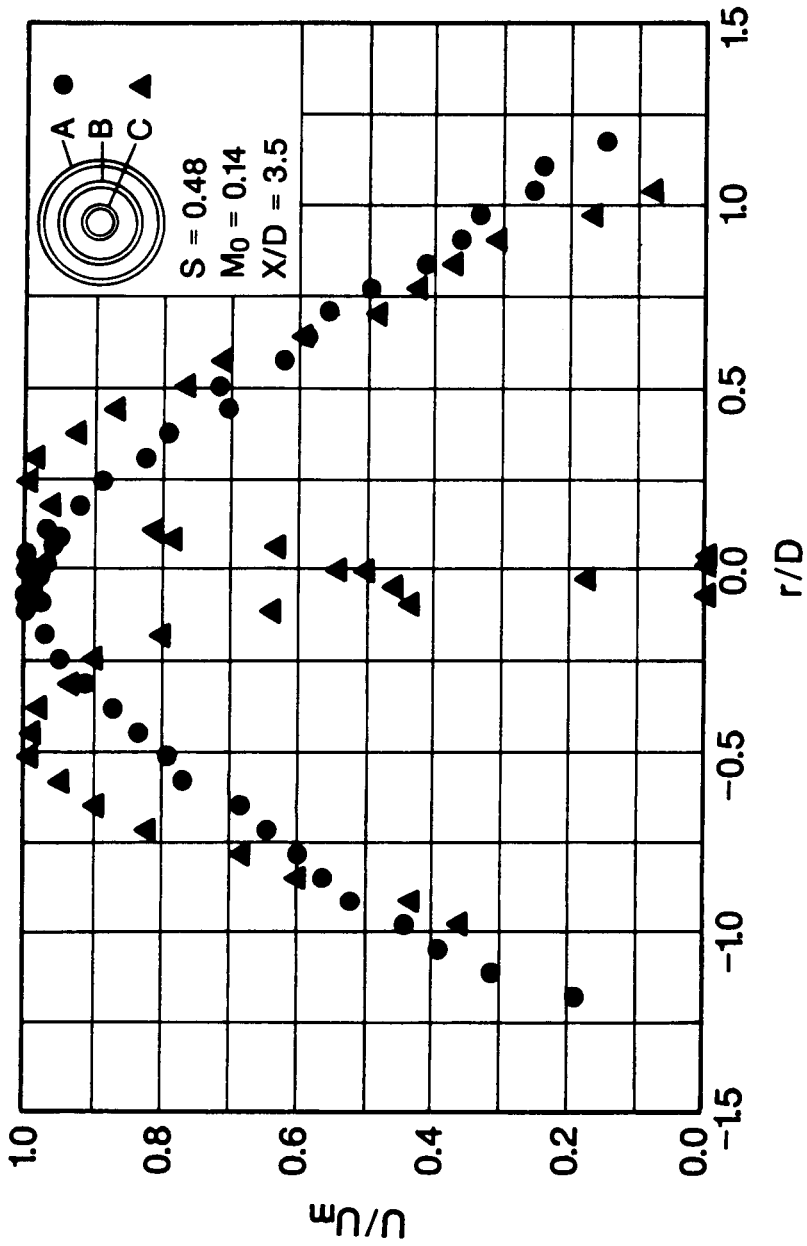
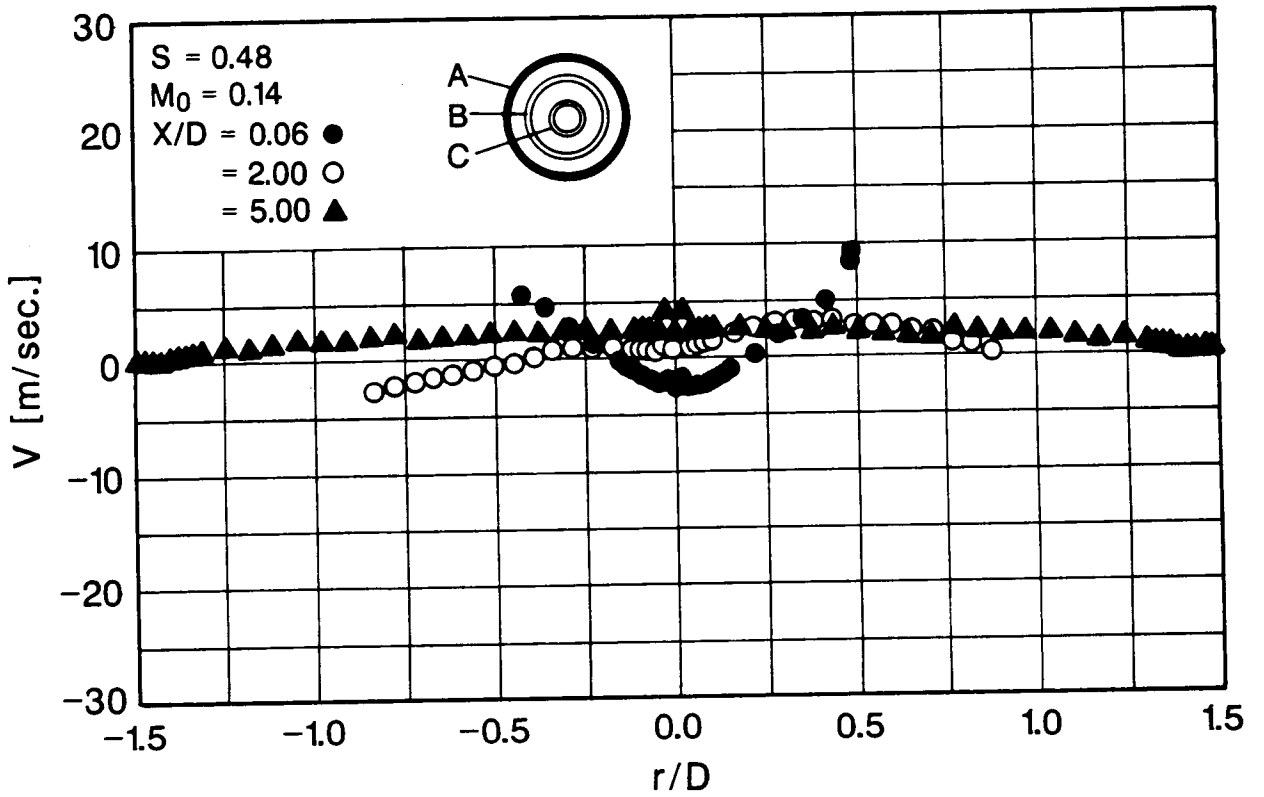
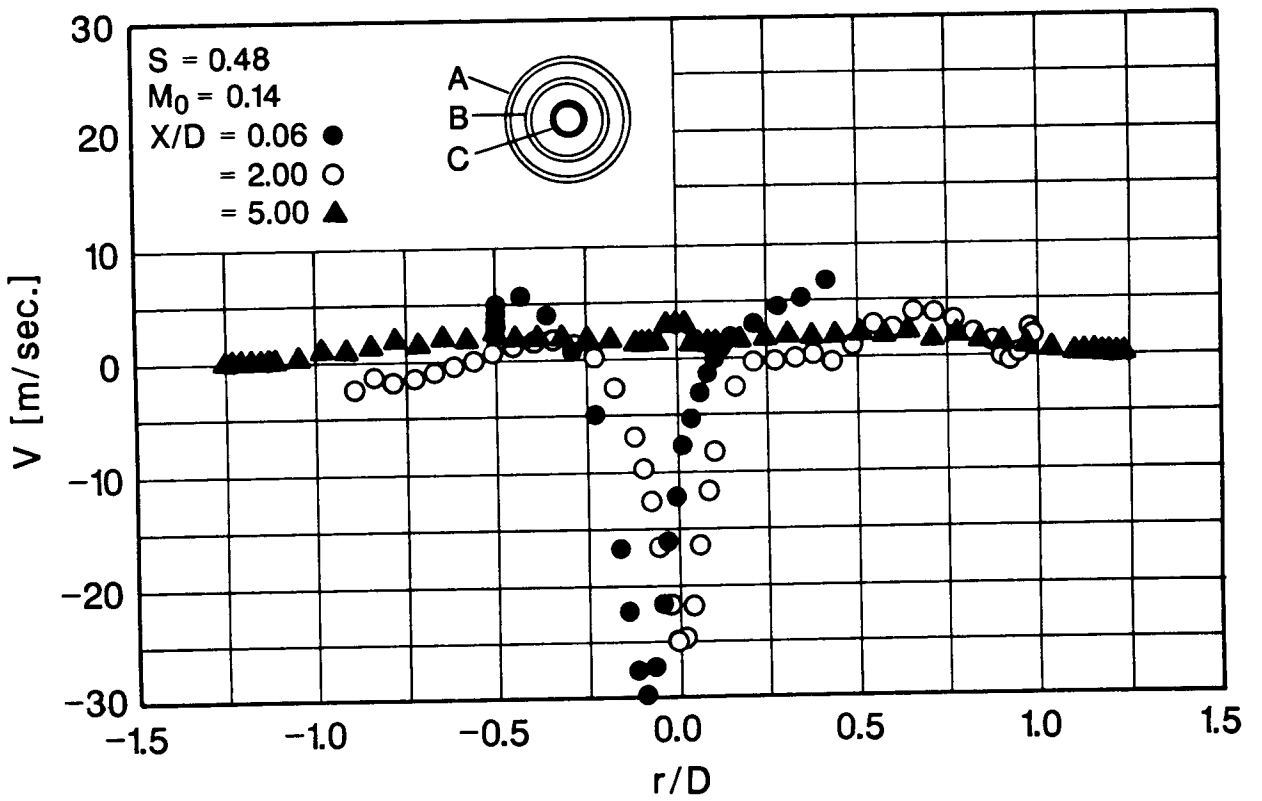


Figure 31: Radial Distribution of the Mean Axial Velocity

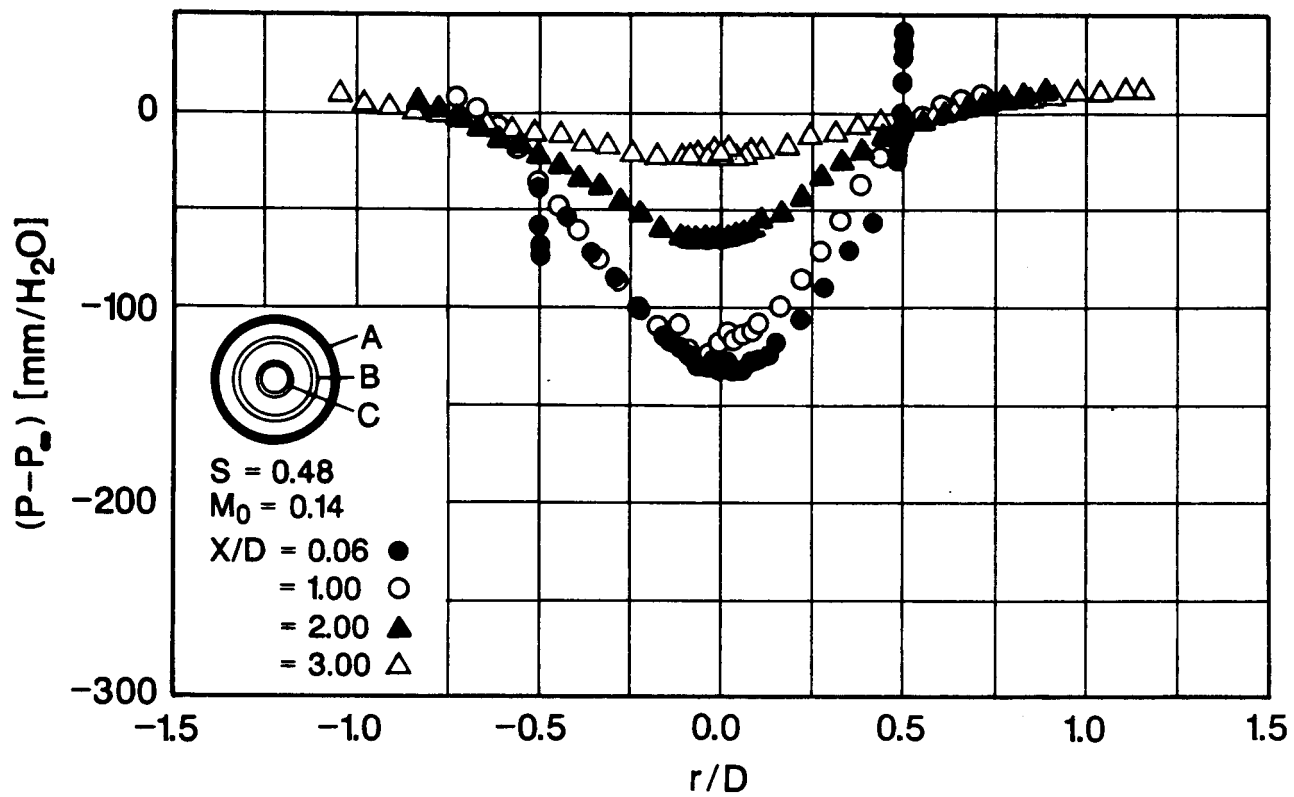


(a) Manifold A

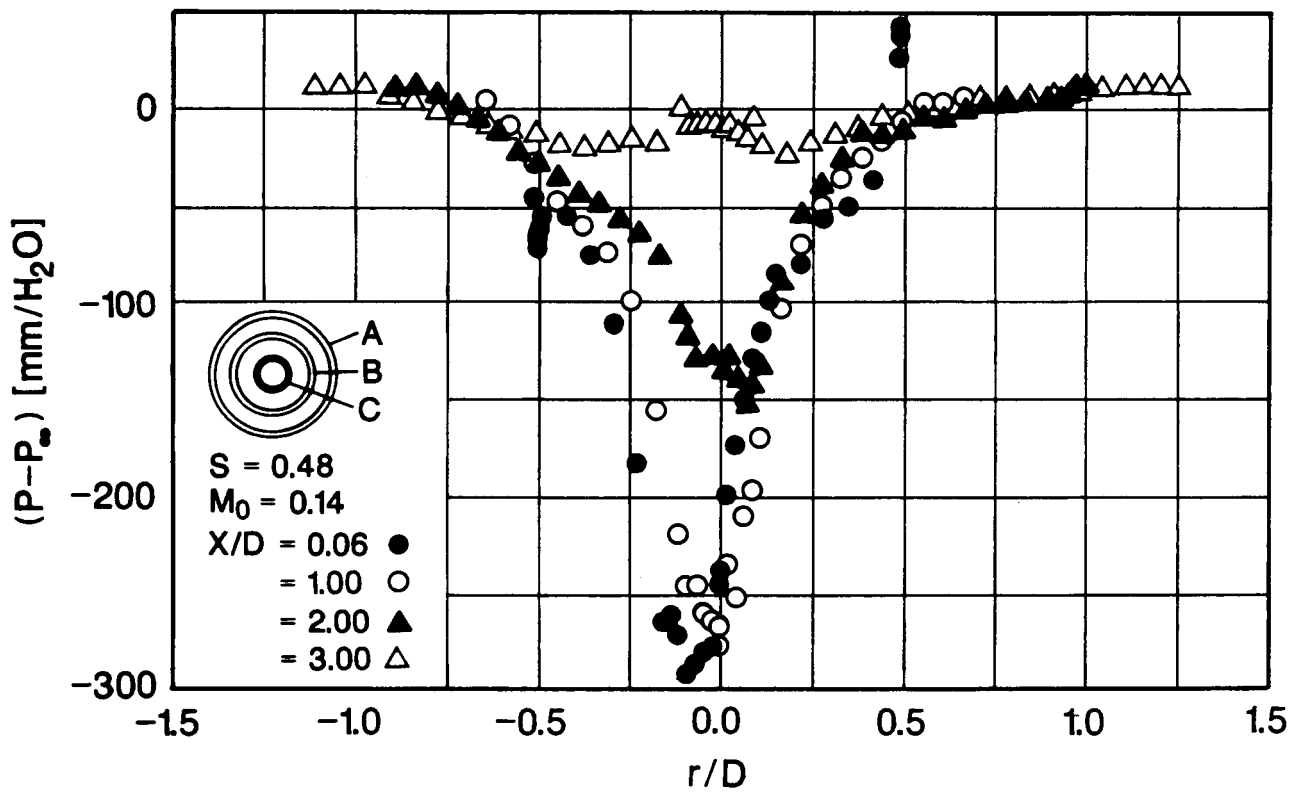


(b) Manifold C

Figure 32: Downstream Development of the Mean Radial Velocity



(a) Manifold A



(b) Manifold C

Figure 33: Downstream Development of the Mean Static Pressure Deficit

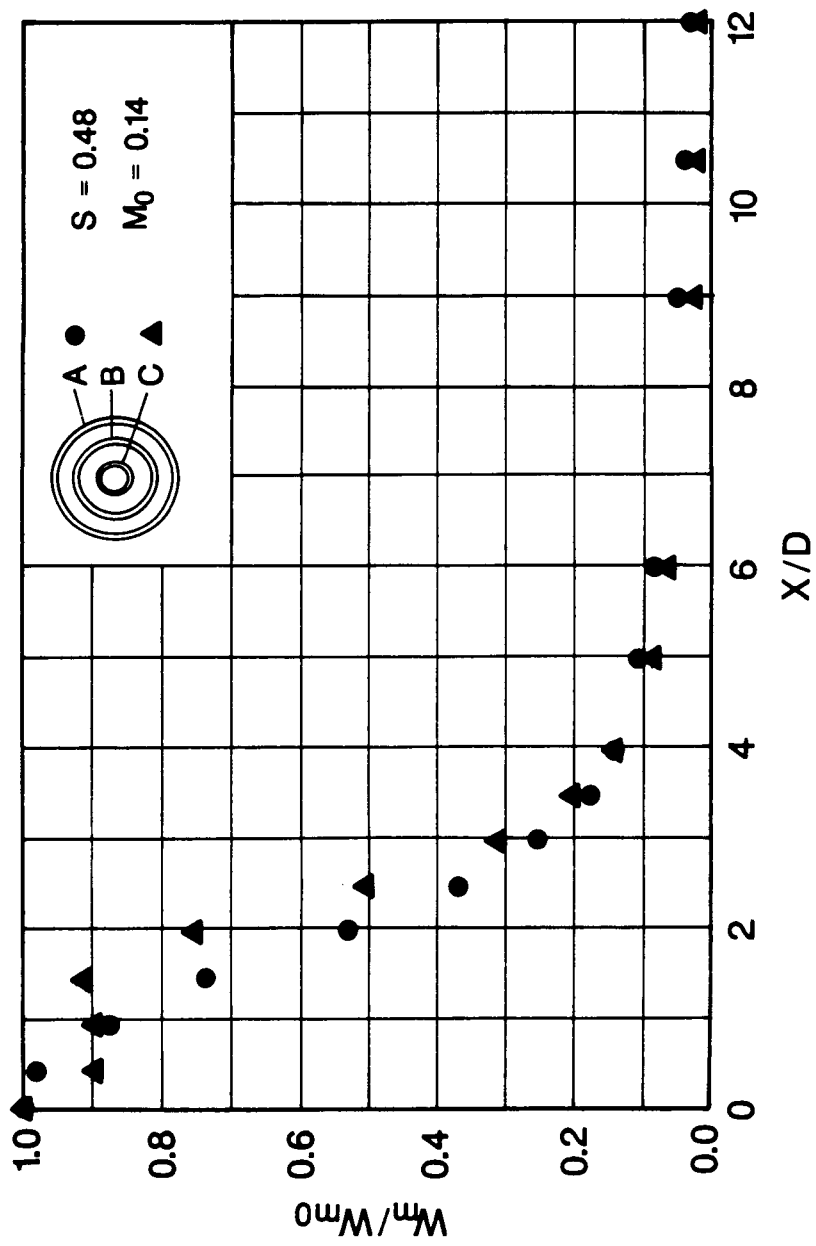


Figure 34: Decay of the Mean Tangential Velocity Maximum with Axial Distance

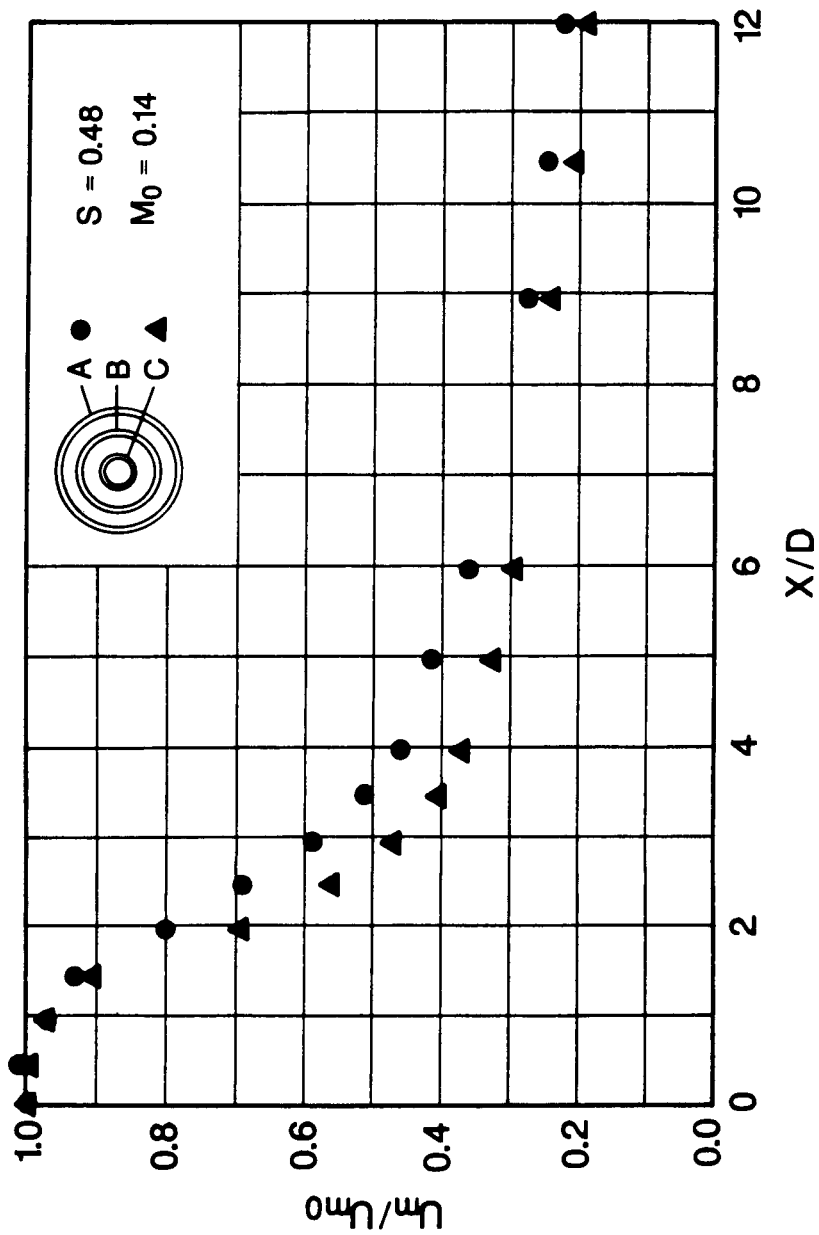


Figure 35: Decay of the Mean Axial Velocity Maximum with Axial Distance

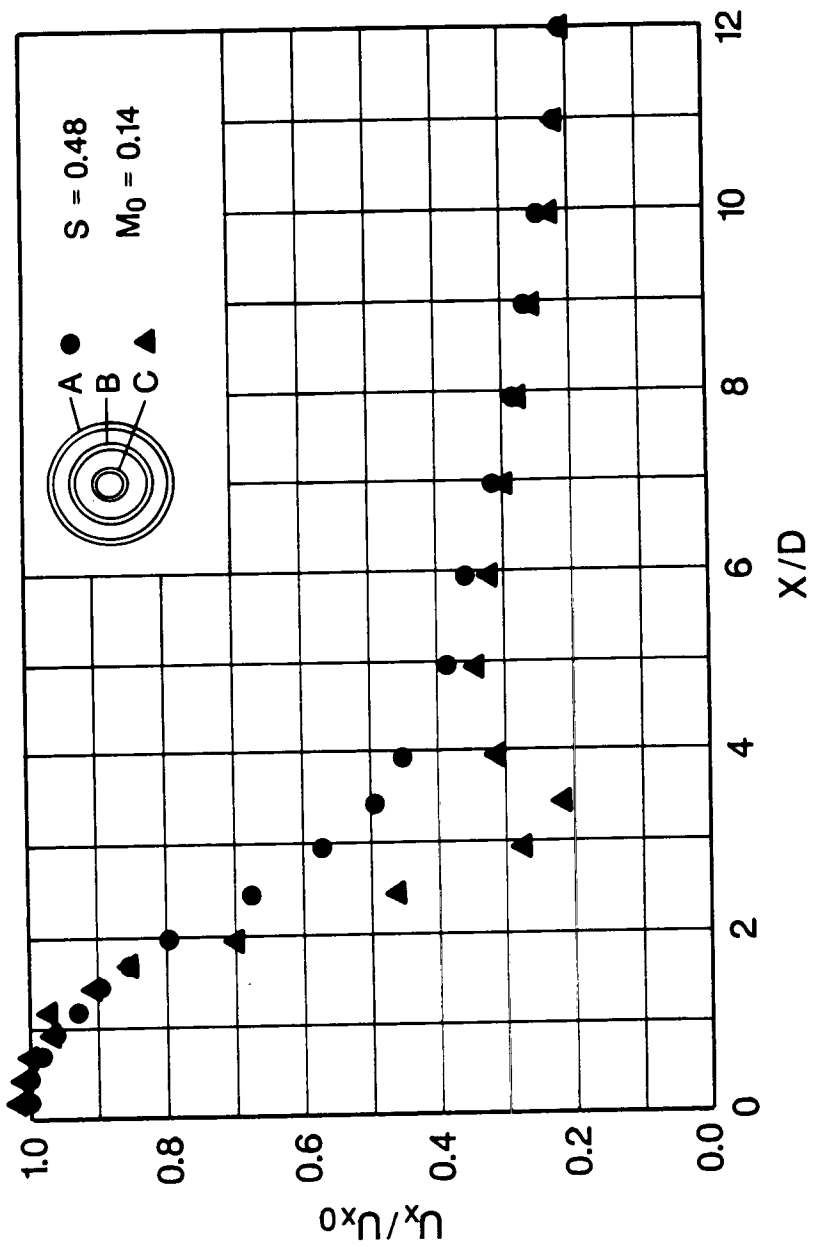


Figure 36: Decay of the Mean Axial Velocity Component Along the Jet Axis

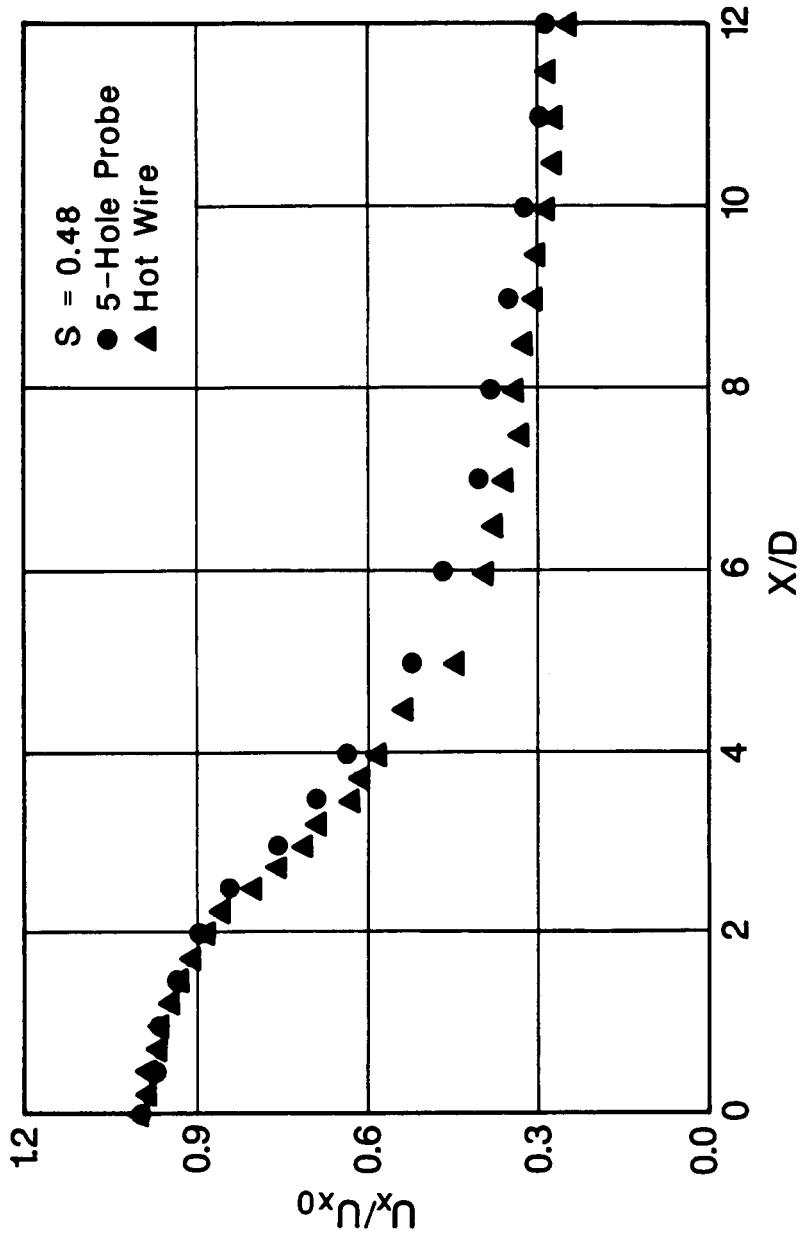


Figure 37: Comparison Between Hot-Wire and 5-Hole Probe Data Along the Jet Axis

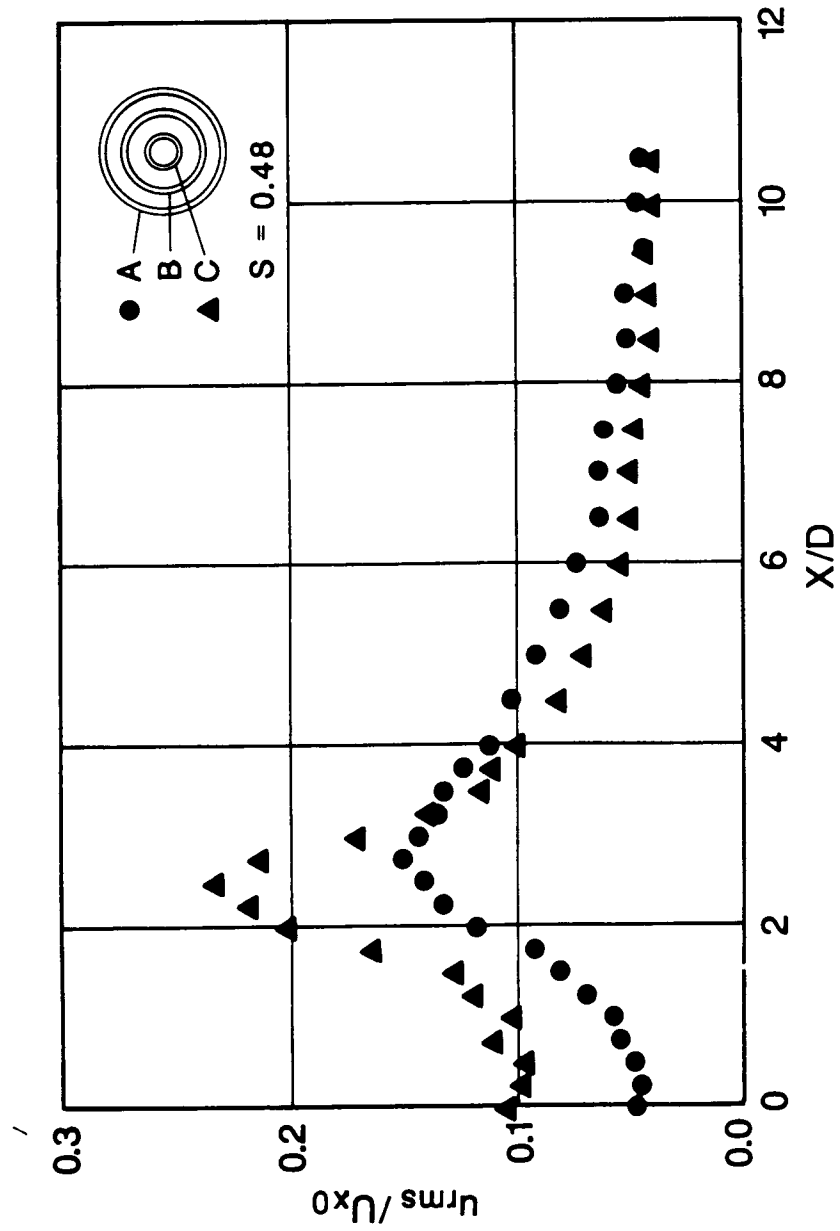


Figure 38: Downstream Development of Axial Turbulence Intensities

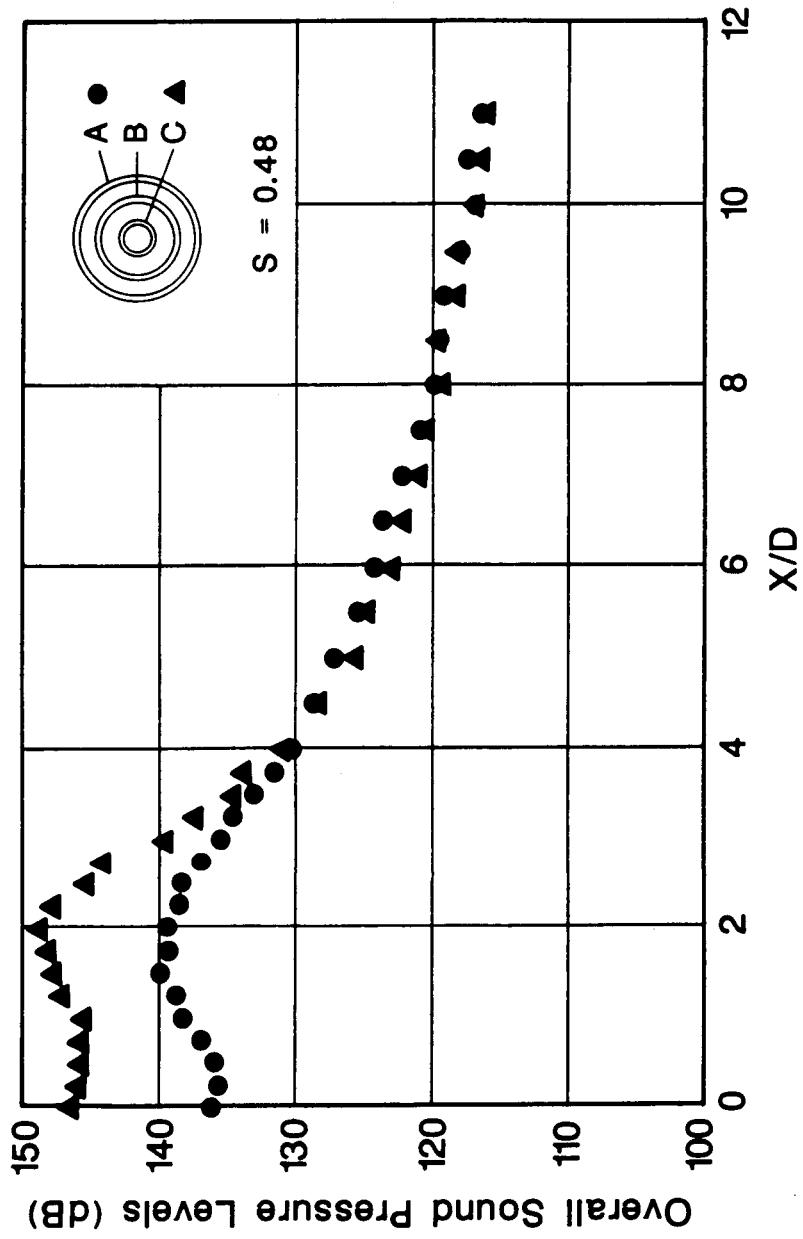


Figure 39: Overall Sound Pressure Levels Along the Jet Axis

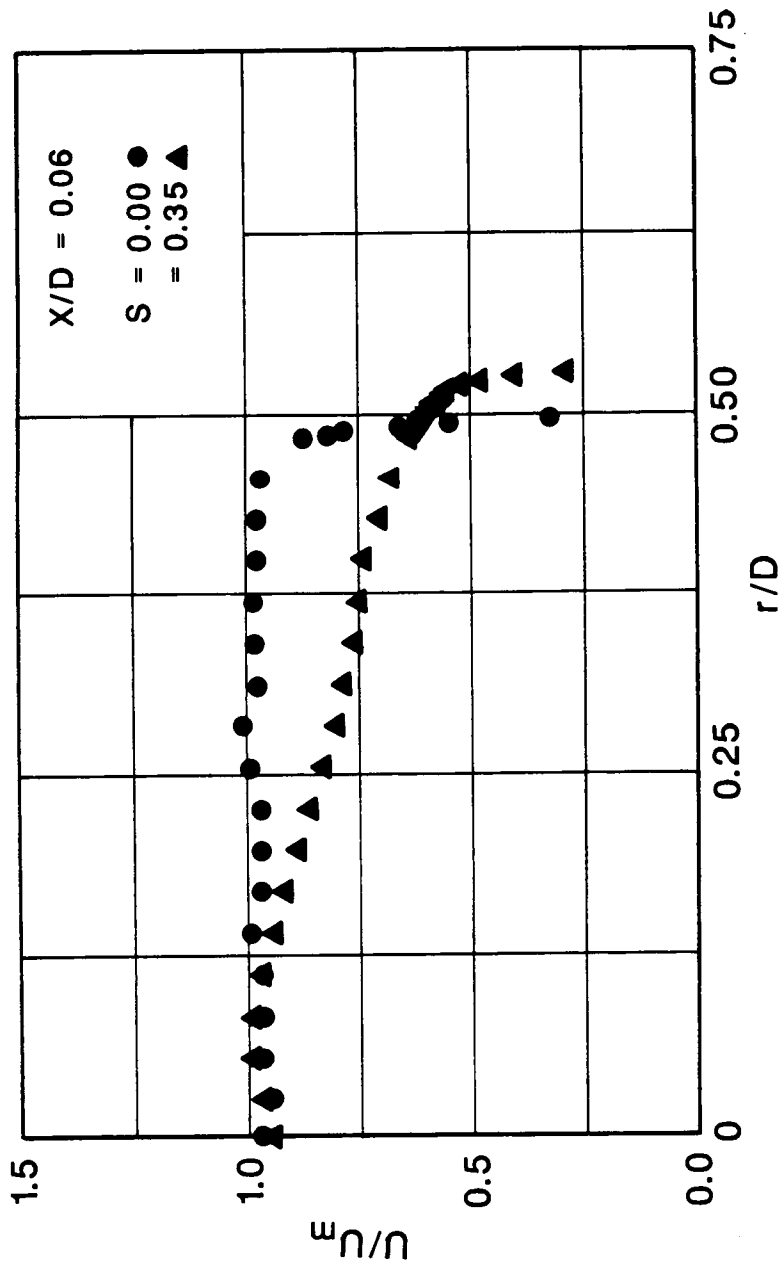


Figure 40: Radial Distributions of Mean Axial Velocities

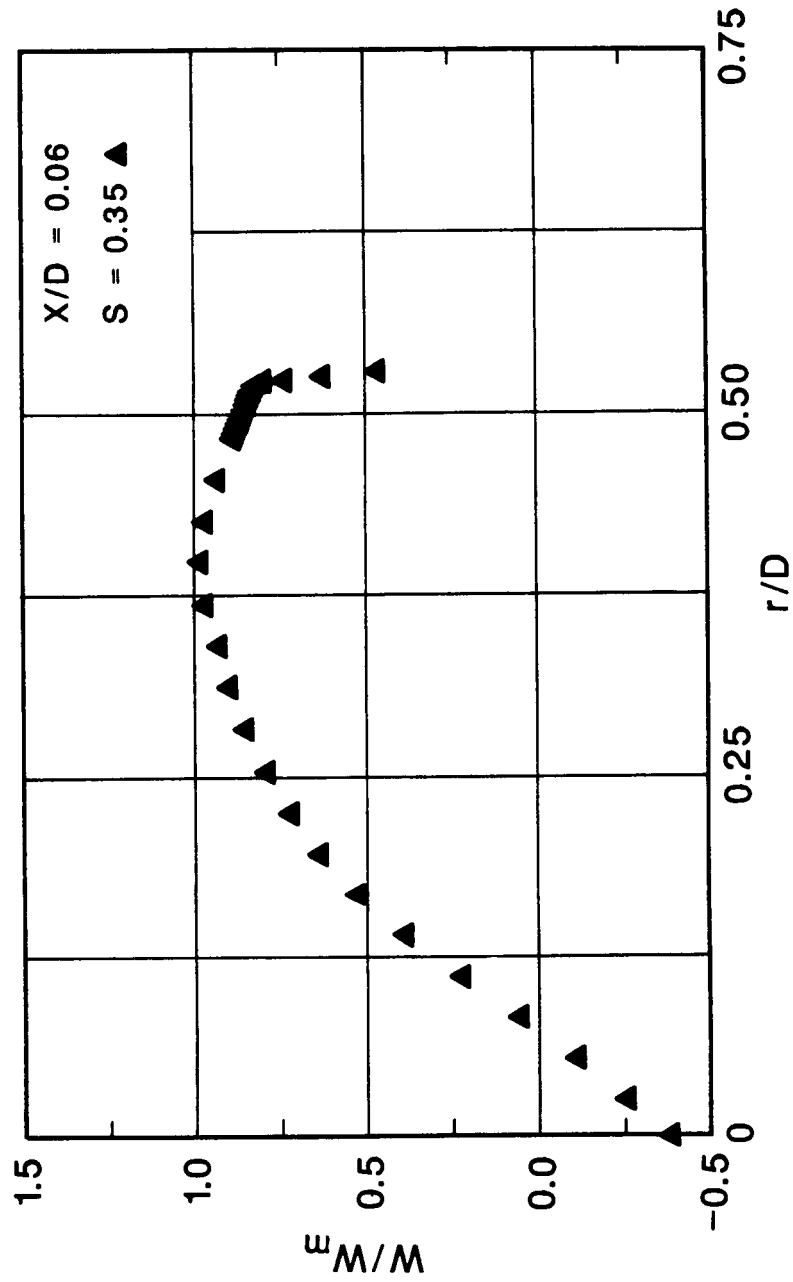


Figure 41: Radial Distribution of Mean Tangential Velocity

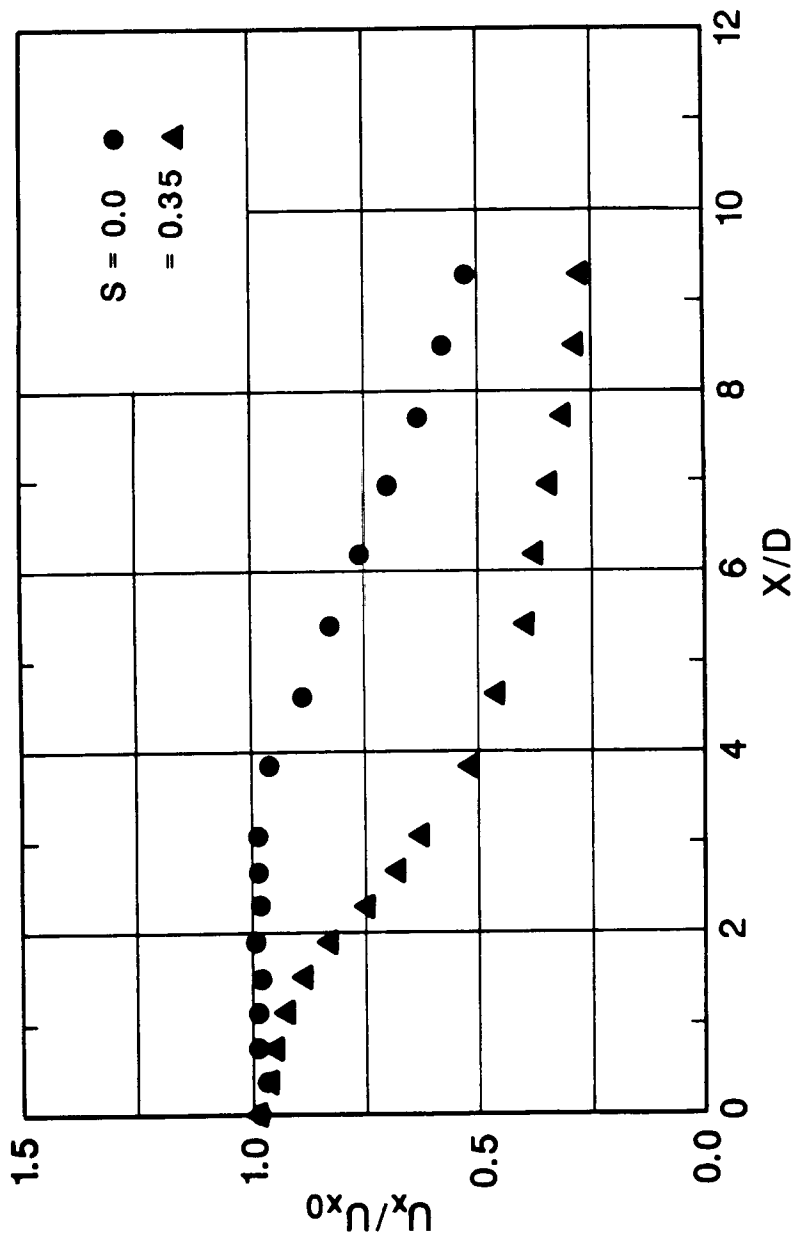


Figure 42: Decay of Mean Axial Velocities Along the Jet Axis

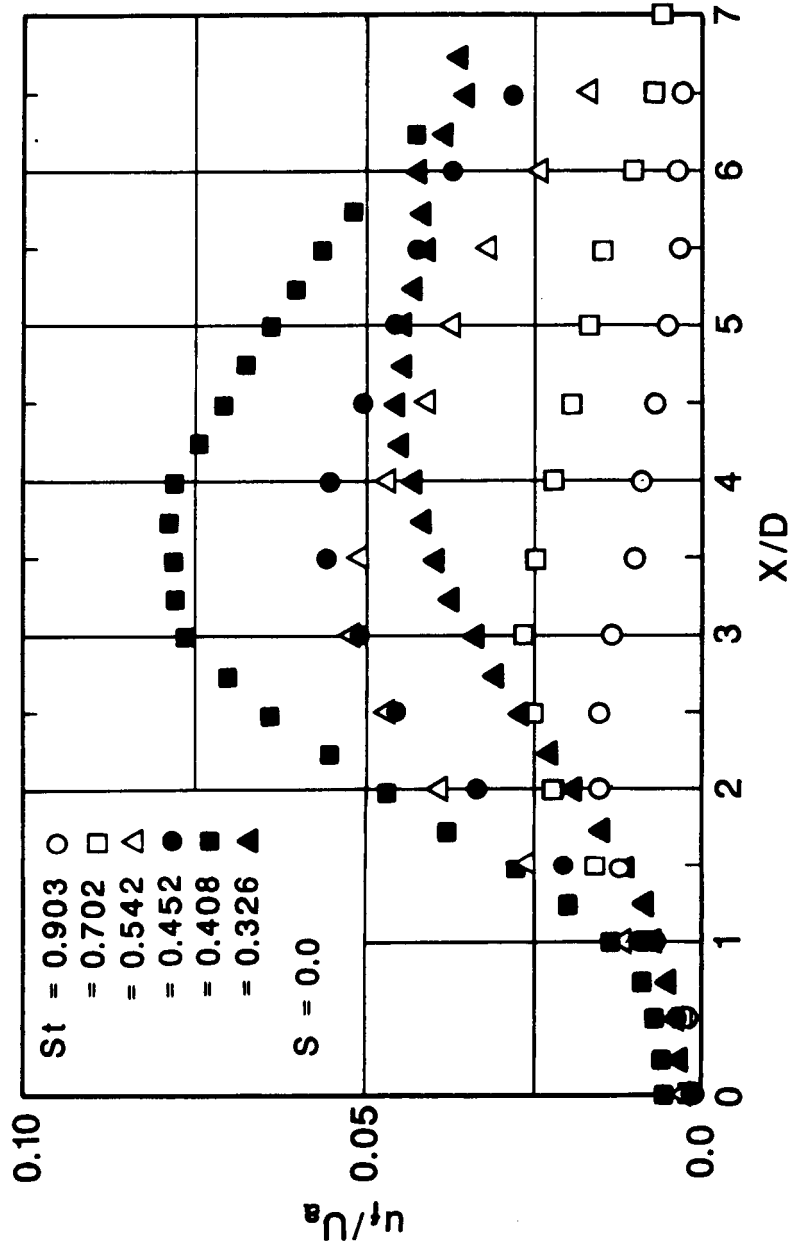


Figure 43: Variation of Fundamental rms Amplitude Along the Jet Axis

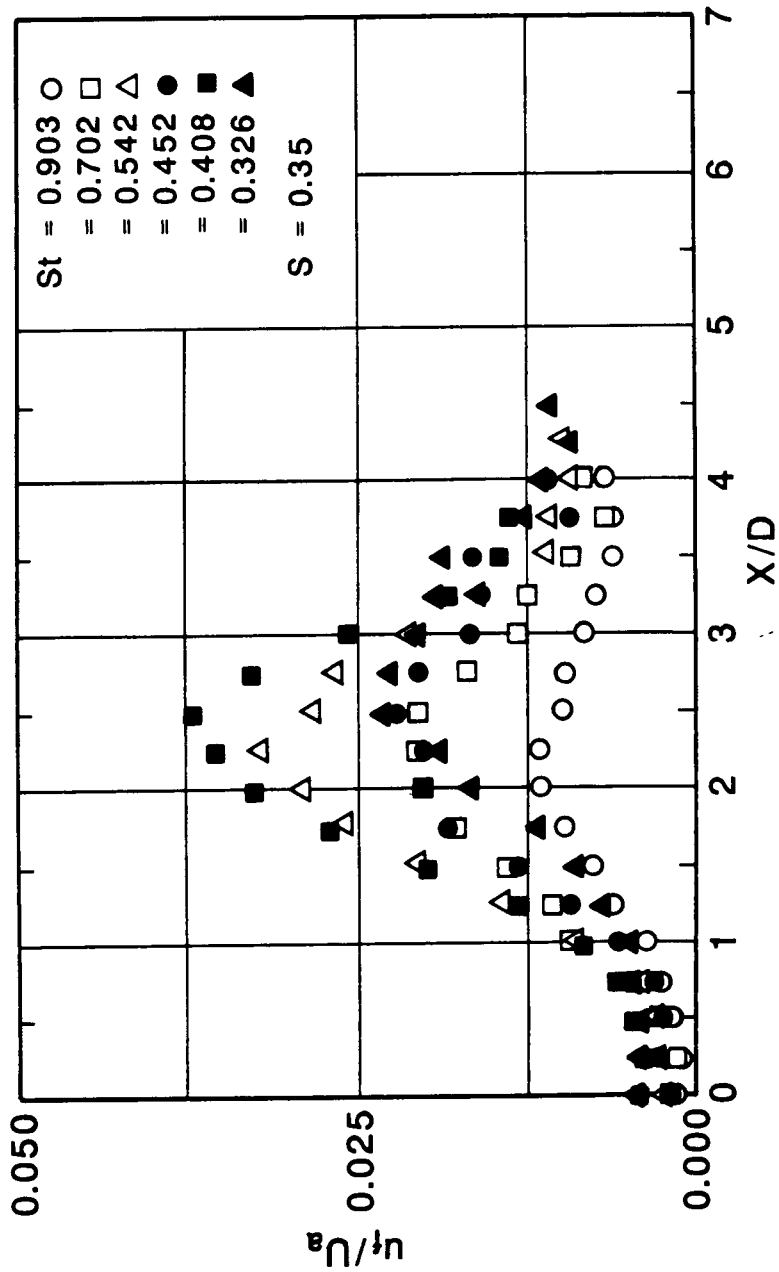


Figure 44: Variation of Fundamental rms Amplitude Along the Jet Axis.

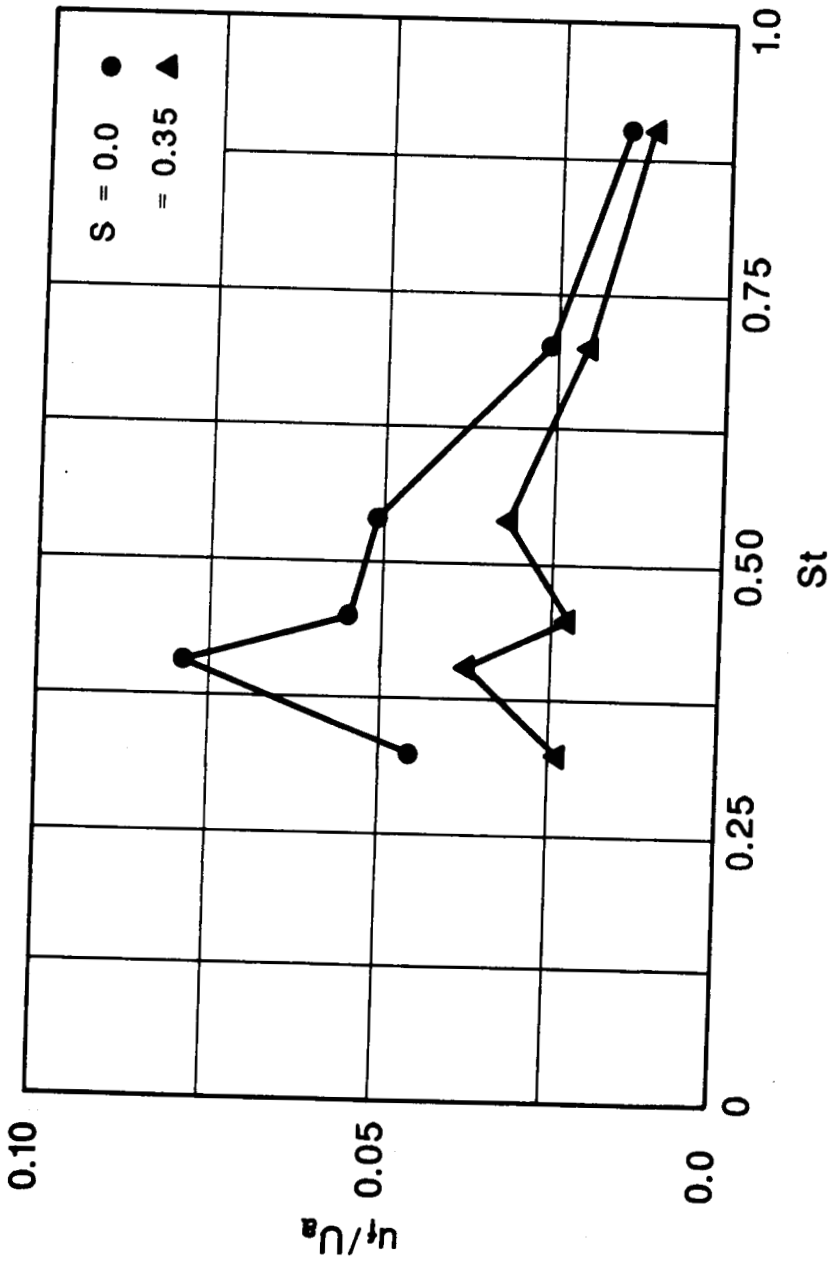


Figure 45: Variation of Peak (rms) Amplitude of the Fundamental with Excitation Strouhal Number

ORIGINAL PAGE IS
OF POOR QUALITY

Table 1: Mean Flow Data at $x/D = .06$; MAN(A)

x/D	P_s	β	δ	U	V	W
	psig	deg.	deg.	fps	fps	fps
0	-1.136	-7.91	-1.39	203	-7.09	3.23
.1	-1.132	-8.99	-1.56	202	-5.52	14.1
.2	-1.137	-6.78	-2.02	203	-7.2	24.2
.3	-1.137	-10	-1.89	201	-6.76	35.5
.4	-1.131	-13	-1.73	198	-6.14	45.8
.5	-1.179	-15.4	-1.4	196	-4.99	54
.6	-1.177	-18.4	-1.06	194	-3.78	64.6
.7	-1.168	-20.8	-1.639	189	-2.26	71.9
1	-1.149	-27.8	1.607	177	2.12	93.4
1.3	-1.127	-24.3	2.03	163	6.97	111
1.6	-1.1	-38.8	3.65	149	12.2	120
1.9	-1.0791	-40	5.28	143	17.2	120
2.2	-1.0301	-34.7	9.71	136	28.3	94.1
2.21	-1.0278	-34.2	10.1	135	28.9	91.6
2.22	-1.0197	-33.7	10.9	132	30.5	87.7
2.23	-1.00995	-33.2	12.2	126	32.7	82.6
2.24	1.000722	-32.6	13.7	119	34.5	76.1
2.25	1.0234	-32.4	18	102	39.5	64.9
2.26	1.0416	-32.2	24.3	84.7	45.2	53.3
2.27	1.0602	-32.5	34.7	62.7	51.5	39.9
2.28	1.0523	-33.8	34.8	35.6	29.8	23.9
2.29	1.0431	-35.8	0	0	0	0

 MASS FLOW RATE = 1.27 lbs/Sec.
 MACH NO. (Based On Average Axial Velocity) = .14
 REYNOLDS NO. = 360337

ORIGINAL PAGE IS
OF POOR QUALITY

Table 2: Mean Flow Data at $x/D = .06$; $MAN(C)$

x/D	P_s	β	δ	U	V	W
	psig	deg.	deg.	fps	fps	fps
0	-.339	-30.2	-9.34	206	-39.2	120
.1	-.282	-32.2	-6.22	196	-25.2	123
.2	-.246	-32.7	-4.43	190	-17.5	122
.3	-.212	-32.6	-2.59	185	-9.92	118
.4	-.182	-31.7	-1.15	180	-4.24	111
.5	-.162	-31.4	-.081	177	-.293	108
.6	-.138	-30.7	1.03	171	3.59	102
.7	-.119	-29.9	1.88	167	6.33	96.1
1	-.111	-28.4	2.98	172	10.2	93.2
1.3	-.078	-27.8	4.74	160	15	84.4
1.6	-.069	-27	5.5	160	17.3	81.6
1.9	-.0482	-24.8	7.36	157	22.3	72.3
2.2	.0408	-16.1	23.4	101	45.5	29.2
2.21	.0615	-15.9	33.3	76.8	52.4	21.9
2.22	.0565	-15.9	33.7	24.3	16.8	6.92
2.23	.0417	-16.6	0	0	0	0

 MASS FLOW RATE = 1.19 Lbs/Sec.
 MACH NO. (Based On Average Axial Velocity) = .14
 REYNOLDS NO. = 356250
 AVERAGE AXIAL VELOCITY = 152 fps

Table 3: Mean Flow Data at $x/D = .5$; MAN(A)

x/D	P_s	β	δ	U	V	W
	psig	deg.	deg.	fps	fps	fps
0	-.192	-1.65	-1.72	206	-6.21	5.94
.1	-.187	-4.69	-1.25	205	-4.48	16.8
.2	-.191	-7.39	-1.52	206	-5.5	26.7
.3	-.186	-10.7	-1.48	202	-5.32	38.1
.4	-.182	-13.1	-1.06	200	-3.81	46.6
.5	-.175	-16.5	-7.51	196	-2.68	58
.75	-.162	-23.2	.332	187	1.18	80
1	-.14	-29.5	1.56	173	5.42	97.8
1.25	-.121	-35.1	2.85	161	9.78	113
1.5	-.0974	-39.1	4.3	149	14.4	121
1.75	-.0709	-39.9	5.97	139	18.9	116
2	-.0346	-37.6	8.68	124	23.9	95.6
2.25	-.00158	-34	11.5	90.9	22.3	61.3
2.5	.00945	-34.3	10.1	46.4	10	31.7
2.75	.0186	-43.1	0	0	0	0

 MASS FLOW RATE = 1.33 Lbs/Sec.
 MACH NO. (Based On Average Axial Velocity) = .071
 REYNOLDS NO. = 188437
 AVERAGE AXIAL VELOCITY = 80.4 fps

ORIGINAL PAGE IS
 OF POOR QUALITY

ORIGINAL PAGE IS
OF POOR QUALITY

Table 4: Mean Flow Data at $x/D = .5$; MAN(C)

x/D	P_s	β	δ	U	V	W
	psig	deg.	deg.	fps	fps	fps
0	-.385	-24.9	-15.3	214	-64.6	99.2
.1	-.338	-28.5	-12.7	206	-52.6	112
.2	-.303	-30.3	-9.66	201	-39.7	118
.3	-.251	-31.7	-6.91	190	-27.1	117
.4	-.225	-31.4	-4.53	190	-17.6	116
.5	-.194	-31	-2.72	186	-10.3	112
.75	-.135	-29.4	1.03	176	3.63	98.9
1	-.0954	-28.4	3.25	164	10.6	88.8
1.25	-.0782	-28.3	4.8	160	15.3	86.2
1.5	-.0645	-28.8	5.95	156	18.6	85.8
1.75	-.049	-28.9	7.32	152	22.2	83.7
2	-.0268	-26	9.68	143	27.1	69.6
2.25	.00827	-21.2	13.9	98.4	26.2	38.2
2.5	.00908	-25.9	7.18	44.3	6.2	21.5
2.75	.0192	-34.8	0	0	0	0

 MASS FLOW RATE = 1.38 LBS/Sec.
 MACH NO. (Based On Average Axial Velocity) = .073
 REYNOLDS NO. = 195234
 AVERAGE AXIAL VELOCITY = 83.3 fps

Table 5: Mean Flow Data at $x/D = 1$; MAN(A)

x/D	P_g	β	δ	U	V	W
	psig	deg.	deg.	fps	fps	fps
0	-.165	-1.82	-2.25	195	-7.64	6.18
.1	-.158	-5.05	-1.49	191	-4.98	16.8
.2	-.162	-7.93	-1.91	192	-6.45	26.7
.3	-.159	-10.9	-1.7	190	-5.76	36.6
.4	-.156	-14.3	-1.39	188	-4.69	47.8
.5	-.151	-17.5	-1.02	184	-3.44	57.9
.75	-.139	-24.3	-.0132	173	-.0438	78.3
1	-.12	-30.5	1.31	161	4.27	94.9
1.25	-.099	-35.1	2.59	147	8.16	104
1.5	-.0768	-37.4	3.98	135	11.8	103
1.75	-.0495	-36.9	5.71	121	15.2	90.9
2	-.0302	-35	7.08	108	16.4	75.8
2.25	-.0137	-32.9	7.77	90.8	14.8	58.7
2.5	.000982	-31.5	9.88	68.7	14	42.1
2.75	.00016	-32.6	10.2	46.6	9.95	29.8
3	.0125	-32.4	7.91	27.2	4.48	17.3
3.25	.0163	-33.5	-9.52	6.21	-1.25	4.11
3.5	.018	-34.1	0	0	0	0

 MASS FLOW RATE = 1.46 LBS/Sec.
 MACH NO.(Based On Average Axial Velocity)= .067
 REYNOLDS NO.= 177656
 AVERAGE AXIAL VELOCITY = 75.8 fps

Table 6: Mean Flow Data at x/D = 1; MAN(C)

x/D	P _s	β	δ	U	V	W
	psig	deg.	deg.	fps	fps	fps
0	-.376	-12.5	-23.3	205	-90.6	45.6
.1	-.332	-20.6	-22.7	188	-84.1	70.7
.2	-.355	-26.2	-16.7	201	-67.3	98.8
.3	-.297	-30.7	-13.3	186	-51.2	110
.4	-.278	-34.2	-9.89	185	-39	126
.5	-.24	-36	-7.11	178	-27.4	129
.75	-.144	-33.6	-1.116	167	-.407	111
1	-.0963	-32.7	3.36	157	10.9	100
1.25	-.0673	-31.9	5.89	149	18.1	92.6
1.5	-.0469	-30.7	8.16	144	24	85.6
1.75	-.0322	-29.7	9.64	138	27	78.8
2	-.0198	-26.5	10.8	131	28	65.3
2.25	-.00543	-23.7	12.1	112	26.3	49.2
2.5	.00753	-22.3	14.4	83.7	23.1	34.3
2.75	.00729	-22.9	11.1	56.4	12	23.8
3	.0107	-27.5	1.79	30.5	1.07	15.9
3.25	.0173	-22	0	0	0	0

MASS FLOW RATE = 1.61 Lbs/Sec.

MACH NO. (Based On Average Axial Velocity) = .073

REYNOLDS NO. = 194297

AVERAGE AXIAL VELOCITY = 82.9 fps

ORIGINAL PAGE IS
OF POOR QUALITY

Table 7: Mean Flow Data at $x/D = 1.5$; MAN(A)

x/D	P_g	β	δ	U	V	W
	psig	deg.	deg.	fps	fps	fps
0	-.138	-1.81	-.208	188	-.683	5.94
.1	-.132	-4.71	.27	185	.876	15.2
.2	-.131	-7.62	-.0437	184	-.142	24.6
.3	-.127	-10.8	.179	181	.575	34.6
.4	-.13	-14	.341	181	1.11	45.2
.5	-.129	-16.6	.536	180	1.76	53.7
.75	-.115	-23.3	1.6	169	5.14	73
1	-.0987	-28.5	2.64	156	8.19	84.8
1.25	-.0757	-32.4	3.79	139	10.9	88.5
1.5	-.0543	-33.5	4.85	124	12.7	82.4
1.75	-.042	-33.2	5.47	115	13.1	74.9
2	-.0304	-32.4	6.3	104	13.6	66
2.25	-.0171	-30.5	7.1	91.9	13.3	54.1
2.5	-.00582	-29.8	8.12	76.4	12.6	43.8
2.75	.00227	-29	9.78	60.7	12	33.6
3	.00583	-29.2	9.36	48.1	9.09	26.9
3.25	.00981	-31	9.51	33.8	6.6	20.3
3.5	.0129	-30.4	7.4	19.8	2.98	11.6
3.75	.0145	-30.5	-40	5.19	-5.06	3.06
3.85	.016	-32.2	0	0	0	0

 MASS FLOW RATE = 1.61 Lbs/Sec.
 MACH NO. (Based On Average Axial Velocity) = .063
 REYNOLDS NO. = 165469
 AVERAGE AXIAL VELOCITY = 70.6 fps

Table 8: Mean Flow Data at $x/D = 1.5$; MAN(C)

x/D	P_g	β	δ	U	V	W
	psig	deg.	deg.	fps	fps	fps
0	-.333	.771	-26.4	191	-94.7	-2.57
.1	-.321	-12.9	-27	184	-96.1	42.2
.2	-.329	-22.9	-23.1	186	-86.2	78.7
.3	-.302	-31.2	-17.6	177	-65.8	107
.4	-.277	-35.3	-14	170	-52	121
.5	-.269	-40.6	-10.7	166	-41.2	142
.75	-.143	-42.1	-5.48	134	-17.3	121
1	-.113	-42.5	-1.55	128	-4.7	117
1.25	-.0724	-38	2.17	123	5.94	96.3
1.5	-.0364	-33.5	6.17	112	14.5	74.1
1.75	-.0381	-30.5	6.37	120	15.5	70.4
2	-.0222	-25.9	9.48	116	21.5	56.3
2.25	-.00772	-24.1	11.6	109	24.4	48.6
2.5	-.00261	-21.2	12.8	102	24.8	39.5
2.75	-.00934	-20.6	9.85	97.1	18	36.5
3	.00416	-20.8	13.6	73	18.9	27.7
3.25	.00536	-22.5	10.2	52.5	10.2	21.8
3.5	.00755	-24.3	5.8	39	4.35	17.6
3.75	.0113	-28.8	.3	23.1	.138	12.7
3.85	.0157	-30.2	-6.87	3.04	-.424	1.77
3.95	.0157	-31.8	0	0	0	0

 MASS FLOW RATE = 1.91 LBS/Sec.
 MACH NO. (Based On Average Axial Velocity) = .07
 REYNOLDS NO. = 186328
 AVERAGE AXIAL VELOCITY = 79.5 fps

Table 9: Mean Flow Data at $x/D = 2$; MAN(A)

x/D	P_s	β	δ	U	V	W
	psig	deg.	deg.	fps	fps	fps
0	-.0917	-2.53	1.3	163	3.69	7.18
.1	-.0986	-5.22	2.02	162	5.75	14.8
.2	-.0873	-7.93	1.52	159	4.25	22.1
.3	-.0878	-10.9	1.88	160	5.34	30.8
.4	-.0852	-14	2.04	157	5.76	39.1
.5	-.0785	-16.2	2.36	151	6.48	43.8
.75	-.0748	-21.6	2.97	146	8.15	57.8
1	-.0624	-25.9	3.92	134	10.2	65
1.25	-.0479	-27.6	4.72	122	11.4	63.7
1.5	-.0361	-28.2	5.36	111	11.8	59.6
1.75	-.0292	-28.5	5.53	103	11.3	55.9
2	-.0175	-28.3	6.43	91.4	11.7	49.2
2.25	-.0128	-27.3	6.24	84.7	10.4	43.7
2.5	-.00607	-27.2	6.97	74.4	10.2	38.2
2.75	-.003313	-25.6	7.81	64.6	9.84	31
3	.0018	-26.7	7.62	57.6	8.62	28.9
3.25	.00589	-26.8	8.53	47.7	8.01	24.1
3.5	.00871	-27.7	6.88	37.9	5.17	19.9
3.75	.0131	-27.7	9.66	24.1	4.64	12.7
4	.015	-30.9	7.89	11.6	1.87	6.91
4.25	.0166	-30.8	0	0	0	0

 MASS FLOW RATE = 1.74 LbS/Sec.
 MACH NO. (Based On Average Axial Velocity) = .048
 REYNOLDS NO. = 127031
 AVERAGE AXIAL VELOCITY = 54.2 fps

Table 10: Mean Flow Data at $x/D = 2$; MAN(C)

x/D	P_g	β	δ	U	V	W
	psig	deg.	deg.	fps	fps	fps
0	-.192	-.172	-31	135	-80.8	.404
.1	-.183	-8.93	-31.3	131	-80.3	20.5
.2	-.199	-21.9	-25.7	137	-71.1	55
.3	-.217	-29.5	-17.4	148	-53.4	83.8
.4	-.204	-34.7	-11.8	148	-37.7	103
.5	-.19	-38.2	-8.09	147	-26.5	115
.75	-.126	-41.1	-2.65	130	-7.98	113
1	-.0771	-40.7	-.355	111	-.908	95.7
1.25	-.0558	-39.6	-.334	99	-.749	81.9
1.5	-.0366	-37.5	.219	86.6	.418	66.4
1.75	-.0165	-34.2	.817	74	1.28	50.3
2	-.0206	-33.7	-.231	78	-.378	52
2.25	-.0145	-28.9	2.36	78.8	3.7	43.5
2.5	-.00495	-24.5	6.89	74.8	9.92	34.1
2.75	-.00568	-23.6	5.92	77.2	8.74	33.7
3	.00161	-19.2	9.93	70.9	13.1	24.7
3.25	.0041	-19.6	10.9	64.8	13.3	23.1
3.5	.00666	-19.2	10.4	56.1	10.8	19.5
3.75	.00734	-18.6	8.07	46.6	6.97	15.7
4	.00956	-18.2	6.58	38.9	4.73	12.8

continues...

Table 10, concluded

x/D	P _s	β	δ	U	V	W
	psig	deg.	deg.	fps	fps	fps
4.1	.00964	-19.7	.605	32.3	.362	11.6
4.2	.0105	-22.8	-1.04	28.5	-.562	12
4.3	.0124	-24	2.92	26.1	1.46	11.6
4.4	.0169	-23.6	26.9	15.1	8.36	6.59
4.5	.0167	-24.5	26.9	11.6	6.5	5.31
4.6	.017	-22	0	0	0	0

 MASS FLOW RATE = 2 Lbs/Sec.
 MACH NO. (Based On Average Axial Velocity) = .052
 REYNOLDS NO. = 139687
 AVERAGE AXIAL VELOCITY = 59.6 fps

Table 11: Mean Flow Data at $x/D = 2.5$; MAN(A)

x/D	P_s	β	δ	U	V	W
	psig	deg.	deg.	fps	fps	fps
0	-.0536	-1.66	2.42	139	5.87	4.02
.1	-.0475	-4.76	4.15	135	9.82	11.2
.2	-.0539	-6.4	2.75	139	6.71	15.6
.3	-.0492	-8.64	3.24	135	7.72	20.5
.4	-.0512	-11	3.37	136	8.16	26.4
.5	-.0501	-13.5	3.47	134	8.35	32.1
.75	-.0437	-17.2	4.36	128	10.2	39.6
1	-.0376	-20.6	4.92	120	11	45.1
1.25	-.0285	-22.4	5.46	110	11.4	45.4
1.5	-.0212	-22.5	6.16	103	12	42.7
1.75	-.0169	-23.3	6.08	95.5	11.1	41.1
2	-.00988	-23.3	6.56	86.8	10.9	37.4
2.25	-.0074	-23.4	6.32	81.4	9.82	35.2
2.5	-.000131	-23.2	8.21	70.3	11	30.1
2.75	-.00114	-22.6	6.64	68.8	8.68	28.6
3	.00359	-23.2	7.97	59.2	9.01	25.4
3.25	.00616	-23.5	7.52	52.1	7.5	22.7
3.5	.00809	-24.6	6.91	45.1	6.01	20.6
3.75	.0126	-25	8.74	33.5	5.68	15.6
4	.0121	-25.3	6.29	31.3	3.82	14.8

continues...

Table 11, concluded

x/D	P _g	β	δ	U	V	W
	psig	deg.	deg.	fps	fps	fps
4.25	.0156	-25.3	10.8	18.2	3.84	8.59
4.5	.0157	-28.8	-3.23	15	-1.967	8.27
4.6	.0163	-28.7	-10.8	12.1	-2.62	6.61
4.7	.0169	-28.5	-32.9	7.3	-5.39	3.97
4.8	.017	-28.3	0	0	0	0

 MASS FLOW RATE = 1.88 Lbs/Sec.
 MACH NO. (Based On Average Axial Velocity) = .046
 REYNOLDS NO. = 123047
 AVERAGE AXIAL VELOCITY = 52.5 fps

Table 12: Mean Flow Data at $x/D = 2.5$; MAN(C)

x/D	P_g	β	δ	U	V	W
	psig	deg.	deg.	fps	fps	fps
0	-.0579	-.0504	-38.9	72.5	-58.5	.0638
.1	-.0572	-9.94	-36.3	71.3	-53.2	12.5
.2	-.0722	-17.8	-28	86.7	-48.4	27.8
.3	-.0775	-25	-19.8	94.7	-37.6	44.2
.4	-.08	-28.1	-12.1	103	-25.1	55
.5	-.0747	-31.4	-8.31	105	-17.9	63.9
.75	-.0658	-33.3	-1.15	114	-2.73	74.9
1	-.0432	-32.8	2.1	104	4.55	67.1
1.25	-.0277	-31.2	3.29	94.5	6.35	57.2
1.5	-.0221	-31	2.35	86.5	4.13	52
1.75	-.0138	-30.3	1.89	75.8	2.9	44.3
2	-.0103	-29.9	1.49	69.6	2.08	40
2.25	-.00497	-28	1.39	63.3	1.74	33.7
2.5	-.00361	-27.1	.637	61.2	.765	31.3
2.75	-4.91E-5	-24.5	.802	58.4	.899	26.6
3	.00397	-22.2	2.87	54.4	2.95	22.2
3.25	.00352	-21.6	3.27	56	3.45	22.2
3.5	.0073	-19.2	5.89	51	5.58	17.8
3.75	.0126	-18.4	9.21	40	6.83	13.3

continues...

Table 12, concluded

x/D	P _g	β	δ	U	V	W
	psig	deg.	deg.	fps	fps	fps
4	.0137	-17	9.62	36.1	6.39	11
4.25	.0134	-17.9	8.39	35.4	5.49	11.4
4.5	.0151	-19.8	7.48	26.8	3.74	9.64
4.6	.0143	-20.2	-2.14	24.2	-1.096	8.89
4.7	.0161	-16.7	4.2	20.8	1.59	6.23
4.8	.0161	-17.8	8.48	21.8	3.41	6.99
4.9	.0184	-17.3	8.86	5.52	.902	1.72
5	.0181	-17	26.9	9.2	4.88	2.81
5.1	.0189	-14.5	0	0	0	0

 MASS FLOW RATE = 1.9 LbS/Sec.
 MACH NO. (Based On Average Axial Velocity) = .041
 REYNOLDS NO. = 110391
 AVERAGE AXIAL VELOCITY = 47.1 fps

Table 13: Mean Flow Data at $x/D = 3$; MAN(A)

x/D	P_s	β	δ	U	V	W
	psig	deg.	deg.	fps	fps	fps
0	-.032	-2.07	3.15	120	6.59	4.33
.1	-.0263	-3.89	5.38	117	11	7.95
.2	-.0313	-5.76	3.51	119	7.34	12
.3	-.0318	-7.07	3.6	119	7.52	14.7
.4	-.0287	-8.61	4.16	117	8.62	17.7
.5	-.0284	-10.1	4.15	116	8.52	20.6
.8	-.0244	-13.9	4.63	111	9.22	27.4
1.1	-.0171	-16.5	5.48	102	10.2	30.2
1.4	-.0151	-18	5.41	97.5	9.7	31.7
1.7	-.00979	-18.4	5.99	90.5	10	30.1
2	-.00531	-19.4	6.51	82.6	9.99	29.1
2.3	-.00292	-18.9	6.77	77.1	9.67	26.4
2.6	-.00143	-19.7	6.48	71.8	8.67	25.7
2.9	.00209	-20.4	6.79	64.1	8.14	23.8
3.2	.00464	-19.8	6.64	57.1	7.07	20.6
3.5	.0088	-21.5	8.08	47.4	7.22	18.7
3.8	.0102	-23	7.88	41.7	6.27	17.7
4.1	.0127	-23.5	8.52	33.2	5.42	14.4
4.4	.0154	-23.5	10.2	22.1	4.33	9.6
4.7	.015	-25.4	3.47	21.4	1.44	10.2

continues...

Table 13, concluded

x/D	P _g	β	δ	U	V	W
	psig	deg.	deg.	fps	fps	fps
5	.0163	-25.7	.593	14.6	.168	7.02
5.2	.0172	-25.7	-32	7.1	-4.93	3.42
5.4	.0174	-27.1	0	0	0	0

 MASS FLOW RATE = 2.06 LbS/Sec.
 MACH NO. (Based On Average Axial Velocity) = .04
 REYNOLDS NO. = 106641
 AVERAGE AXIAL VELOCITY = 45.5 fps

ORIGINAL PAGE IS
OF POOR QUALITY

Table 14: Mean Flow Data at $x/D = 3$; MAN(C)

x/D	P_s	β	δ	U	V	W
	psig	deg.	deg.	fps	fps	fps
0	-.0132	-.455	-40	41.4	-34.7	1.329
.1	-.0103	-8.95	-40	42	-35.7	6.62
.2	-.0158	-13.2	-31.4	51.7	-32.4	12.1
.3	-.0183	-18.8	-24.2	55.6	-26.4	18.9
.4	-.0057	-22.1	-16.7	49.5	-16	20.1
.5	-.025	-23.4	-11.2	73.9	-16	32
.8	-.0322	-26.4	-4.475	94.8	-1.877	47.1
1.1	-.0232	-25.5	2.12	93.7	3.85	44.7
1.4	-.0162	-24.3	3.57	89.1	6.09	40.2
1.7	-.011	-24.1	3.83	81.7	5.99	36.5
2	-.00485	-23.6	4.87	71.8	6.68	31.4
2.3	-.00247	-23	3.76	65.1	4.65	27.6
2.6	.00223	-22.8	2.23	55.4	2.34	23.3
2.9	.00368	-22.2	1.96	52	1.92	21.2
3.2	.00978	-21.5	4.6	40.6	3.51	16
3.5	.00939	-20.7	.58	40.9	.443	15.5
3.8	.0113	-19.7	3.95	36.6	2.69	13.1
4.1	.0116	-20	3.58	36.2	2.41	13.2
4.4	.0145	-17.2	2.95	27.1	1.46	8.38
4.7	.0158	-19.1	6.7	22.1	2.75	7.67

continues...

Table 14, concluded

x/D	P _g	β	δ	U	V	W
	psig	deg.	deg.	fps	fps	fps
5	.0174	-15.4	9.59	12.9	2.26	3.55
5.2	.0179	-16.4	.701	7.03	.0897	2.07
5.4	.0173	-13.6	-5.93	13	-1.39	3.15
5.6	.018	-13.9	-33.6	6.29	-4.31	1.56
5.8	.0187	-14.6	0	0	0	0

 MASS FLOW RATE = 1.86 LBS/Sec.
 MACH NO. (Based On Average Axial Velocity) = .031
 REYNOLDS NO. = 83671.9
 AVERAGE AXIAL VELOCITY = 35.7 fps

ORIGINAL PAGE IS
OF POOR QUALITY

Table 15: Mean Flow Data at $x/D = 3.5$; MAN(A)

x/D	P_g	β	δ	U	V	W
	psig	deg.	deg.	fps	fps	fps
0	-.0187	-1.7	4.02	104	7.32	3.09
.1	-.0133	-2.86	6.06	101	10.7	5.04
.2	-.0175	-4.05	4.15	104	7.53	7.33
.3	-.0143	-5.66	4.76	100	8.37	9.92
.4	-.0139	-6.39	4.8	99	8.36	11.1
.5	-.0155	-7.62	4.96	101	8.8	13.4
.8	-.0123	-9.96	5.09	95.9	8.66	16.8
1.1	-.0108	-12.4	5.2	92.5	8.63	20.3
1.4	-.00583	-13.3	5.95	86	9.21	20.3
1.7	-.00452	-14.4	6.74	82.8	10.1	21.3
2	.000845	-15.2	7.74	73.6	10.4	20
2.3	-.00237	-15.1	6.14	74.9	8.33	20.2
2.6	.00329	-15.9	8.02	65.1	9.54	18.5
2.9	.00403	-16.9	7.82	61.5	8.83	18.7
3.2	.00411	-18	6.72	58.2	7.21	18.9
3.5	.00648	-18.5	6.54	51.8	6.26	17.3
3.8	.00976	-19.2	7.95	43.3	6.41	15.1
4.1	.0111	-20.7	7.99	37.9	5.69	14.3
4.4	.0113	-21	6.72	35.1	4.43	13.5
4.7	.0139	-20.9	8.08	26.7	4.05	10.2

continues...

Table 15, concluded

x/D	P _s	β	δ	U	V	W
	psig	deg.	deg.	fps	fps	fps
5	.0136	-24.7	4.21	25.3	2.05	11.6
5.3	.0154	-23	-5.22	15.6	-1.55	6.64
5.6	.0169	-23.7	0	0	0	0

MASS FLOW RATE = 2.21 Lbs/Sec.

MACH NO. (Based On Average Axial Velocity) = .04

REYNOLDS NO. = 105234

AVERAGE AXIAL VELOCITY = 44.9 fps

Table 16: Mean Flow Data at $x/D = 3.5$; MAN(C)

x/D	P_g	β	δ	U	V	W
	psig	deg.	deg.	fps	fps	fps
0	-.00207	-1.38	-20.7	45.2	-17.1	1.09
.1	.0166	-5.39	0	0	0	0
.2	.0221	-8.54	0	0	0	0
.3	-.00173	-10.9	-11.5	52.6	-10.9	10.1
.4	-.0108	-13.8	-8.32	65	-9.79	16
.5	-.0111	-15.6	-6.19	67.4	-7.58	18.8
.8	-.0158	-18.9	-1.54	79.9	-2.27	27.4
1.1	-.0134	-19.2	1.43	82.6	2.19	28.8
1.4	-.0102	-18.6	2.76	81.7	4.16	27.5
1.7	-.00623	-18.3	3.91	76.8	5.52	25.4
2	-.00376	-18.1	4.29	72.3	5.7	23.6
2.3	.000735	-17.6	5.45	63.6	6.37	20.2
2.6	.00181	-18.3	4.83	59.1	5.04	19.5
2.9	.00537	-18.9	3.36	49.6	3.07	17
3.2	.00883	-20.2	3.64	40.4	2.74	14.9
3.5	.0103	-19.3	2.81	35.4	1.84	12.4
3.8	.0115	-18.4	.391	31.2	.225	10.4
4.1	.0131	-21.1	-3.23	25.8	-1.56	9.95
4.4	.0159	-18.7	-8.71	13.9	-2.24	4.69
4.7	.017	-17	-11.5	6.75	-1.44	2.06

continues...

Table 16, concluded

x/D	P _s	β	δ	U	V	W
	psig	deg.	deg.	fps	fps	fps
5	.0177	-17.1	0	0	0	0
5.3	.0171	-13.9	0	0	0	0
5.6	.0168	-12.2	0	0	0	0
5.8	.0181	-9.27	0	0	0	0
6	.018	-9.57	0	0	0	0
6.2	.0183	19.1	0	0	0	0
6.4	.0182	11.3	0	0	0	0
6.6	.0185	63.4	0	0	0	0

 MASS FLOW RATE = 1.51 Lbs/Sec.
 MACH NO. (Based On Average Axial Velocity) = .019
 REYNOLDS NO. = 51562.5
 AVERAGE AXIAL VELOCITY = 22 fps

Table 17: Mean Flow Data at $x/D = 4$; MAN(A)

x/D	P_g	β	δ	U	V	W
	psig	deg.	deg.	fps	fps	fps
0	-.0112	-1.4	4.22	94.7	6.98	2.31
.1	-.00561	-2.36	7.14	91.4	11.5	3.77
.2	-.00993	-3.34	4.65	94.1	7.66	5.49
.3	-.0102	-4.85	4.54	94	7.5	7.98
.4	-.0109	-4.79	4.16	94.4	6.9	7.91
.5	-.0114	-6.16	4.57	95.1	7.64	10.3
.8	-.00784	-8.27	4.88	89.9	7.75	13.1
1.1	-.00617	-9.32	5.29	86.6	8.12	14.2
1.4	-.00457	-10.3	5.34	82.7	7.86	15
1.7	-.00267	-12.1	5.97	78.6	8.4	16.9
2	.000181	-12.8	6.45	72.4	8.39	16.4
2.3	.00146	-13.4	6.35	68.2	7.8	16.2
2.6	.00321	-14.1	6.74	63.7	7.76	16
2.9	.00443	-14.9	6.43	59.6	6.96	15.9
3.2	.0054	-15.6	6.83	56.3	7	15.7
3.5	.00749	-16.1	6.74	50.5	6.21	14.6
3.8	.0085	-17.2	6.48	46.5	5.52	14.4
4.1	.00976	-17.5	6.53	41.8	5.01	13.2
4.4	.0117	-19.9	6.39	35.3	4.21	12.8
4.7	.0132	-21.4	8.44	29.9	4.77	11.7

continues...

Table 17, concluded

x/D	P_s	β	δ	U	V	W
	psig	deg.	deg.	fps	fps	fps
5	.0128	-22.8	4.7	28.8	2.57	12.1
5.3	.0142	-23.8	4.14	23	1.82	10.1
5.5	.0157	-24.4	6.76	15.2	1.98	6.9
5.7	.0159	-23.6	8.27	14.6	2.32	6.39
5.9	.0159	-21.5	-3.03	14.1	-1.806	5.57
6.1	.0168	-26.8	-10.8	6.35	-1.36	3.21
6.3	.0171	-24.7	0	0	0	0

MASS FLOW RATE = 2.42 Lbs/Sec.

MACH NO. (Based On Average Axial Velocity) = .034

REYNOLDS NO. = 90468.8

AVERAGE AXIAL VELOCITY = 38.6 fps

Table 18: Mean Flow Data at $x/D = 4$; MAN(C)

x/D	P_s	β	δ	U	V	W
	psig	deg.	deg.	fps	fps	fps
0	-.00288	-1.44	-4.88	59.6	-5.09	1.5
.1	-.00125	-3.69	-1.34	60.9	-1.43	3.93
.2	-.00535	-6.79	-4.09	66	-4.76	7.86
.3	-.00374	-7.73	-3.88	64.3	-4.4	8.73
.4	-.00643	-9.58	-2.92	69.6	-3.6	11.7
.5	-.00627	-10.7	-2.08	70.3	-2.6	13.3
.8	-.00706	-13.6	.162	74.2	.216	18
1.1	-.00659	-14.4	1.52	76.1	2.08	19.5
1.4	-.00524	-15	2.91	75.9	3.99	20.3
1.7	-.00213	-14.5	3.67	71.6	4.74	18.5
2	.00166	-15.3	4.95	64.5	5.79	17.6
2.3	.000451	-15.2	3.84	64.2	4.47	17.4
2.6	.00304	-14.7	4.53	59.2	4.85	15.5
2.9	.00428	-16.6	3.76	54.2	3.72	16.1
3.2	.00816	-17	4.87	44.8	3.99	13.7
3.5	.00971	-18.5	5.15	39	3.7	13
3.8	.0106	-19.4	1.29	34.5	.826	12.2
4.1	.0113	-20.2	-.409	31.5	-.239	11.6
4.4	.0141	-19.2	-1.12	22.1	-.457	7.68
4.7	.0148	-19.4	-6.6	17.9	-2.2	6.32

continues...

Table 18, concluded

x/D	P _g	β	δ	U	V	W
	psig	deg.	deg.	fps	fps	fps
5	.0161	-20.2	-21.5	8.63	-3.62	3.18
5.3	.0166	-22.9	0	0	0	0

MASS FLOW RATE = 1.67 Lbs/Sec.

MACH NO. (Based On Average Axial Velocity) = .033

REYNOLDS NO. = 88359.4

AVERAGE AXIAL VELOCITY = 37.7 fps

Table 19: Mean Flow Data at $x/D = 5$; MAN(A)

x/D	P_g	β	δ	U	V	W
	psig	deg.	deg.	fps	fps	fps
0	-.00468	-2.26	4.77	84.4	7.05	3.33
.1	.00286	-2.41	9.84	78.3	13.6	3.29
.2	-.0035	-3.42	5.17	83.2	7.54	4.97
.3	-.00361	-3.42	4.97	83.2	7.26	4.97
.4	-.00228	-4.12	5.6	81.5	8.01	5.87
.5	-.00281	-4.2	5.48	82.1	7.89	6.03
.8	-.00311	-5.58	5.26	81.7	7.56	7.98
1.1	-.00131	-6.27	5.73	78.3	7.9	8.6
1.4	-.000561	-7.03	5.67	75.7	7.57	9.34
1.7	-.000382	-7.9	5.59	74.5	7.35	10.3
2	.000769	-9.52	6.32	71.3	8	12
2.3	.0027	-10.2	6.16	66.2	7.25	11.9
2.6	.00352	-10	6.19	63.6	7	11.2
2.9	.00353	-12.3	5.68	61.2	6.23	13.3
3.2	.00377	-12.9	5.39	59.6	5.77	13.6
3.5	.00754	-14	7.84	52	7.38	13
3.8	.00751	-13.5	7.13	50.5	6.49	12.1
4.1	.0101	-14.7	7.24	42.8	5.62	11.2
4.4	.0109	-17.4	8.09	39.3	5.86	12.3
4.7	.0124	-19	9.27	34.1	5.88	11.7

continues...

Table 19, concluded

x/D	P _g	β	δ	U	V	W
	psig	deg.	deg.	fps	fps	fps
5	.0126	-19.8	8.19	31.1	4.75	11.2
5.3	.0131	-20	7.06	28	3.7	10.2
5.6	.0147	-21.6	10.4	21.9	4.3	8.67
5.9	.0149	-19.8	8.26	19.3	2.98	6.96
6	.014	-23.5	5.12	22.2	2.17	9.64
6.1	.015	-24.9	6.17	17.4	2.07	8.08
6.2	.0152	-26.2	6.21	15.7	1.9	7.72
6.3	.0152	-27.9	1.83	14.6	.529	7.75
6.4	.0152	-26.5	1.83	14.8	.529	7.39
6.5	.0145	-23.1	2.91	19.1	1.05	8.14
6.6	.0155	-21.6	5.76	13.2	1.43	5.24
6.7	.0158	-26	3.1	10.7	.644	5.22
6.8	.0158	-29.1	7.01	11.2	1.58	6.24
6.9	.0155	-28	2.58	11.8	.603	6.28
7	.0157	-26.3	-5.17	10.9	-1.11	5.41
7.1	.0162	-24.5	7.26	6.7	.938	3.05
7.2	.0164	-30.2	-40	3.05	-2.96	1.78
7.3	.0166	-29.9	0	0	0	0

 MASS FLOW RATE = 2.79 Lbs/Sec.
 MACH NO.(Based On Average Axial Velocity)= .03
 REYNOLDS NO.= 79687.5
 AVERAGE AXIAL VELOCITY = 34 fps

Table 20: Mean Flow Data at $x/D = 5$; MAN(C)

x/D	P_s	β	δ	U	V	W
	psig	deg.	deg.	fps	fps	fps
0	.00578	-2.04	8.18	62.7	9.01	2.23
.1	.00583	-3.36	8.26	62	9.03	3.64
.2	-.000449	-3.65	3.04	69.9	3.72	4.46
.3	.000641	-5.14	3.5	68	4.17	6.11
.4	-.000496	-5.45	2.89	69.4	3.52	6.63
.5	-.00129	-5.99	3.13	70.9	3.9	7.44
.8	.000713	-7.8	3.97	68.1	4.78	9.33
1.1	.000123	-8.89	3.9	68.8	4.75	10.8
1.4	.00148	-9.74	4.83	66.7	5.71	11.4
1.7	.000727	-10.8	4.22	67.2	5.05	12.8
2	.00328	-10.7	5.07	62.6	5.65	11.8
2.3	.00434	-10.6	5.52	60.3	5.94	11.3
2.6	.00492	-12.1	5.45	57.3	5.59	12.3
2.9	.00702	-12.7	6.8	52.4	6.4	11.8
3.2	.00549	-12.9	4.48	53.1	4.26	12.2
3.5	.00931	-13.8	7.01	44.6	5.65	11
3.8	.00965	-14.8	5.45	41	4.04	10.8
4.1	.00984	-15.8	3.92	38.6	2.74	10.9
4.4	.0125	-14.3	5.16	30.3	2.82	7.73
4.7	.0123	-19.4	1.85	28.6	.983	10.1

continues...

Table 20, concluded

x/D	P _s	β	δ	U	V	W
	psig	deg.	deg.	fps	fps	fps
5	.0144	-19.5	.533	20	.197	7.07
5.1	.0139	-21.2	.507	21.7	.206	8.44
5.2	.0146	-20.6	2.35	18.3	.803	6.88
5.3	.0147	-22.3	-.357	16.8	-.113	6.91
5.4	.0148	-21.2	-.379	16.8	-.119	6.5
5.5	.0159	-24.4	.681	8.18	.107	3.71
5.6	.0146	-23	-2.28	16.2	-.701	6.89
5.7	.0148	-25.6	-3.33	15.5	-.998	7.41
5.8	.0159	-20	-8.19	7.67	-1.18	2.79
5.9	.0158	-25	-22.3	8.66	-3.92	4.04
6	.0158	-24.8	-11.1	9.24	-1.99	4.27
6.1	.016	-25.2	-31.7	4.33	-2.96	2.04
6.2	.0161	-24.4	0	0	0	0

MASS FLOW RATE = 2.02 Lbs/Sec.
MACH NO. (Based On Average Axial Velocity) = .03
REYNOLDS NO. = 79921.9
AVERAGE AXIAL VELOCITY = 34.1 fps

Table 21: Mean Flow Data along the Jet Axis; MAN(C)

x/D	P _g	β	δ	U	V	W
	psig	deg.	deg.	fps	fps	fps
0	-.193	-1.39	-2.38	208	-8.64	5.05
.25	-.197	-.991	-2.3	209	-8.4	3.62
.5	-.196	-1.38	-2.45	209	-8.98	5.04
.75	-.184	-1.29	-1.96	205	-7.03	4.61
1	-.17	-1.1	-1.39	201	-4.86	3.85
1.3	-.152	-1.45	-.902	194	-3.05	4.91
1.5	-.135	-1.56	-.419	187	-1.37	5.1
1.8	-.117	-1.81	.15	178	.467	5.63
2	-.0956	-2.09	.687	166	1.99	6.05
2.5	-.0605	-2.06	1.56	141	3.85	5.07
3	-.0358	-2.27	2.4	120	5.02	4.74
3.5	-.0183	-2.14	3.75	103	6.72	3.83
4	-.0124	-1.54	3.84	94.7	6.36	2.54
5	-.00314	-1.6	5.18	81	7.34	2.26
6	-.000915	-1.59	4.66	75	6.12	2.08
7	.00356	-1.39	5.92	65.9	6.84	1.6
8	.00618	-.224	6.43	59.4	6.7	.232
9	.00733	-.424	5.95	55.2	5.75	.408
10	.00883	.9	6.52	50.9	5.82	-.799
11	.0103	.879	6.73	46.7	5.51	-.716
12	.0112	1.83	7.1	43.5	5.42	-1.39

Table 22: Mean Flow Data along the Jet Axis; MAN(C)

x/D	P _s	β	δ	U	V	W
	psig	deg.	deg.	fps	fps	fps
0	-.327	-27.1	-11.1	206	-45.4	105
.25	-.352	-26.6	-13.7	210	-57.3	105
.5	-.355	-23.7	-16.9	209	-69.1	91.6
.75	-.357	-19.1	-19.5	207	-77.4	71.7
1	-.34	-13.5	-23.1	200	-87.8	48
1.3	-.357	-6.80	-25	191	-94.5	23.4
1.5	-.324	-2.66	-27.0	188	-97.4	8.75
1.8	-.291	.0226	-27.9	177	-93.4	-1.101
2	-.213	-.0867	-30.9	145	-86.9	.22
2.5	-.0925	-1.77	-32.8	96.5	-62.3	2.98
3	-.0275	-2.69	-34	58.4	-39.4	2.74
3.5	-.00305	-1.1	-17.6	46.3	-14.7	.89
4	-.00747	-.86	-4.88	66	-5.64	.991
5	-.00297	-1.59	2.99	72.2	9.77	.744
6	.00128	-1.725	5.1	67.6	6.03	.855
7	.00426	-.0699	6.42	62.6	7.04	.0763
8	.00601	-1.52	6.76	57.8	6.84	.524
9	.00715	1.09	6.51	53.7	6.13	-1.02
10	.009	2.07	6.87	48.2	5.82	-1.74
11	.00955	1.08	7.07	46.2	5.73	-1.871
12	.0103	1.24	7.13	43.4	5.43	-1.939

Table 23: Hot-Wire Data along the Jet Axis; MAN(A)

x/D	U/U_0	U_{rms}/U_0
0	1	.0491
.25	1.04	.0468
.5	1.02	.05
.75	.998	.0562
1	.967	.0594
1.25	.94	.0704
1.5	.893	.0828
1.75	.843	.0935
2	.781	.12
2.25	.726	.134
2.5	.675	.143
2.75	.613	.152
3	.578	.145
3.25	.528	.137
3.5	.505	.134
3.75	.475	.125
4	.41	.113
4.5	.361	.104
5	.326	.0926
5.5	.337	.0824
6	.29	.0746
6.5	.289	.0648
7	.277	.0648
7.5	.26	.0627
8	.256	.0561
8.5	.247	.0521
9	.232	.0536
9.5	.23	.046
10	.22	.0477
10.5	.214	.0467

Table 24: Hot-Wire Data along the Jet Axis; MAN(C)

x/D	U/U_0	U_{rms}/U_0
0	1	.101
.25	1.02	.0941
.5	1.01	.0964
.75	.988	.0921
1	.995	.0908
1.25	.954	.117
1.5	.938	.146
1.75	.95	.169
2	.889	.203
2.25	.814	.248
2.5	.652	.241
2.75	.416	.194
3	.257	.175
3.25	.24	.123
3.5	.249	.117
3.75	.249	.107
4	.246	.0932
4.5	.241	.0799
5	.243	.0675
5.5	.231	.0636
6	.243	.0525
6.5	.221	.0528
7	.222	.0475
7.5	.209	.0478
8	.203	.0431
8.5	.199	.0393
9	.187	.0379
9.5	.188	.0366
10	.186	.0377
10.5	.178	.0377

Table 25: Overall Sound Pressure Levels along the Jet Axis

x/D	MAN(A)	MAN(C)
	OASPL(dB)	OASPL(dB)
0	136.3	146.5
.25	135.8	146.1
.5	136.1	145.9
.75	137.1	145.9
1	138.5	145.8
1.25	139	147.2
1.5	140.1	147.9
1.75	139.5	148.3
2	139.5	148.9
2.25	138.7	147.9
2.5	138.6	145.5
2.75	137.1	144.2
3	135.7	139.7
3.25	134.8	137.5
3.5	133.3	134.7
3.75	131.8	133.9
4	130.6	131
4.5	128.9	128.5
5	127.5	125.9
5.5	125.7	125
6	124.5	123.3
6.5	123.9	122.4
7	122.5	121.3
7.5	121.1	120.7
8	120	119.6
8.5	119.7	119.7
9	119.3	118.4
9.5	118.2	118.3
10	117	117
10.5	117.6	116.7
11	116.6	116.2

APPENDIX A:
FIVE-HOLE PROBE CALIBRATION PROCEDURE

* * * * *

FIGURES INCLUDED IN APPENDIX A

<u>Number</u>	<u>Title</u>	<u>Page</u>
A1	Five-Hole Probe Calibration Curve.....	A.4
A2	Five-Hole Probe Calibration Curve.....	A.5
A3	Five-Hole Probe Calibration Curve.....	A.6

TABLES INCLUDED IN APPENDIX A

	<u>Title</u>	<u>Page</u>
A1	Five-Hole Probe Calibration (M = 0.06).....	A.7
A2	Five-Hole Probe Calibration (M = 0.08).....	A.8
A3	Five-Hole Probe Calibration (M = 0.11).....	A.9
A4	Five-Hole Probe Calibration (M = 0.14).....	A.10
A5	Five-Hole Probe Calibration (M = 0.19).....	A.11
A6	Five-Hole Probe Calibration (M = 0.21).....	A.12
A7	Five-Hole Probe Calibration (M = 0.23).....	A.13
A8	Five-Hole Probe Calibration (M = 0.28).....	A.14
A9	Five-Hole Probe Calibration (M = 0.3).....	A.15
A10	Five-Hole Probe Calibration (M = 0.34).....	A.16
A11	Five-Hole Probe Calibration (M = 0.4).....	A.17

APPENDIX A:

FIVE-HOLE PROBE CALIBRATION PROCEDURE

The calibration of the probe is done in a free jet facility where the flow direction can be measured within 0.5 degrees. The first step to calibrate the probe was to set the probe tip in the horizontal plane so that the yaw was aerodynamically nulled. This condition was maintained by frequently checking the zero reading for $(P_2 - P_4)$ during the whole calibration procedure. The next step consisted of reading the output from the Digi Quartz transducers which have an output frequency as a function of the applied pressure. These measurements were made at five-degree increments in δ over the range $-30^\circ < \delta < +25^\circ$. These pressures were then used to calculate the following nondimensional coefficients for each pitch angle (δ) setting:

1) Normalized pitch pressure difference, $NPPD = \frac{P_3 - P_1}{HIP}$.

2) Normalized static pressure difference,

$$NSPD = \frac{1/4(P_1 + P_2 + P_3 + P_4) - P_s}{HIP}$$

3) Normalized total pressure difference, $NTPD = \frac{P_5 - P_t}{HIP}$

In the above coefficients, half impact pressure, $HIP = P_5 - \frac{1}{4}(P_1 + P_2 + P_3 + P_4)$ and P_5 , are the five-hole probe pressures. The above measurements were made at a range of Mach numbers ranging from 0.06 up to 0.4, and the results are tabulated in Tables A1 through A11 and plotted in Figures A1 through A3. These tables are

directly used in the computer program. An interpolation and iteration scheme is applied between the tables and within each table to increase the accuracy and include the compressibility effects. Total Mach number, pitch angle, and static and total pressures are calculated from this procedure at each measuring point. With yaw angle and temperatures known, the three components of velocity vector are then calculated.

The calibration of the five-hole probe is based on the assumption that the calibration coefficients are independent of Reynolds number based on the probe tip diameter.

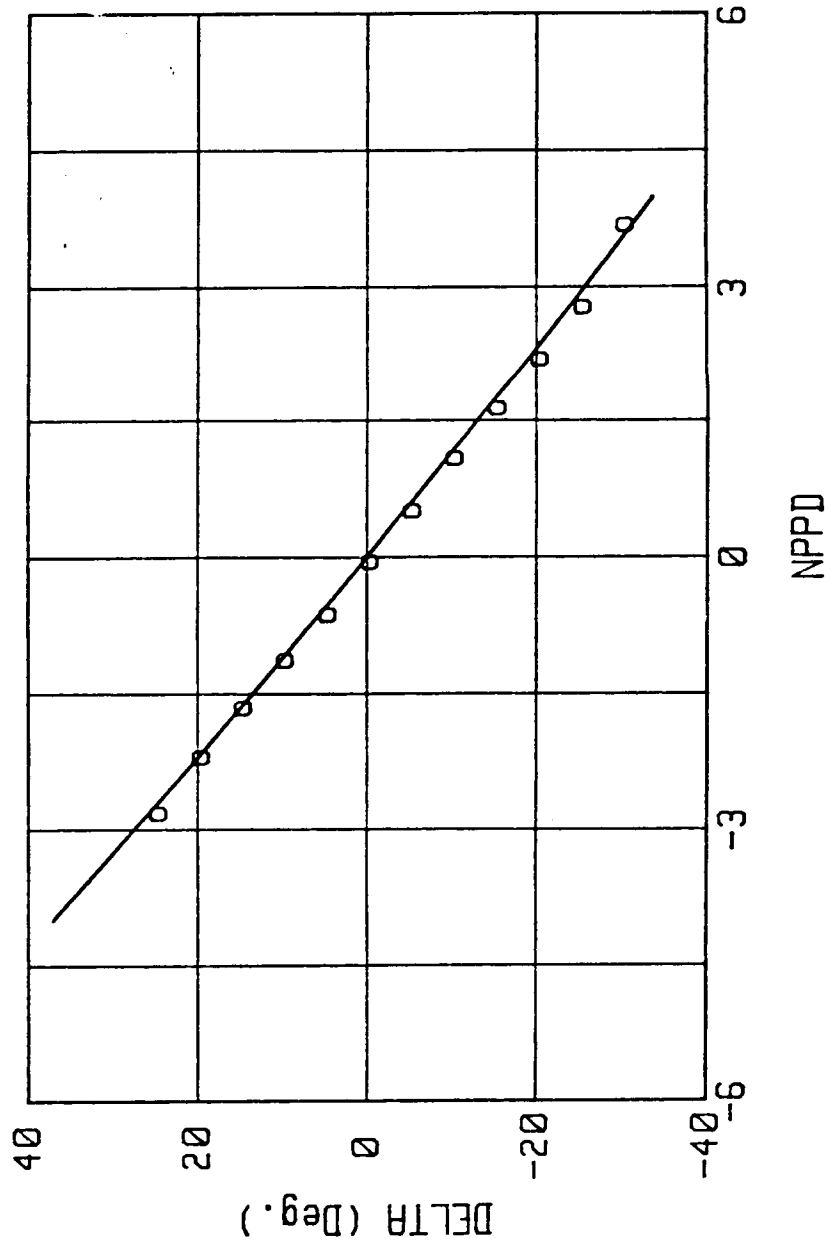


Figure A1: Five-Hole Probe Calibration Curve

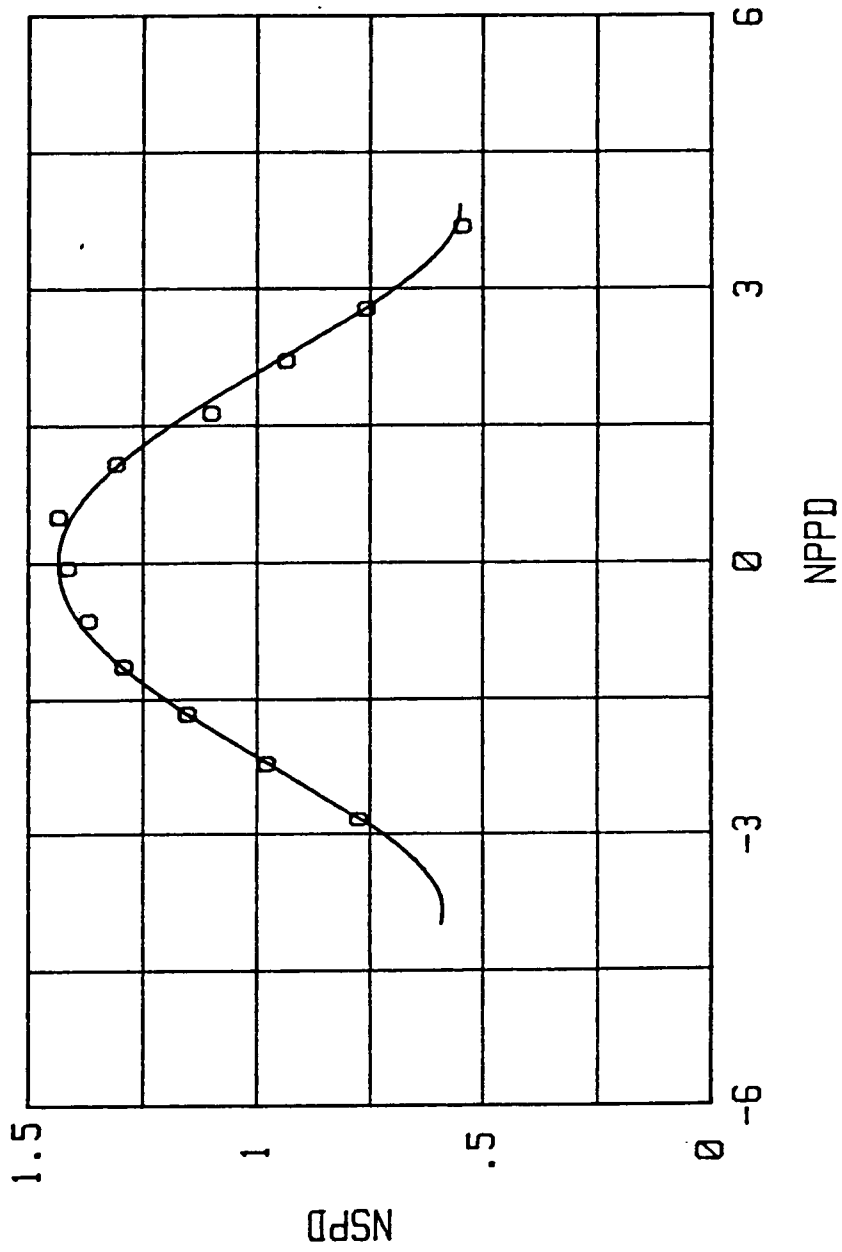


Figure A2: Five-Hole Probe Calibration Curve ($M = 0.08$)

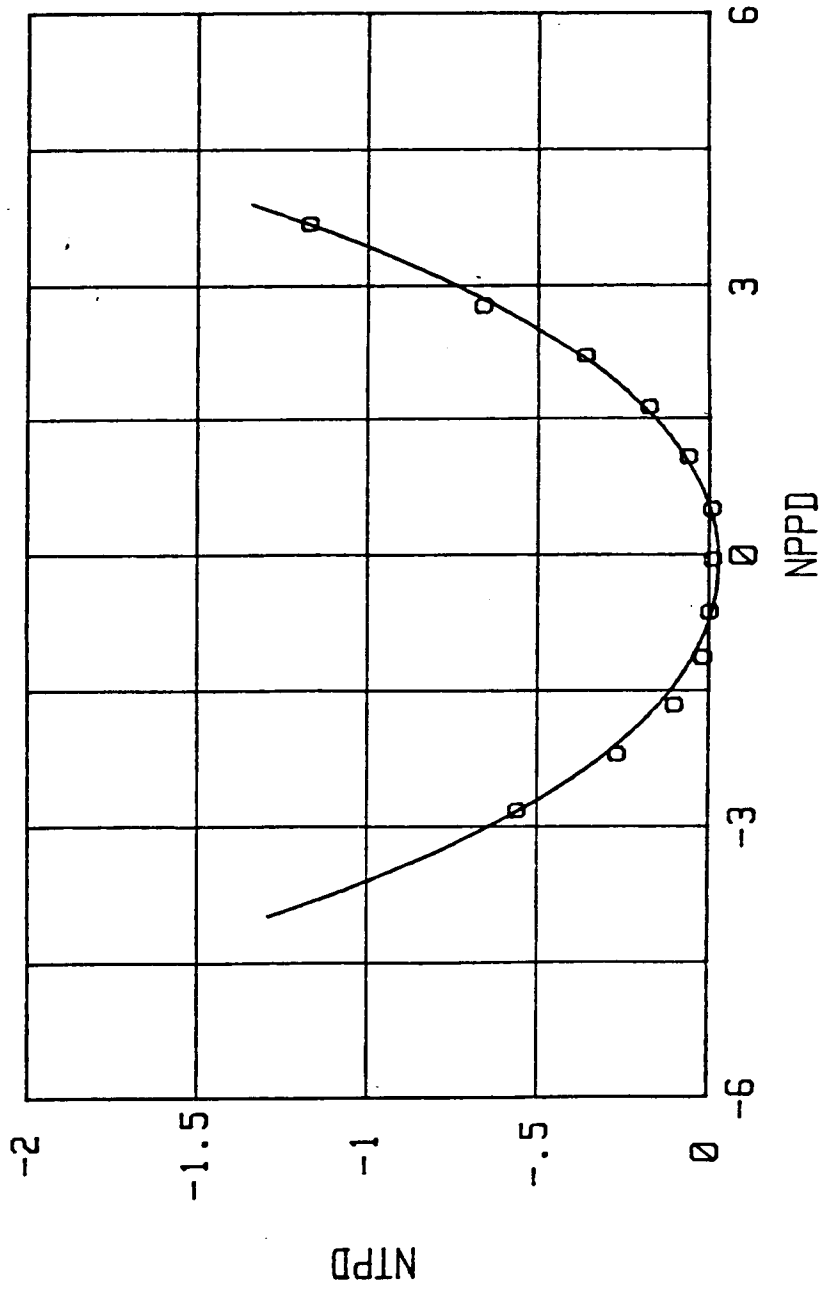


Figure A3: Five-Hole Probe Calibration Curve ($M = 0.08$)

Table A1: Five-Hole Probe Calibration

M = .06

δ (deg)	HIP	NSPD	NPPD	NTPD
-30	.0243	.4763	3.5546	-1.1505
-25	.0251	.7371	2.9283	-.6932
-20	.0263	.9486	2.2417	-.3654
-15	.0253	1.1761	1.7527	-.2255
-10	.0259	1.2934	1.0772	-.0502
-5	.0248	1.4420	.5530	-.0040
0	.0242	1.5057	-.0041	-.0041
5	.0243	1.4954	-.5591	0.000
10	.0256	1.3516	-1.0703	-.0234
15	.0156	1.9646	-2.7910	.1479
20	.0225	.8999	-1.8598	-.3426
25	.0248	.7782	-2.6694	-.5766

Table A2: Five-Hole Probe Calibration

M = .08

δ (deg)	HIP	NSPD	NPPD	NTPD
-30	.0310	.5516	3.7032	-1.1774
-25	.0333	.7654	2.7970	-.6677
-20	.0355	.9422	2.2241	-.3693
-15	.0372	1.1063	1.6490	-.1856
-10	.0351	1.3146	1.0961	-.0712
-5	.0344	1.4407	.5178	-.0029
0	.0348	1.4201	-.0345	-.0000
5	.0353	1.3751	-.6143	-.0085
10	.0362	1.2983	-1.1160	-.0276
15	.0371	1.1578	-1.6399	-.1106
20	.0373	.9853	-2.1835	-.2760
25	.0358	.7806	-2.8092	-.5674

Table A3: Five-Hole Probe Calibration

M = .11

δ (deg)	HIP	NSPD	NPPD	NTPD
-30	.0566	.4741	3.6111	-1.1542
-25	.0616	.7263	2.8226	-.6837
-20	.0649	.9121	2.1881	-.3763
-15	.0661	1.0764	1.6272	-.1739
-10	.0634	1.2751	1.0926	-.0678
-5	.0617	1.3987	.4878	-.0097
0	.0607	1.4422	-.1021	.0016
5	.0612	1.4157	-.6011	-.0049
10	.0632	1.3205	-1.1144	-.0269
15	.0667	1.1260	-1.6594	-.0975
20	.0667	.9505	-2.1529	-.2729
25	.0632	.7799	-2.8409	-.5732

Table A4: Five-Hole Probe Calibration

M = .14

δ (deg)	HIP	NSPD	NPPD	NTPD
-30	.0831	.4580	3.6848	-1.1898
-25	.0923	.7129	2.8028	-.6685
-20	.0988	.8841	2.2069	-.3481
-15	.0960	1.1069	1.6461	-.1775
-10	.0929	1.2809	1.0581	-.0495
-5	.0914	1.3934	.5089	-.0109
0	.0907	1.4159	-.0342	-.0022
5	.0913	1.3987	-.6309	-.0033
10	.0950	1.2812	-1.0879	-.0305
15	.0980	1.1367	-1.6429	-.1031
20	.1006	.9180	-2.1964	-.2675
25	.0911	.8034	-2.9039	-.6063

Table A5: Five-Hole Probe Calibration

M = .19

δ (deg)	HIP	NSPD	NPPD	NTPD
-30	.1353	.4957	3.7887	-1.2814
-25	.1572	.7181	2.8164	-.6586
-20	.1670	.8775	2.2105	-.3749
-15	.1663	1.0759	1.6594	-.1714
-10	.1635	1.2232	1.1089	-.0599
-5	.1576	1.3665	.5528	-.0114
0	.1555	1.4051	-.0219	-.0013
5	.1548	1.4183	-.6480	-.0032
10	.1663	1.2195	-1.1537	-.0289
15	.1669	1.1291	-1.6809	-.1103
20	.1691	.9199	-2.2575	-.2927
25	.1623	.7190	-2.8644	-.5823

Table A6: Five-Hole Probe Calibration

M = .21

δ (deg)	HIP	NSPD	NPPD	NTPD
-30	.1730	.5102	3.6636	-1.2322
-25	.1996	.6967	2.8118	-.6843
-20	.2107	.8802	2.1901	-.3730
-15	.2101	1.0852	1.6529	-.1771
-10	.2102	1.2110	1.0860	-.0547
-5	.2013	1.3538	.5660	-.0129
0	.1920	1.4590	0.0521	-.0219
5	.1915	1.3762	-.5602	.0365
10	.2017	1.3069	-1.1160	-.0283
15	.2153	1.0629	-1.6728	-.1129
20	.2168	.8971	-2.2012	-.2690
25	.1999	.7449	-2.8849	-.6043

Table A7: Five-Hole Probe Calibration

M = .23

δ (deg)	HIP	NSPD	NPPD	NTPD
-30	.2170	.4838	3.4280	-1.1473
-25	.2406	.7009	2.7916	-.6663
-20	.2516	.8853	2.2589	-.3803
-15	.3548	1.0571	1.6733	-.1817
-10	.2483	1.2354	1.0619	-.0560
-5	.2401	1.3611	.5264	-.0104
0	.2389	1.3990	-.0100	.0029
5	.2398	1.3841	-.5855	-.0050
10	.2458	1.3035	-1.0785	-.0277
15	.2651	1.0419	-1.6945	-.1252
20	.2600	.9269	-2.2112	-.2862
25	.2380	.7821	-2.9406	-.6341

Table A8: Five-Hole Probe Calibration

M = .28

δ (deg)	HIP	NSPD	NPPD	NTPD
-30	.3054	.5025	3.4167	-1.1158
-25	.3282	.7357	2.8253	-.6896
-20	.3578	.8607	2.1732	-.3631
-15	.3457	1.1015	1.6908	-.1927
-10	.3487	1.2231	1.1331	-.0502
-5	.3417	1.3670	.5620	-.0243
0	.3408	1.4255	.0112	-.0023
5	.3433	1.4132	-.5776	.0044
10	.3532	1.3088	-1.2037	-.0405
15	.3758	1.0777	-1.6892	-.1285
20	.3772	.9201	-2.2345	-.2892
25	.3358	.8204	-2.9325	-.6597

Table A9: Five-Hole Probe Calibration

M = .3

δ (deg)	HIP	NSPD	NPPD	NTPD
-30	.3316	.5209	3.5865	-1.2299
-25	.3727	.7441	2.7448	-.7022
-20	.3919	.9256	2.2091	-.4037
-15	.4096	1.0623	1.6252	-.1611
-10	.4022	1.1988	1.1302	-.0666
-5	.3783	1.3869	.5509	-.0204
0	.3797	1.3875	.0287	.0005
5	.3827	1.3629	-.5440	-.0112
10	.3906	1.2922	-1.1169	-.0364
15	.4117	1.0905	-1.6385	-.1241
20	.3951	.9853	-2.2703	-.3161
25	.3770	.7980	-2.8751	-.6193

Table A10: Five-Hole Probe Calibration

M = .34

δ (deg)	HIP	NSPD	NPPD	NTPD
-30	.4531	.5488	3.5196	-1.1836
-25	.4806	.8551	2.8086	-.6980
-20	.5265	.9717	2.1261	-.3694
-15	.5431	1.0794	1.6026	-.1852
-10	.5354	1.2406	1.0314	-.0637
-5	.5205	1.3553	.5130	-.0167
0	.5065	1.4237	-.0677	-.0085
5	.4992	1.4638	-.6004	-.0060
10	.5381	1.2688	-1.1653	-.2079
15	.5520	1.1185	-1.6483	-.1198
20	.5645	.9351	-2.1294	-.2581
25	.5115	.8111	-2.8122	-.6068

Table All: Five-Hole Probe Calibration

M = .4

δ (deg)	HIP	NSPD	NPPD	NTPD
-30	.6201	.5200	3.4287	-1.0953
-25	.6658	.7727	2.7578	-.6623
-20	.6958	.9606	2.1535	-.3626
-15	.7803	1.1185	1.6395	-.1635
-10	.6963	1.2666	1.1327	-.0500
-5	.6722	1.3990	.5905	-.0040
0	.6582	1.4524	.0469	-.0029
5	.6694	1.4238	-.4412	-.0022
10	.7063	1.2824	-.9777	-.0133
15	.7294	1.1425	-1.5582	-.0872
20	.7409	.9596	-2.0692	-.2401
25	.6897	.8570	-2.6205	-.5069

**APPENDIX B:
HOT-FILM CALIBRATION PROCEDURE**

* * * * *

TABLES INCLUDED IN APPENDIX B:

<u>Number</u>	<u>Title</u>	<u>Page</u>
B1	Hot-Film Calibration Data.....	B.2

APPENDIX B:

HOT-FILM CALIBRATION PROCEDURE

As mentioned in Sections 3.2.2 and 4.2, some qualitative turbulence data were collected along the jet centerline using a TSI model 1210-20 hot-film probe. The calibration procedure was similar to Reference [109]. The probe was first mounted on a TSI model 1125 calibrator and connected to the DISA model 55M01 anemometer by the same cable used for actual measurements. The probe resistance was then measured by setting the anemometer to the "resistance measure" mode with no air flow in the calibration tunnel. The resistance value was then multiplied by the overhead ratio of 1.5 and set on the "decade" of the anemometer. The next step was adjustment of bridge balance by square wave test using an oscilloscope and adjusting gain and filter knobs of the anemometer for best response. Finally the calibration data were taken by recording the anemometer dc and ac output voltages for a range of Mach numbers from zero (no flow) to 0.3. The dc voltages are tabulated in Table B1. The calibration data were then curve fitted to the relationship $V_{CTA}^2 = a + b\sqrt{u}$ where V_{CTA} was the bridge voltage and u the axial velocity. Values of a and b which were determined and input into the data acquisition program are

$$V_{CTA}^2 = 4.1482\sqrt{M \times 1120} + 12.637$$

Table B1: Hot-Film Calibration Data

M	V _{CTA}
.025	5.992
.05	6.589
.075	7.086
.10	7.502
.125	7.885
.150	8.188
.175	8.467
.200	8.715
.225	8.925
.250	9.125
.275	9.304
.300	9.469
.325	9.621
.350	9.759
.375	9.883
.400	10.002

APPENDIX C:
COMPUTER PROGRAMS

* * * * *

<u>Section Number</u>	<u>Title</u>	<u>Page</u>
C.1	COMPUTER PROGRAM FOR MEAN FLOW MEASUREMENTS.....	C.2
C.2	COMPUTER PROGRAM FOR HOT-WIRE MEASUREMENTS.....	C.17

C.1 COMPUTER PROGRAM FOR MEAN FLOW MEASUREMENTS

ORIGINAL COPY OF FOUR QUALITY

```

10  ! ZRUN FEB.5,1987
11  ! PLASTIC NOZZLE
13  ! NEW CALIBRATION (OLD PROBE , NEW CALIBRATION"
20  ! 5-HOLE PROBE TRAVEL AND READOUT AND CALCULATIONS (NO PLOTS)
30  ! RADIAL TRAVERSE IN POSITIVE "Z" DIRECTION FROM CENTER LINE
70  ! CONNECT LC SMITH READOUT TO 702 EXTERNALLY
80  ! SCANNIVALVE READOUT IS THROUGH 703 (OPEN SERV AIR FOR OPERATION)
90  OPTION BASE 1
100 DIM A(11,16,4),M(11),U(70,3),C(170),V(170),W(170),R(170),Beta(70),Delta(
70),Psf(70),Ptf(70),Vf(70),Head(35)
110 DIM Mach(70),Vel(70),Pr(70),Rr(170),Rrwd(70),Rrui(70),Rrwi(70),Dummi(70)
120 DIM Zz(70),P(70,6),Rp(70)
121 PRINTER IS 710
124 INPUT "INSERT DATA DISC INPUT RECORD NO?",Rech
126 INPUT "MANIFOLD OPEN =",Man IA=1 B=2 C=3
130 INPUT "REFERENCE X/D STATION",Xst
131 INPUT "INPUT REF Z STATION",Zst
140 INPUT "INPUT 3 POSITIVE Z-STEP SIZES(IN THOUSANDTHS IN)",Step1,Step2,Step
150 INPUT "INPUT 3 NO OF STEPS (TOTAL MAX 70)",Nn1,Nn2,Nn3
160 INPUT "INPUT AMBIENT PRESSURE",Pa
170 INPUT "INPUT AMBIENT TEMP IN DEG F",Ta
180 INPUT "INPUT TANK PRESSURE",Pt
190 INPUT "INPUT TANK TEMP IN DEG F",Tt !REQ FOR STATIC TEMP CALCULATION
200 INPUT "INPUT PLENUM PRESSURE",Pp1
210 INPUT "INPUT PLENUM TEMP",Tp1
220 INPUT "INPUT MANIFOLD A PRESSURE DIFF",Dpa
230 INPUT "INPUT MANIFOLD B PRESSURE DIFF",Dpb
240 INPUT "INPUT MANIFOLD C PRESSURE DIFF",Dpc
241 INPUT "DO YOU WANT SWIRL NO ? (1 = YES , 2 = NO )",Swi
243 INPUT "DO YOU WANT TO PLOT ? (1 = YES 2 = NO)",Np
250 DATA -40,-.4682,7.9306,-4.0848,-35,.1231,5.2614,-2.1024
260 DATA -30,.4763,3.5546,-1.1505,-25,.7371,2.9283,-.6932
270 DATA -20,.9486,2.2417,-.3654,-15,.1761,1.7527,-.2255
280 DATA -10,1.2934,1.0772,-.0502,-5,1.442,.5530,-.0040
290 DATA 0,1.5057,-.0041,-.0041,5,1.4954,-.5591,0.000
300 DATA 10,1.3516,-1.0703,-.0234,15,1.9646,-2.7910,.1479
310 DATA 20,.8999,-1.8598,-.3426,25,.7782,-2.6694,-.5766
320 DATA 30,.5800,-3.8411,-1.1124,35,.2246,-5.0321,-1.8984
330 !
340 DATA -40,-.3535,6.8744,-3.2930,-35,.1621,4.7476,-1.8671
350 DATA -30,.5516,3.7032,-1.1774,-25,.7654,2.7970,-.6677
360 DATA -20,.9422,2.2241,-.3693,-15,1.1063,1.6490,-.1856
370 DATA -10,1.3146,1.0961,-.0712,-5,1.4407,.5178,-.0029
380 DATA 0,1.4201,-.0345,0,5,1.3751,-.6143,-.0085
390 DATA 10,1.2983,-1.1160,-.0276,15,1.1578,-1.6399,-.1106
400 DATA 20,.9853,-2.1835,-.2760,25,.7806,-2.8092,-.5674
410 DATA 30,.5216,-3.6264,-1.0205,35,.2041,-5.0923,-1.9199
420 !
430 DATA -40,-.4432,7.6749,-3.9157,-35,.1193,4.9060,-2.0190
440 DATA -30,.4741,3.6111,-1.1542,-25,.7263,2.8226,-.6837
450 DATA -20,.9121,2.1881,-.3763,-15,1.0764,1.6272,-.1739
460 DATA -10,1.2751,1.0926,-.0678,-5,1.3987,.4878,-.0097
470 DATA 0,1.4422,-.1021,.0016,5,1.4157,-.6011,-.0049
480 DATA 10,1.3205,-1.1144,-.0269,15,1.126,-1.6594,-.0975
490 DATA 20,.9505,-2.1529,-.2729,25,.7799,-2.8409,-.5732
500 DATA 30,.5266,-3.7205,-1.0603,35,.2120,-5.1349,-.7636
510 !
520 DATA -40,-.3922,7.4770,-3.7698,-35,.1140,4.8443,-1.9936
530 DATA -30,.4580,3.6848,-1.1898,-25,.7129,2.8028,-.6685
540 DATA -20,.8841,2.2069,-.3481,-15,1.1069,1.6461,-.1775
550 DATA -10,1.2809,1.0581,-.0495,-5,1.3934,.5089,-.0109
560 DATA 0,1.4159,-.0342,-.0022,5,1.3987,-.6309,-.0033
570 DATA 10,1.2812,-1.0879,-.0305,15,1.1367,-1.6429,-.1031
580 DATA 20,.9180,-2.1964,-.2675,25,.8034,-2.9039,-.6063
590 DATA 30,.5234,-3.6717,-1.0374,35,.2238,-4.9390,-1.8780
600 !

```

```

610 DATA -40,-.2930,7.8108,-4.1682,-35,.2128,4.6914,-1.9944
620 DATA -30,.4957,3.7887,-1.2814,-25,.7181,2.8164,-.6586
630 DATA -20,.8775,2.2105,-.3749,-15,1.0749,1.6594,-.1714
640 DATA -10,1.2232,1.1889,-.0599,-5,1.3665,.5528,-.0114
650 DATA 0,1.4051,-.0219,-.0013,5,1.4183,-.6480,-.0032
660 DATA 10,1.2195,-1.1537,-.0289,15,1.1291,-1.6809,-.1103
661 DATA 20,.9199,-2.2575,-.2927,25,.7190,-2.8644,-.5823
662 DATA 30,.5137,-3.5857,-1.0353,35,.2504,-5.1296,-2.0123
663 !
664 DATA -40,-.2603,6.9356,-3.6421,-35,.1977,4.8194,-2.1297
665 DATA -30,.5102,3.6636,-1.2322,-25,.6967,2.8118,-.6843
666 DATA -20,.8802,2.1901,-.3730,-15,1.0852,1.6529,-.1771
667 DATA -10,1.2110,1.0860,-.0547,-5,1.3538,.5660,-.0129
668 DATA 0,1.4590,-.0521,-.0219,5,1.3762,-.5602,.0365
669 DATA 10,1.3069,-1.1160,-.0283,15,1.0629,-1.6728,-.1129
670 DATA 20,.8971,-2.2012,-.2690,25,.7449,-2.8849,-.6043
671 DATA 30,.5049,-3.4889,-.9976,35,.2949,-5.0535,-2.0269
672 !
673 DATA -40,-.2300,6.9902,-3.7487,-35,.2304,5.1721,-2.3411
674 DATA -30,.4838,3.4280,-1.1473,-25,.7009,2.7916,-.6663
675 DATA -20,.8853,2.2589,-.3803,-15,1.0571,1.6733,-.1817
676 DATA -10,1.2354,1.0619,-.0560,-5,1.3611,.5264,-.0104
677 DATA 0,1.3990,-.0100,.0029,5,1.3841,-.5855,-.0050
678 DATA 10,1.3035,-1.0785,-.0277,15,1.0419,-1.6945,-.1252
679 DATA 20,.9269,-2.2112,-.2862,25,.7821,-2.9406,-.6341
680 DATA 30,.5266,-3.4780,-1.0288,35,.3194,-5.5783,-2.3144
681 !
682 DATA -40,-.2383,8.3238,-4.5659,-35,.2466,4.6273,-1.9727
683 DATA -30,.5025,3.4167,-1.1158,-25,.7357,2.8253,-.6896
684 DATA -20,.8607,2.1732,-.3631,-15,1.1015,1.6908,-.1927
685 DATA -10,1.2231,1.1331,-.0502,-5,1.3670,.5620,-.0243
686 DATA 0,1.4255,.0112,-.0023,5,1.4132,-.5776,-.0044
687 DATA 10,1.3088,-1.2037,-.0405,15,1.0777,-1.6892,-.1285
688 DATA 20,.9201,-2.2345,-.2892,25,.8204,-2.9325,-.6597
689 DATA 30,.5928,-3.7332,-1.1497,35,.3658,-5.7192,-2.4910
690 !
691 DATA -40,-.3067,7.0182,-3.6985,-35,.1776,4.4365,-1.8482
692 DATA -30,.5209,3.5865,-1.2299,-25,.7441,2.7448,-.7022
693 DATA -20,.9256,2.2091,-.4037,-15,1.0623,1.6252,-.1611
694 DATA -10,1.1988,1.1302,-.0666,-5,1.3869,.5509,-.0204
695 DATA 0,1.3875,.0287,.0005,5,1.3629,-.5440,-.0112
696 DATA 10,1.2922,-1.1169,-.0364,15,1.0905,-1.6385,-.1241
697 DATA 20,.9853,-2.2703,-.3161,25,.7980,-2.8751,-.6193
698 DATA 30,.6652,-3.8716,-1.2323,35,.3220,-5.3255,-2.2251
699 !
700 DATA -40,-.2187,6.0234,-2.9445,-35,.1808,4.4694,-1.8816
701 DATA -30,.5488,3.5196,-1.1836,-25,.8551,2.8086,-.6980
702 DATA -20,.9717,2.1261,-.3694,-15,1.0794,1.6026,-.1852
703 DATA -10,1.2406,1.0314,-.0637,-5,1.3553,.5130,-.0167
704 DATA 0,1.4237,-.0677,-.0085,5,1.4638,-.6004,-.0060
705 DATA 10,1.2688,-1.1653,-.0279,15,1.1185,-1.6483,-.1198
706 DATA 20,.9351,-2.1294,-.2581,25,.8111,-2.8122,-.6068
707 DATA 30,.5583,-3.5170,-1.0706,35,.3017,-4.9376,-1.9957
708 !
709 DATA -40,-.3306,6.5526,-3.3191,-35,.2040,4.7035,-1.9963
710 DATA -30,.5200,3.4287,-1.0953,-25,.7727,2.7578,-.6623
711 DATA -20,.9606,2.1535,-.3626,-15,1.1185,1.6395,-.1635
712 DATA -10,1.2666,1.1327,-.0500,-5,1.3990,.5905,-.0040
713 DATA 0,1.4524,.0469,-.0029,5,1.4238,-.4412,-.0022
714 DATA 10,1.2824,-.9777,-.0133,15,1.1425,-1.5582,-.0872
715 DATA 20,.9596,-2.0692,-.2401,25,.8570,-2.6205,-.5069
716 DATA 30,.6761,-3.4994,-1.0182,35,.3374,-4.8436,-1.9050
717 !
718 !
719 DATA .06,.08,.11,.14,.19,.21,.23,.28,.3,.34,.4
720 READ A(*),M(*)
722 Rho=Pa*144/(53.3*(Ta+460))

```

```

723 Rho=DROUND(Rho,6)
724 PRINT "4.5 INCH PLASTIC NOZZLE DATA"
726 PRINT "RADIAL TRAVERSE"
727 PRINT "DATA STORED IN DISC NO 24 ; RECORD NO",Recn
728 PRINT "MANIFOLD OPEN =",Man ! A=1 ,B=2 ,C=3
729 Xst=DROUND(Xst,3)
730 PRINT "REF X/D STATION =",Xst
731 PRINT "REF Z STATION =",Zst
732 Ls1=Step1/1000
733 Ls2=Step2/1000
734 Ls3=Step3/1000
736 PRINT "STEP SIZES =",Ls1,Ls2,Ls3
737 PRINT "NO OF STEPS =",Nn1,Nn2,Nn3
740 PRINT "AMBIENT PRESSURE =",Pa
750 PRINT "AMBIENT TEMP =",Ta
751 PRINT "DENSITY =",Rho," Lbs/CU.FT"
760 PRINT "TANK PRESSURE=",Pt
770 PRINT "TANK TEMP =",Tt
780 PRINT "PLENUM PRESSURE=",Pp1
790 PRINT "PLENUM TEMP = ",Tp1
800 PRINT "MAN(A) DP =",Dpa,"MAN(B) DP =",Dpb,"MAN(C) DP =",Dpc
811 !
840 PRINT "*****"
841 Diameter=4.5
842 Radius=2.25
843 Area=.11 ! .11 SQ.FT
850 Zz9=0
851 Dp=Dpa+Dpb+Dpc ! ASSUMED ONE MANIFOLD OPERATING THEREFORE 2 DPS ARE ZERO
853 Ru=0 ! FOR MASS FLOW CALCULATIONS
854 Rruw=0 ! FOR SWIRL NO CALCULATIONS
855 Ruu=0
856 Rww=0
857 Dumm=0
858 Rp=0
860 Nn=Nn1+Nn2+Nn3
861 Rr(1)=0
862 Rr(1)=Zst
863 FOR I=2 TO Nn1
864 Rr(I)=Rr(I-1)+Ls1/12
865 Rr1(I)=Rr1(I-1)+Ls1
866 NEXT I
867 FOR J=Nn1+1 TO Nn1+Nn2
868 Rr(J)=Rr(J-1)+Ls2/12
869 Rr1(J)=Rr1(J-1)+Ls2
870 NEXT J
871 FOR K=Nn1+Nn2+1 TO Nn
872 Rr(K)=Rr(K-1)+Ls3/12
873 Rr1(K)=Rr1(K-1)+Ls3
874 .NEXT K
875 Step=Step1
876 FOR L1=1 TO Nn
877 IF L1>Nn1-1 THEN Step=Step2
878 IF L1>Nn1+Nn2-1 THEN Step=Step3
879 Stp=Step
880 Ls=Step/1000
881 Zz(L1)=DROUND((Zz9/1000),4)
882 !
890 REMOTE 702 ! TAKING 20 AVERAGES FOR BETA
900 OUTPUT 702;"V D5 T1","Vdc
910 WAIT 10
920 Kk1=0
930 FOR Ii=1 TO 20
940 WAIT .5
950 TRIGGER 702
960 K1=0
970 ENTER 702;K1

```

ORIGINAL PAGE IS
OF POOR QUALITY

```

980 KK1=KK1+K1
990 NEXT Ii
1000 Beta(L1)=KK1/20
1010 !
1020 REMOTE 706
1030 OUTPUT 706;"R2"
1040 WAIT 3
1050 OUTPUT 706;"B2"
1060 Mm=5
1061 IF L1=1 THEN Mm=6
1070 FOR I=1 TO Mm
1080 OUTPUT 706;"A1"
1081 WAIT 1
1082 OUTPUT 706;"B1"
1090 WAIT 5
1100 REMOTE 703
1110 OUTPUT 703;"V D5 T1,",Vdc
1120 Kk2=0
1130 FOR Ij=1 TO 20
1140 WAIT .5
1150 TRIGGER 703
1160 K2=0
1170 ENTER 703;K2
1180 Kk2=Kk2+K2
1190 NEXT Ij
1191 Kk3=Kk2/20
1192 Pp=.093424+85.686*Kk3+368.2+(Kk3^2) TRANSDUCER CALIBRATION CURVE-FITTED
1202 P(L1,I)=Pp
1230 NEXT I
1240 Zz9=Zz9+Stp
1250 IF L1=Nn THEN Stp=-Zz9+Stp
1260 FOR I1=1 TO 6
1270 P(L1,I1)=DROUND(P(L1,I1),3)
1280 NEXT I1
1290 Beta(L1)=DROUND(-(Beta(L1)-5)+17.5),3)
1320 PRINT L1,"P1=",P(L1,1),"P2=",P(L1,2),"P3=",P(L1,3),"P4=",P(L1,4),"P5=",P(L
1,5)
1328 IF L1=1 THEN PRINT "P6=",P(L1,6)
1330 Dxx=0
1340 Dzz=Stp
1350 !
1360 !
1810 !FOR Ii=1 TO 13
1820 !PRINT A(1,Ii,1)
1830 !NEXT Ii
1840 !FOR Jj=1 TO 6
1850 !PRINT A(Jj,13,4)
1860 !NEXT Jj
1870! Ls1=-Stp/1000
1880 N=0 ! COUNTS NO OF ITERATIONS
1890! P1=P(L1,1)+Pa
1900! P2=P(L1,2)+Pa
1910! P3=P(L1,3)+Pa
1920 !P4=P(L1,4)+Pa
1930! P5=P(L1,5)+Pa
1931 P1=P(L1,1)
1932 P2=P(L1,2)
1933 P3=P(L1,3)
1934 P4=P(L1,4)
1935 P5=P(L1,5)
1940 Pav=.25*(P1+P2+P3+P4)
1950 Hip=P5-Pav
1951 IF Hip=0 THEN GOTO 2092
1960 Nppd=(P3-P1)/Hip
1970 ! PRINT "NPPD=",NPPD
1980 FOR I=1 TO 16

```

ORIGINAL PAGE IS
OF POOR QUALITY

ORIGINAL PAGE IS
OF POOR QUALITY

```
1990 IF Nppd<A(1,I,3) THEN GOTO 2040
1991 IF I>1 THEN GOTO 2000
1992 Nspd1=A(1,1,2)
1993 Ntpd1=A(1,1,4)
1994 Delta1=A(1,1,1)
1995 GOTO 2070
2000 Nspd1=A(1,I-1,2)+((A(1,I,2)-A(1,I-1,2))/(A(1,I,3)-A(1,I-1,3)))*(Nppd-A(1,I-1,3))
2010 Ntpd1=A(1,I-1,4)+((A(1,I,4)-A(1,I-1,4))/(A(1,I,3)-A(1,I-1,3)))*(Nppd-A(1,I-1,3))
2020 Delta1=A(1,I-1,1)+((A(1,I,1)-A(1,I-1,1))/(A(1,I,3)-A(1,I-1,3)))*(Nppd-A(1,I-1,3))
2030 GOTO 2070
2040 NEXT I
2050 M2=M(1)
2070 Ps1=Pav-Nspd1*Hip
2080 Pt1=P5-Ntpd1*Hip
2081 Ps11=Ps1+Pa !CONVERSION TO ABSOLUTE
2082 Pt11=Pt1+Pa !CONVERSION TO ABSOLUTE
2090 Q=5.0*((Pt11/Ps11)^.286-1)
2091 IF Q>0 THEN GOTO 2111
2092 PRINT "VERY LOW VELOCITY"
2093 Psf(L1)=Ps1
2094 Ptf(L1)=Pt1
2096 Ps1=DROUND(Ps1,3)
2097 Pt1=DROUND(Pt1,3)
2098 PRINT "PS=",Ps1 !,"PT=",Pt1
2099 U1(L1)=0
2100 V1(L1)=0
2101 W1(L1)=0
2102 Ru1(L1)=0
2103 Rruw1(L1)=0
2104 Ruu1(L1)=0
2105 Rww1(L1)=0
2106 Dumm1(L1)=0
2110 GOTO 2790
2111 M1=SQR(Q)
2112 IF ABS(M1-M2)<.0001 THEN GOTO 2410
2113 M2=M1
2120 !THE FOLLOWING MESSAGES WARN CALIBRATION LIMITS AVAILABLE
2130 !IF M1>M(11) THEN PRINT "WARNING ; M>.4"
2140 !IF M1<M(1) THEN PRINT "WARNING ; M<.06 "
2150 FOR J=1 TO 11
2160 IF M1<M(J) THEN GOTO 2180
2170 NEXT J
2180 FOR K=1 TO 16
2190 IF ABS(J-1)<.5 THEN J=2
2200 IF Nppd<A(J-1,K,3) THEN GOTO 2250
2201 IF K>1 THEN GOTO 2210
2202 Nspd2=A(J-1,1,2)
2203 Ntpd2=A(J-1,1,4)
2204 Delta2=A(J-1,1,1)
2205 GOTO 2260
2210 Nspd2=A(J-1,K-1,2)+((A(J-1,K,2)-A(J-1,K-1,2))/(A(J-1,K,3)-A(J-1,K-1,3)))*(Nppd-A(J-1,K-1,3))
2220 Ntpd2=A(J-1,K-1,4)+((A(J-1,K,4)-A(J-1,K-1,4))/(A(J-1,K,3)-A(J-1,K-1,3)))*(Nppd-A(J-1,K-1,3))
2230 Delta2=A(J-1,K-1,1)+((A(J-1,K,1)-A(J-1,K-1,1))/(A(J-1,K,3)-A(J-1,K-1,3)))*(Nppd-A(J-1,K-1,3))
2240 GOTO 2260
2250 NEXT K
2260 FOR L=1 TO 16
2270 IF Nppd<A(J,L,3) THEN GOTO 2320
2271 IF L>1 THEN GOTO 2280
2272 Nspd3=A(J,1,2)
2273 Ntpd3=A(J,1,4)
```

```

2274 Delta3=A(J,1,1)
2275 GOTO 2330
2280 Nspd3=A(J,L-1,2)+((A(J,L,2)-A(J,L-1,2))/((A(J,L,3)-A(J,L-1,3))))*(Nppd-A(J,L-1,3))
2290 Ntpd3=A(J,L-1,4)+((A(J,L,4)-A(J,L-1,4))/((A(J,L,3)-A(J,L-1,3))))*(Nppd-A(J,L-1,3))
2300 Delta3=A(J,L-1,1)+((A(J,L,1)-A(J,L-1,1))/((A(J,L,3)-A(J,L-1,3))))*(Nppd-A(J,L-1,3))
2310 GOTO 2330
2320 NEXT L
2330 Nspd=Nspd2+((Nspd3-Nspd2)/(M(J)-M(J-1)))*(M1-M(J-1))
2340 Ntpd=Ntpd2+((Ntpd3-Ntpd2)/(M(J)-M(J-1)))*(M1-M(J-1))
2350 Delta=Delta2+((Delta3-Delta2)/(M(J)-M(J-1)))*(M1-M(J-1))
2360 Nspd1=Nspd
2370 Ntpd1=Ntpd
2380 Delta1=Delta
2390 N=N+1
2400 GOTO 2070
2410 Ps1=DROUND(Ps1,3)
2420 Pt1=DROUND(Pt1,3)
2430 M1=DROUND(M1,3)
2440 Delta1=DROUND(Delta1,3)
2441 Psf(L1)=Ps1
2442 Ptf(L1)=Pt1
2450 PRINT "PS=",Ps1,"PT=",Pt1,"ITERATION=",N
2460 Ts=(Tt+460)/(1+.2*(M1^2))
2470 Vs=SQRT(1.4*32.2*53.3*Ts)
2480 V=M1*Vs
2490 DEG
2500 Vx=V*COS(Delta)*COS(Beta(L1))
2510 Vy=V*COS(Delta)*SIN(Beta(L1))
2520 Vz=V*SIN(Delta)
2530 V=DROUND(V,4)
2540 !THE FOLLOWING IF STATEMENT IS TO STORE V0 FOR NORMALIZING
2550 IF L1>1 THEN GOTO 2570
2560 V0=V
2570 Vx=DROUND(Vx,3)
2580 Vy=DROUND(Vy,3)
2590 Vz=DROUND(Vz,3)
2591 Vf(L1)=V
2592 Deltaf(L1)=Delta1
2595 PRINT "V=",V,"BETA=",Beta(L1),"DELTA=",Delta1
2600! PRINT "VX=",Vx,"VY=",Vy,"VZ=",Vz
2601 PRINT "U=",Vx,"V=",Vz,"W=", -Vy
2610 !Vxu=Vx/V0
2620 !Vyu=Vy/V0
2630 !Vzu=Vz/V0
2640 !Vxu=DROUND(Vxu,4)
2650! .Vyu=DROUND(Vyu,3)
2660 !Vzu=DROUND(Vzu,3)
2670 !PRINT "VX/V=",Vxu,"VY/V=",Vyu,"VZ/V",VzuEDIT
2690 Mach(L1)=M1
2700 Vel(L1)=V
2710 U(L1,1)=Vx
2720 U(L1,2)=Vy
2730 U(L1,3)=Vz
2740 U1(L1)=Vx
2750 V1(L1)=Vz
2760 W1(L1)=-Vy
2761 Rp1(L1)=ABS(Rr(L1))*Psf(L1)*144
2762 Rp=Rp+Rp1(L1)
2770 Ru1(L1)=ABS(Rr(L1))*U1(L1)
2771 Ru=Ru+Ru1(L1)
2772 Rruw1(L1)=ABS(Rr(L1))*ABS(Rr(L1))*U1(L1)*W1(L1)
2773 Rruw=Rruw+Rruw1(L1)
2774 Ruu1(L1)=ABS(Rr(L1))*U1(L1)*U1(L1)

```

ORIGINAL PAGE IS
OF POOR QUALITY

```

2775 Rww1(L1)=ABS(Rr(L1))*W1(L1)*W1(L1)
2777 Ruu=Ruu+Ruu1(L1)
2778 Rww=Rww+Rww1(L1)
2779 Dumml(L1)=Ruu1(L1)-Rww1(L1)/2
2780 Dumml=Dumml+Dumml(L1)
2781 !PRINT "M=",MACH(L1),"V=",VEL(L1),"VX=",VX,"VY=",VY,"VZ=",VZ
2782 !PRINT "VX/V0=",Vxu1(L1),"VY/V0=",Vyu1(L1),"VZ/V0=",Vzu1(L1)
2790 Rr(L1)=DROUND(Rr(L1),3)
2791 Rr1(L1)=DROUND(Rr1(L1),4)
2800 !PRINT "r=",Rr(L1)
2803 PRINT "r=",Rr1(L1)
2805 *PRINT "*****"
*****
2806! IF U1(L1)=0 THEN Nn=L1
2808 !IF U1(L1)=0 THEN GOTO 2810
2809 IF U1(L1)=0 THEN
2810 IF L1>Nn1 THEN
2811 Nn=L1
2812 GOTO 2817
2813 END IF
2814 END IF
2816 IF L1<Nn THEN GOTO #128
2817 Yy=1-.00313*Dp
2818 Wflow=.8484*Yy*SQR(Dp)
2819 Wflow=DROUND(Wflow,3)
2820 PRINT "MASS FLOW RATE MEASURED BY ORIFICE RUNS =",Wflow," LBS/SEC"
2821 !
2822 !
2823 Umax=U1(1)
2824 Wmax=W1(1)
2825 FOR I=2 TO Nn
2826 IF W1(I)>Wmax THEN Wmax=W1(I)
2827 IF U1(I)>Umax THEN Umax=U1(I)
2828 NEXT I
2829 Wmax=DROUND(Wmax,3)
2830 Umax=DROUND(Umax,3)
2831 IF Sw1=2 THEN GOTO 2977
2832 Ra1=0
2833 Ra2=0
2834 Ra3=0
2835 Bb1=0
2836 Bb2=0
2837 Bb3=0
2838 Cc1=0
2839 Cc2=0
2840 Cc3=0
2841 Dd1=0
2842 Dd2=0
2843 Dd3=0
2844 Ee1=0
2845 Ee2=0
2846 Ee3=0
2847 Ff1=0
2848 Ff2=0
2849 Ff3=0
2850 FOR I=1 TO (Nn1-1)
2851 X11=Ru1(I)+Ru1(I+1)
2852 Y11=Rruw1(I)+Rpuw1(I+1)
2853 Z11=Ruu1(I)+Rou1(I+1)
2854 T11=Rww1(I)+Rww1(I+1)
2855 Q11=ABS(Rr(I))+ABS(Rr(I+1))
2856 H11=Rp1(I)+Rp1(I+1)
2857 A1=X11*ABS(Ls1)/12/2
2858 B1=Y11*ABS(Ls1)/12/2
2859 C1=Z11*ABS(Ls1)/12/2
2860 D1=T11*ABS(Ls1)/12/2

```

```

2861 E1=011*ABS(Ls1)/12/2
2862 F1=H11*ABS(Ls1)/12/2
2863 Aa1=Aa1+A1
2864 Bb1=Bb1+B1
2865 Cc1=Cc1+C1
2866 Dd1=Dd1+D1
2867 Ee1=Ee1+E1
2868 Ff1=Ff1+F1
2869 NEXT I
2870 FOR I=Nn1 TO (Nn1+Nn2-1)
2871 X22=Ru1(I)+Ru1(I+1)
2872 Y22=Rruw1(I)+Rruw1(I+1)
2873 Z22=Ruu1(I)+Ruu1(I+1)
2874 T22=Rww1(I)+Rww1(I+1)
2875 Q22=ABS(Rr(I))+ABS(Rr(I+1))
2876 H22=Rp1(I)+Rp1(I+1)
2877 A2=X22*ABS(Ls2)/12/2
2878 B2=Y22*ABS(Ls2)/12/2
2879 C2=Z22*ABS(Ls2)/12/2
2880 D2=T22*ABS(Ls2)/12/2
2881 E2=Q22*ABS(Ls2)/12/2
2882 F2=H22*ABS(Ls2)/12/2
2884 Aa2=Aa2+A2
2885 Bb2=Bb2+B2
2886 Cc2=Cc2+C2
2887 Dd2=Dd2+D2
2888 Ee2=Ee2+E2
2889 Ff2=Ff2+F2
2891 NEXT I
2892 !
2893 FOR I=(Nn1+Nn2) TO (Nn-1)
2894 X33=Ru1(I)+Ru1(I+1)
2895 Y33=Rruw1(I)+Rruw1(I+1)
2896 Z33=Ruu1(I)+Ruu1(I+1)
2897 T33=Rww1(I)+Rww1(I+1)
2898 Q33=ABS(Rr(I))+ABS(Rr(I+1))
2899 H33=Rp1(I)+Rp1(I+1)
2901 A3=X33*ABS(Ls3)/12/2
2902 B3=Y33*ABS(Ls3)/12/2
2903 C3=Z33*ABS(Ls3)/12/2
2904 D3=T33*ABS(Ls3)/12/2
2905 E3=Q33*ABS(Ls3)/12/2
2906 F3=H33*ABS(Ls3)/12/2
2908 Aa3=Aa3+A3
2909 Bb3=Bb3+B3
2910 Cc3=Cc3+C3
2911 Dd3=Dd3+D3
2912 Ee3=Ee3+E3
2913 Ff3=Ff3+F3
2915 NEXT I
2916 !
2917 Aa=Aa1+Aa2+Aa3
2918 Bb=Bb1+Bb2+Bb3
2919 Cc=Cc1+Cc2+Cc3
2920 Dd=Dd1+Dd2+Dd3
2921 Ee=Ee1+Ee2+Ee3
2922 Ff=Ff1+Ff2+Ff3
2924 Mflow=2*PI*Rho*Aa
2925 Anflux=Bb
2926 Axflux=Cc+.5*Dd-.5*Wmax*Wmax*Ee
2927 Jarea=2*PI*Ee
2928 Jarea=DROUND(Jarea,3)
2930 Swirl=Bb/(Cc+.5*Dd-.5*Wmax*Wmax*Ee)/(Radius/12)
2931 Axflux1=Cc-.5*Dd
2933 Swirl1=Bb/(Cc-.5*Dd)/(Radius/12)
2934 Axflux2=Cc+Ff/Rho

```

ORIGINAL PAGE IS
OF POOR QUALITY

ORIGINAL PART IS
OF POOR QUALITY

```
2936 Swirl2=Bb/(Cc+Ff/Rho)/(Radius/12)
2937 Axflux3=Cc
2939 Swirl3=Bb/Cc/(Radius/12)
2940 Swirl1=DROUND(Swirl1,2)
2941 Swirl2=DROUND(Swirl2,2)
2942 Swirl3=DROUND(Swirl3,2)
2943 Mflow=DROUND(Mflow,3)
2944 Swirl=DROUND(Swirl,2)
2945 Anflux=DROUND(Anflux,3)
2946 Axflux1=DROUND(Axflux1,3)
2947 Axflux2=DROUND(Axflux2,3)
2948 Axflux3=DROUND(Axflux3,3)
2949 Axflux=DROUND(Axflux,3)
2951 PRINT "MASS FLOW RATE BY INTEGRATION =",Mflow," Lba/Sec"
2952 PRINT "JET CROSS SECTION AREA =",Jarea,"SQ.FT"
2953 PRINT "ANGULAR MOMENTUM FLUX =",Anflux
2954 PRINT "AXIAL MOMENTUM FLUX 1=",Axflux1,"WMAX DELETED FROM DENOMINATOR"
2955 PRINT "AXIAL MOMENTUM FLUX 2=",Axflux2,"Pa USED IN DENOMINATOR"
2956 PRINT "AXIAL MOMENTUM FLUX 3=",Axflux3,"SIMPEST FORM ;PRESSURE OMITTED"
2957 PRINT "AXIAL MOMENTUM FLUX =",Axflux,"COMPLETE FORMULA"
2959 PRINT "SWIRL NO.=",Swirl,"COMPLETE FORMULA"
2960 PRINT "SWIRL NO. 1 =",Swirl1,"Wmax DELETED FROM DENOMINATOR"
2961 PRINT "SWIRL NO. 2 =",Swirl2,"(Pa USED IN DENOMINATOR)"
2962 PRINT "SWIRL NO. 3 =",Swirl3,"SIMPLEST FORM ;PRESSURE TERM OMITTED"
2963 ! MACH NO CALCULATION
2964 Vave=Mflow/(Jarea*Rho)
2965 Mave=Vave/Vs !MAVE=MACH NO BASED ON AVERAGE AXIAL VELOCITY
2966 Mave=DROUND(Mave,2)
2967 Vave=DROUND(Vave,3)
2968 PRINT "AVERAGE AXIAL VELOCITY=",Vave,"FPS "
2969 PRINT "MAX AXIAL VELOCITY =",Umax,"FPS"
2970 PRINT "MAX TANGENTIAL VELOCITY =",Wmax,"FPS"
2971 !
2972 ! REYNOLDS NO CALCULATION
2973 Rave=Vave*Diameter/12/1.6*10000
2974 Rave=DROUND(Rave,6)
2975 PRINT "REYNOLDS NO.=",Rave," (BASED ON AVERAGE AXIAL VELOCITY)"
2976 PRINT "MACH NO.=",Mave," (BASED ON AVERAGE AXIAL VELOCITY)"
2977 PRINT "*****"
*****"
2978 IF Np=2 THEN GOTO 4128
2979 GINIT
2980 GRAPHICS ON
2981 DUMP DEVICE IS 710
2982 ! PLOTTER IS 705,"HPGL"
2983 VIEWPORT 20,100,30,80
2984 FRAME
2985 CSIZE 4,.4
2986 MOVE 20,70
2987 GCLEAR
2988 J=0
2989 MOVE 25,80
2990 GCLEAR,
2991 WINDOW 0,1,0,100
2992 AXES .5,25,0,0,2,3,5
2994 FRAME
2995 FOR J=1 TO 1
2996 MOVE 0,0
3000 CLIP OFF
3010 MOVE .75,-10
3020 LABEL "r/D "
3040 MOVE .2,-15
3050 LABEL "MEAN TANGENTIAL VELOCITY PROFILE"
3070 MOVE -.1,50
3080 LABEL "W(fps)"
3100 CSIZE 3.5,.5
```

```

3110  LOG 5
3120  FOR I=0 TO 100 STEP 50
3130  MOVE -.05,I
3140  LABEL USING "#,K";I
3150  NEXT I
3160  LOG 5
3170  FOR I=0 TO 1 STEP .5
3180  MOVE I,-2
3190  LABEL USING "#,K";I
3200  NEXT I
3210  NEXT J
3220  FOR I=1 TO Nn
3221  Ror=ABS(Rn1(I))/Diameter
3230  MOVE Ror,W1(I)
3240  LABEL "o"
3250  NEXT I
3260  FOR I=1 TO Nn
3261  Ror=ABS(Rn1(I))/Diameter
3263  PLOT Ror,W1(I)
3264  NEXT I
3266  DUMP GRAPHICS
3267  !
3268  !
3270  GINIT
3280  GRAPHICS ON
3281  DUMP DEVICE IS 710
3290  ! PLOTTER IS 705,"HPGL"
3300  VIEWPORT 20,100,30,80
3310  FRAME
3320  CSIZE 4,.4
3330  MOVE 20,70
3340  GCLEAR
3350  J=0
3360  MOVE 25,80
3370  GCLEAR
3380  WINDOW 0,1,0,200
3390  AXES .25,50,0,0,2,2,5
3400  FRAME
3410  FOR J=1 TO 1
3420  MOVE 0,0
3430  CLIP OFF
3440  MOVE .5,-20
3441  LABEL "r/D"
3442  MOVE .25,-30
3450  LABEL "MEAN AXIAL VELOCITY PROFILE"
3470  MOVE -.1,100
3480  LABEL "U(fps)"
3530  CSIZE 3.5,.5
3540  .LOG 5
3550  FOR I=0 TO 200 STEP 100
3560  MOVE -.05,I
3570  LABEL USING "#,K";I
3580  NEXT K
3590  LOG 5
3600  FOR I=0 TO 1 STEP .5
3610  MOVE I,-5
3620  LABEL USING "#,K";I
3630  NEXT I
3640  NEXT J
3650  FOR I=1 TO Nn
3651  Ror=ABS(Rn1(I))/Diameter
3660  MOVE Ror,U1(I)
3670  LABEL "o"
3680  NEXT I
3681  FOR I=1 TO Nn
3682  Ror=ABS(Rn1(I))/Diameter

```

```

3684 PLOT Ror,U1(I)
3685 NEXT I
3690 DUMP GRAPHICS
3691 !
3700 GINIT
3701 GRAPHICS ON
3702 DUMP DEVICE IS 710
3703 !PLOTTER IS 705,"HPGL"
3704 VIEWPORT 20,100,30,80
3705 FRAME
3706 CSIZE 4,.4
3707 MOVE 20,70
3708 GCLEAR
3709 WINDOW 0,1,-100,100
3710 AXES .5,25,0,-100,2,2,5
3711 FRAME
3712 FOR J=1 TO 1
3713 MOVE 0,0
3714 CLIP OFF
3715 MOVE .5,-115
3716 LABEL "r/D"
3717 MOVE .2,-130
3718 LABEL "MEAN RADIAL VELOCITY DISTRIBUTION"
3719 DEG
3720 LDIR 90
3721 MOVE -.1,-25
3722 LABEL "V(FPS)"
3723 LDIR 0
3724 CSIZE 3.5,.5
3725 LORG 5
3726 FOR I=-100 TO 100 STEP 50
3727 MOVE -.05,I
3728 LABEL USING "#,K";I
3729 NEXT I
3730 LORG 5
3731 FOR I=0 TO 1 STEP .5
3732 MOVE I,-105
3733 LABEL USING "#,K";I
3734 NEXT I
3735 NEXT J
3736 FOR I=1 TO Nn
3737 Ror=ABS(Rr1(I))/Diameter
3738 MOVE Ror,V1(I)
3739 LABEL "o"
3741 NEXT I
3742 FOR I=1 TO Nn
3743 Ror=ABS(Rr1(I))/Diameter
3744 PLOT Ror,V1(I)
3745 NEXT I
3746 DUMP GRAPHICS
3747 !
3748 !
3749 GINIT
3750 GRAPHICS ON
3751 DUMP DEVICE IS 710
3752 !PLOTTER IS 705,"HPGL"
3753 VIEWPORT 20,100,30,80
3760 FRAME
3770 CSIZE 4,.4
3780 MOVE 20,70
3790 GCLEAR
3800 J=0
3810 MOVE 25,80
3820 GCLEAR
3830 WINDOW 0,1,-.3,+.3
3840 AXES .5,.1,0,-.3,2,2,5

```

```

3850 FRAME
3860 FOR J=1 TO 1
3870 MOVE 0,0
3880 CLIP OFF
3890 MOVE .5,-.35
3900 LABEL "r/D"
3910 MOVE .2,-.40
3920 LABEL "STATIC PRESSURE DISTRIBUTION"
3930 MOVE -.5,0
3940 LABEL "P(psig)"
3950 LORG 5
3960 FOR I=-.3 TO .3 STEP .3
3970 MOVE -.05,I
3980 LABEL USING "#,K";I
3990 NEXT I
4000 LORG 5
4010 FOR I=0 TO 1 STEP .5
4020 MOVE I,-.25
4030 LABEL USING "#,K";I
4040 NEXT I
4050 NEXT J
4060 FOR I=1 TO Nn
4061 Ror=ABS(Rr1(I))/Diameter
4070 MOVE Ror,Psf(I)
4080 LABEL "o"
4090 NEXT I
4091 FOR I=1 TO Nn
4092 Ror=ABS(Rr1(I))/Diameter
4093 PLOT Ror,Psf(I)
4094 NEXT I
4100 DUMP GRAPHICS
4120 ! *****
4128! SUB XY TRAV 1/23/86
4129! IF U1(L1)=0 THEN GOTO 4133
4130 IF U1(L1)=0 THEN
4131 IF L1>Nn1 THEN GOTO 4135
4132 END IF
4134 IF L1<Nn THEN GOTO 4178
4135 !
4136 Head(1)=Man
4137 Head(2)=Dpa
4138 Head(3)=Dpb
4139 Head(4)=Dpc
4140 Head(5)=Xst
4141 Head(6)=Zst
4142 Head(7)=Ls1
4143 Head(8)=Nn
4144 Head(9)=Pa
4145 Head(10)=Ta
4146 Head(11)=Rho
4147 Head(12)=Pt
4148 Head(13)=Tt
4149 Head(14)=Pp1
4150 Head(15)=Tp1
4151 Head(16)=Recn
4152 Head(17)=Swirl
4153 Head(18)=Mflow
4154 Head(19)=Wflow
4155 Head(20)=Vave
4156 Head(21)=Mave
4157 Head(22)=Rave
4158 Head(23)=Vs
4159 Head(24)=Ls2
4160 Head(25)=Ls3
4161 Head(26)=Umax
4162 Head(27)=Wmax

```

ORIGINAL PAGE IS
OF POOR QUALITY

```
4163 Head(28)=Anflux
4164 Head(29)=Axflux
4165 Head(30)=Axflux1
4166 Head(31)=Axflux2
4167 Head(32)=Axflux3
4168 Head(33)=Swirl1
4169 Head(34)=Swirl2
4170 Head(35)=Swirl3
4171 !
4172 PRINT "DATA STORAGE STARTED"
4173 ASSIGN @Path TO "ZC "
4174 OUTPUT @Path,Recn;Head(*),Ptf(+),Psf(+),Vf(+),Beta(+),Deltaf(+),Pr1(+),U1
*,V1(*),W1(*),P(*)
4175 PRINT "DATA STORED IN REC NO",Head(16)
4176 !
4177 IF U1(L1)=0 THEN GOTO 4877
4178! MOVE BY DZZ,DXX
4179 DIM C$(6)[6]
4180 DATA "0" ! EXIT PROG MODE
4181 DATA "I" ! ENTER COMMAND MODE
4182 DATA "R 252" ! STEP RATE
4183 DATA "S 3"! SLOPE
4184 DATA "F 30"! STEP RATE FACTOR
4187 DATA "N 0"! NO. OF STEPS
4197 Img$="+,K" ! ASK JEFF
4207 Tkx=707
4217 Tkz=719
4227 GOSUB 4817
4237 ! Unit = 724,716,725 FOR Y,X,Z
4247 FOR I2=1 TO 2
4257 IF I2=2 THEN 4297
4267 Unit=724
4277 Sign$="+"
4287 IF (Dxx<0) THEN Sign$="-"
4297 IF I2=1 THEN 4337
4307 Unit=725
4317 Sign$="+"
4327 IF Dzz<0 THEN Sign$="-"
4337 ! CONTINUE
4347 RESTORE 4180
4357 FOR I1=1 TO 6
4367 READ C$(I1)
4377 OUTPUT Unit USING Img$;"0"
4387 OUTPUT Unit USING Img$;C$(I1)
4397 NEXT I1
4407 Ss=Dxx
4417 IF I2=2 THEN Ss=Dzz
4427 Ss1=Ss
4437 GOSUB 4817
4447 IF Unit=724 THEN M1=VAL(B$)
4457 IF Unit=725 THEN M1=VAL(R$)
4467 Ss2=ABS(Ss1)
4477 D$=VAL$(Ss2)
4487 !PRINT "LINE 822";Ss1,D$
4497 !Ii9 Loop for hp9836 5/28/86
4507 Ii9=0
4517 Ii9=Ii9+1
4527 IF Ii9=2 THEN Ii$="0"
4537 FOR I1=1 TO 5
4547 OUTPUT Unit USING Img$;C$(I1)
4557 NEXT I1
4567 OUTPUT Unit USING Img$;"N ";D$
4577 OUTPUT Unit USING Img$;Sign$
4587 OUTPUT Unit USING Img$;"G"
4597 IF Ii9=1 THEN GOTO 4517
4607 GOSUB 4817
```

```

4617 IF Unit=724 THEN M2=VAL(B$)
4627 IF Unit=725 THEN M2=VAL(A$)
4637 Dm=M2-M1
4647 !IF Dm<3 THEN D$="0"
4657 !PRINT "LINE 931 ";M1,M2,Dm,Ss
4667 !IF Dm<3 THEN GOTO 822
4677 IF Dm<Ss THEN Sign$="+"
4687 IF Dm<Ss THEN Ss1=Ss-Dm
4697 IF Dm>Ss THEN Sign$="-"
4707 IF Dm>Ss THEN Ss1=Dm-Ss
4717 IF Dm<>Ss THEN 4467
4727 WAIT .5
4737 NEXT I2
4747 NEXT L1
4757 PRINT
4767 !ASSIGN @Path TO "PR01"
4777 !FOR L2=1 TO Nn
4787 !OUTPUT @Path;Yy(L2),Uu(L2),Ur(L2),Uref,Xst
4797 !NEXT L2
4807 STOP
4817 OUTPUT Tkx USING Img$;"V 0"! X-AXIS
4827 ENTER Tkx;B$
4837 OUTPUT Tkz USING Img$;"V 0"! Z-AXIS
4847 ENTER Tkz;A$
4857 !PRINT "LINE 1143";B$,A$
4867 RETURN
4877 END

```

C.2 COMPUTER PROGRAM FOR HOT-WIRE MEASUREMENTS

```

10 ! HWZ (HP 9836) FEB 25, 1987
20 ! EQUAL STEP MOVEMENT IN Z DIRECTION
30 OPTION BASE 1
40 DIM Zz(70),Uu(70),Ur(70),Misc(70),Head(70),Rr1(70)
50 INPUT "INPUT RECORD NO ?",Recn
60 ! INPUT "MEAN VOLTAGE AT EXIT CENTER, UREF",Uref1
70 ! Mach=Uref*.1/2 ! FROM HW CAL
80 ! INPUT "MACH NO",Mach
90 ! Red=Mach*1120*3.5/12/1.6*10000
100! Red=DROUND(Red,3)
110 INPUT "MANIFOLDS OPEN =",Man A=1 B=2 C=3
120 INPUT "REFERENCE X/D",Xst
130 INPUT "INPUT 3 POSITIVE Z-STEP SIZE(IN THOUSANDTHS IN )",Step1,Step2,Step3
140 INPUT "INPUT 3 NO OF STEPS (MAX 70)",Nn1,Nn2,Nn3
150 INPUT "INPUT AMBIENT PRESS",Pa
160 INPUT "INPUT AMBIENT TEMP",Ta
170 INPUT "INPUT TANK PRESSURE",Pt
180 INPUT "INPUT TANK TEMP IN DEG F",Tt
190 INPUT "PLENUM PRESSURE =",Pp1
200 INPUT "PLENUM TEMP =",Tp1
210 INPUT "INPUT MAN A PRESSURE DIFF",Dpa
220 INPUT "INPUT MAN B PRESSURE DIFF",Dpb
230 INPUT "INPUT MAN C PRESSURE DIFF",Dpc
240 Ls1=Step1/1000
250 Ls2=Step2/1000
260 Ls3=Step3/1000
270 Rho=Pa*144/(53.3*(Ta+460))
280 Rho=DROUND(Rho,6)
290 Xst=DROUND(Xst,3)
300 !Mach=DROUND(Mach,3)
301 PRINTER IS 710
310 PRINT "HW DATA 4.5 INCH NOZZLE"
320 PRINT "RADIAL TRAVERSE"
330 PRINT "DATA STORED IN DISC NO 26 ; RECORD NO ",Recn
340 PRINT "MANIFOLD OPEN =",Man
350 PRINT "REF X/D STATION=",Xst
360 PRINT "STEP SIZES=",Ls1,Ls2,Ls3
370 PRINT "NO OF STEPS =",Nn1,Nn2,Nn3
380 PRINT "AMBIENT PRESSURE =",Pa
390 PRINT "AMBIENT TEMP = ",Ta
400 PRINT "DENSITY =",Rho,"LBS/CU.FT"
410 PRINT "TANK PRESSURE =",Pt
420 PRINT "TANK TEMP =",Tt
430 PRINT "PLENUM PRESSURE =",Pp1
440 PRINT "PLENUM TEMP =",Tp1
450 PRINT "MAN(A) DP=",Dpa,"MAN(B) DP=",Dpb,"MAN(C) DP=",Dpc
460 ! PRINT "D=3.5 IN JET Mach No.=",Mach
470 ! PRINT "ReD=",Red
480 PRINT "*****"
490 PRINT
500! Uref1=DROUND(Uref1,4)
510! PRINT "U REF [V]",Uref1
550 Diameter=4.5
560 Zz9=0
570 Nn=Nn1+Nn2+Nn3
580 Rr1(1)=0
590 FOR I=2 TO Nn1
600 Rr1(I)=Rr1(I-1)+Ls1
610 NEXT I
620 FOR I=Nn1+1 TO Nn1+Nn2
630 Rr1(I)=Rr1(I-1)+Ls2
640 NEXT I
650 FOR I=Nn1+Nn2+1 TO Nn
660 Rr1(I)=Rr1(I-1)+Ls3
670 NEXT I
680 Step=Step1

```

ORIGINAL PAGE IS
OF POOR QUALITY

```

690 FOR L1=1 TO Nn
700 IF L1>Nn1-1 THEN Step=Step2
710 IF L1>Nn1+Nn2-1 THEN Step=Step3
720 Stp=Step
730 Ls=Step/1000
740 Zz(L1)=DROUND(((Zz9/1000)/Diameter),4)
750 REMOTE 703
760 OUTPUT 703;"V D5 T1," ! READING SPEED AND TRIGGER, V DC
770 WAIT .5
780 Kk1=0
790 FOR Ii=1 TO 20
800 TRIGGER 703
810 K1=0
820 ENTER 703;K1
830 Kk1=Kk1+K1
840 NEXT Ii
850 Uu(L1)=Kk1/20
860 IF L1=1 THEN Uref=Uu(1)
861 IF L1=1 THEN
862 PRINT
864 Uref=DROUND(Uref,4)
865 PRINT
866 PRINT "U REF (V)=",Uref
867 PRINT
869 PRINT " L1          Z/D          U/Ux          Urms /Ux"
870 PRINT
872 END IF
873 Uu(L1)=DROUND((Uu(L1)-Uref),3)
880 OUTPUT 703;"VA D6 T1," ! READING SPEED AND TRIGGER, V AC
890 WAIT 1
900 Kk1=0
910 FOR Ii=1 TO 20
920 K1=0
930 TRIGGER 703
940 ENTER 703;K1
950 Kk1=Kk1+K1
960 NEXT Ii
970 Ur(L1)=Kk1/20
980 Ur(L1)=DROUND((Ur(L1)/Uref),3)
990 Stp=Step
1000 Zz9=Zz9+Stp
1010 IF L1=Nn THEN Stp=-Zz9+Stp
1020 PRINT L1,Zz(L1),Uu(L1),Ur(L1)
1030 Dyy=0
1040 Dzz=Stp
1050! SUB XY TRAV 1/23/86
1051 IF Uu(L1)<.1 THEN Nn=L1
1060 IF L1<Nn THEN GOTO 1830
1070 Head(1)=Man
1080 Head(2)=Dpa
1090 Head(3)=Dpb
1100 Head(4)=Dpc
1110 Head(5)=Xst
1120 Head(7)=Ls1
1130 Head(8)=Nn
1140 Head(9)=Pa
1150 Head(10)=Ta
1160 Head(11)=Rho
1170 Head(12)=Pt
1180 Head(13)=Tt
1190 Head(14)=Pp1
1200 Head(15)=Tp1
1210 Head(16)=Recn
1220 Head(24)=Ls2
1230 Head(25)=Ls3
1240 Head(30)=Uref1

```

```

1250 Head(31)=Unef
1260 PRINT
1261 Unef=DROUND(Unef,4)
1263 PRINT "U REF (V)=",Unef
1270 PRINT
1280 PRINT "DATA STORAGE STARTED"
1290 ASSIGN @Path TO "ZC"
1300 OUTPUT @Path,Rech;Head(*),Uu(*),Ur(*),Rr1(*),Zz(*),Misc(*)
1310 PRINT "DATA STORAGE COMPLETED"
1320 GINIT
1330 GRAPHICS ON
1340 DUMP DEVICE IS 710
1350 ! PLOTTER IS 705,"HPGL"
1360 VIEWPORT 10,110,20,80
1370 FRAME
1380 CSIZE 4,.4
1390 MOVE 20,70
1400 GCLEAR
1410 J=0
1420 MOVE 25,80
1430 GCLEAR
1440 WINDOW 0,1,0,1      A
1450 AXES .10,.10,0,0,2,2,5
1460 FRAME
1470 FOR J=1 TO 1
1480 MOVE 0,0
1490 CLIP OFF
1500 MOVE .5,-.15
1510 LABEL "r/D"
1520 MOVE 0,-.25
1530 LABEL "FIG    RADIAL DISTRIBUTIONS OF MEAN AXIAL VELOCITY (S=.40)"
1540 DEG
1550 LDIR 90
1560 MOVE -.05,.45
1570 LABEL "U/Ux"
1580 LDIR 0
1581 MOVE .5,1.2
1582 LABEL "(HW DATA)"
1590 CSIZE 3.5,.5
1600 LORG 5
1610 FOR I=0 TO 1 STEP .2
1620 MOVE -.02,I
1630 LABEL USING "#,K";I
1640 NEXT I
1650 LORG 5
1660 FOR I=0 TO 1.0 STEP .2
1670 MOVE I,-.05
1680 LABEL USING "#,K";I
1690 NEXT I
1700 NEXT J
1710 FOR I=1 TO Head(8)
1720 Ror=Rr1(I)/Diameter
1730 U=Uu(I)
1740 MOVE Ror,U
1750 LABEL "o"
1760 NEXT I
1770 FOR I=1 TO Head(8)
1780 Ror=Rr1(I)/Diameter
1790 U=Uu(I)
1800 PLOT Ror,U
1810 NEXT I
1820 DUMP GRAPHICS
1821 IF Uu(L1)<.1 THEN GOTO 2560
1830! MOVE BY Dxx Dyy
1840 DIM C$(6)[6]
1850 DATA "Q" ! EXIT PROG MODE

```

```

1860 DATA "I" ! ENTER COMMAND MODE
1870 DATA "R 252" ! STEP RATE
1880 DATA "S 3"! SLOPE
1890 DATA "F 30"! STEP RATE FACTOR
1900 DATA "N 0"! NO. OF STEPS
1910 Img$="+,K" ! ASK JEFF
1920 Tky=706
1930 Tkz=719
1940 GOSUB 2500
1950 ! Unit = 716,724,725 FOR Y,X,Z
1960 FOR I2=1 TO 2
1970 ! IF I2=2 THEN 2010
1980 Unit=716
1990 Sign$="+"
2000 IF (Dyy<0) THEN Sign$="-"
2010 IF I2=1 THEN 2050
2020 Unit=725
2030 Sign$="+"
2040 IF Dzz<0 THEN Sign$="-"
2050 ! CONTINUE
2060 RESTORE 1850
2070 FOR I1=1 TO 6
2080 READ C$(I1)
2090 OUTPUT Unit USING Img$;"0"
2100 OUTPUT Unit USING Img$;C$(I1)
2110 NEXT I1
2120 Ss=Dyy
2130 IF I2=2 THEN Ss=Dzz
2140 Ss1=Ss
2150 GOSUB 2500
2160 IF Unit=716 THEN M1=VAL(B$)
2170 IF Unit=725 THEN M1=VAL(A$)
2180 Ss2=ABS(Ss1)
2190 D$=VAL$(Ss2)
2200 !PRINT "LINE 822";Ss1,D$
2210 !Ii9 Loop for hp9836 5/28/86
2220 Ii9=0
2230 Ii9=Ii9+1
2240 IF Ii9=2 THEN D$="0"
2250 FOR I1=1 TO 5
2260 OUTPUT Unit USING Img$;C$(I1)
2270 NEXT I1
2280 OUTPUT Unit USING Img$;"N ";D$
2290 OUTPUT Unit USING Img$;Sign$
2300 OUTPUT Unit USING Img$;"G"
2310 IF Ii9=1 THEN GOTO 2230
2320 GOSUB 2500
2330 IF Unit=716 THEN M2=VAL(B$)
2340 IF Unit=725 THEN M2=VAL(A$)
2350 Dm=M2-M1
2360 !IF Dm<3 THEN D$="0"
2370 !PRINT "LINE 931 ";M1,M2,Dm,Ss
2380 !IF Dm<3 THEN GOTO 822
2390 IF Dm<Ss THEN Sign$="+"
2400 IF Dm<Ss THEN Ss1=Ss-Dm
2410 IF Dm>Ss THEN Sign$="-"
2420 IF Dm>Ss THEN Ss1=Dm-Ss
2430 IF Dm<>Ss THEN 2180
2440 WAIT .5
2450 NEXT I2
2460 NEXT L1
2470 PRINT
2480 PRINT
2490 STOP
2500 OUTPUT Tky USING Img$;"V 0"! Y-AXIS
2510 ENTER Tky;B$

```

```
2520 OUTPUT Tkz USING Img$; "V 0"! Z-AXIS
2530 ENTER Tkz;A$
2540!PRINT "LINE 1143";B$,A$
2550 RETURN
2560 END
```

APPENDIX D:

BLUEPRINTS

* * * * *

FIGURES INCLUDED IN APPENDIX D

<u>Number</u>	<u>Title</u>	<u>Page</u>
D1	Manifold "A" Dimensions.....	D.2
D2	Manifold "B" Dimensions.....	D.3
D3	Manifold "C" Dimensions.....	D.4
D4	Orifice Plate Dimensions.....	D.5
D5	Elbow Nozzle Alterations.....	D.6

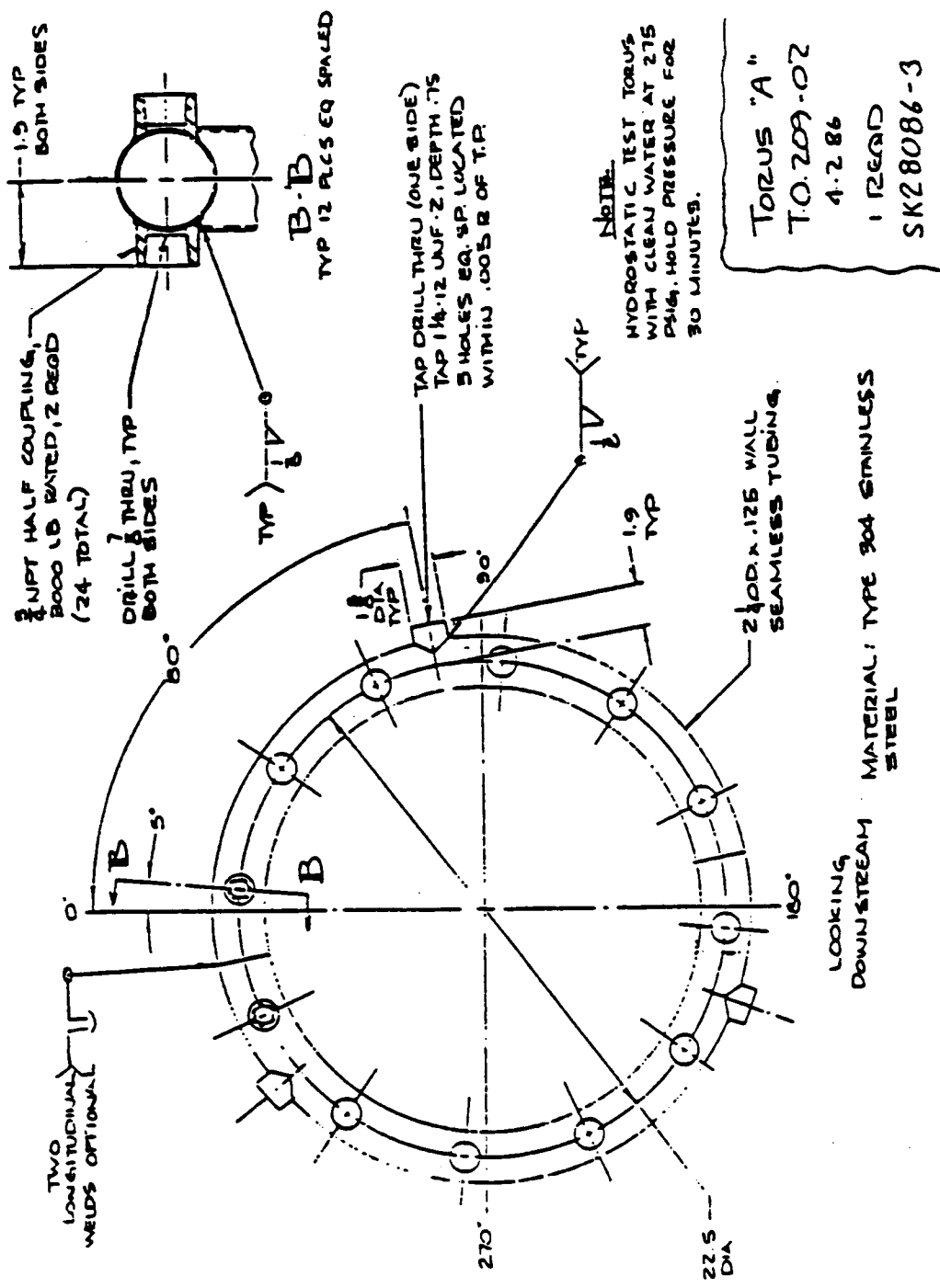
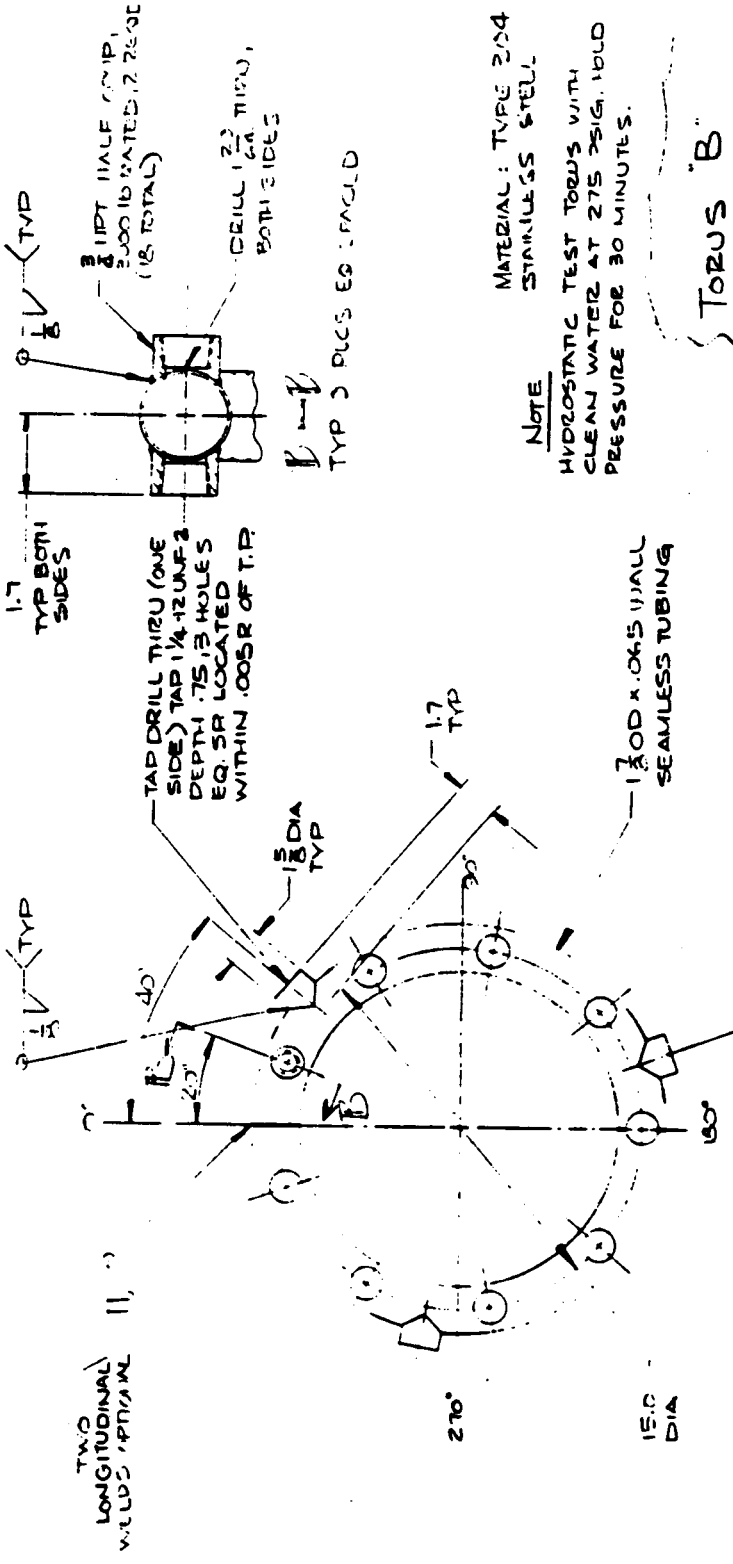


Figure D1: Manifold "A" Dimensions

ORIGINAL PAGE IS
OF POOR QUALITY



NOTE
MATERIAL: TYPE 304
STAINLESS STEEL
HYDROSTATIC TEST TORUS WITH
CLEAN WATER AT 275 PSIG. HOLD
PRESSURE FOR 30 MINUTES.

TORUS 'B'
T.O. 209-02
4-2-86
1 REQD

SK28086-2

Figure D2: Manifold "B" Dimensions

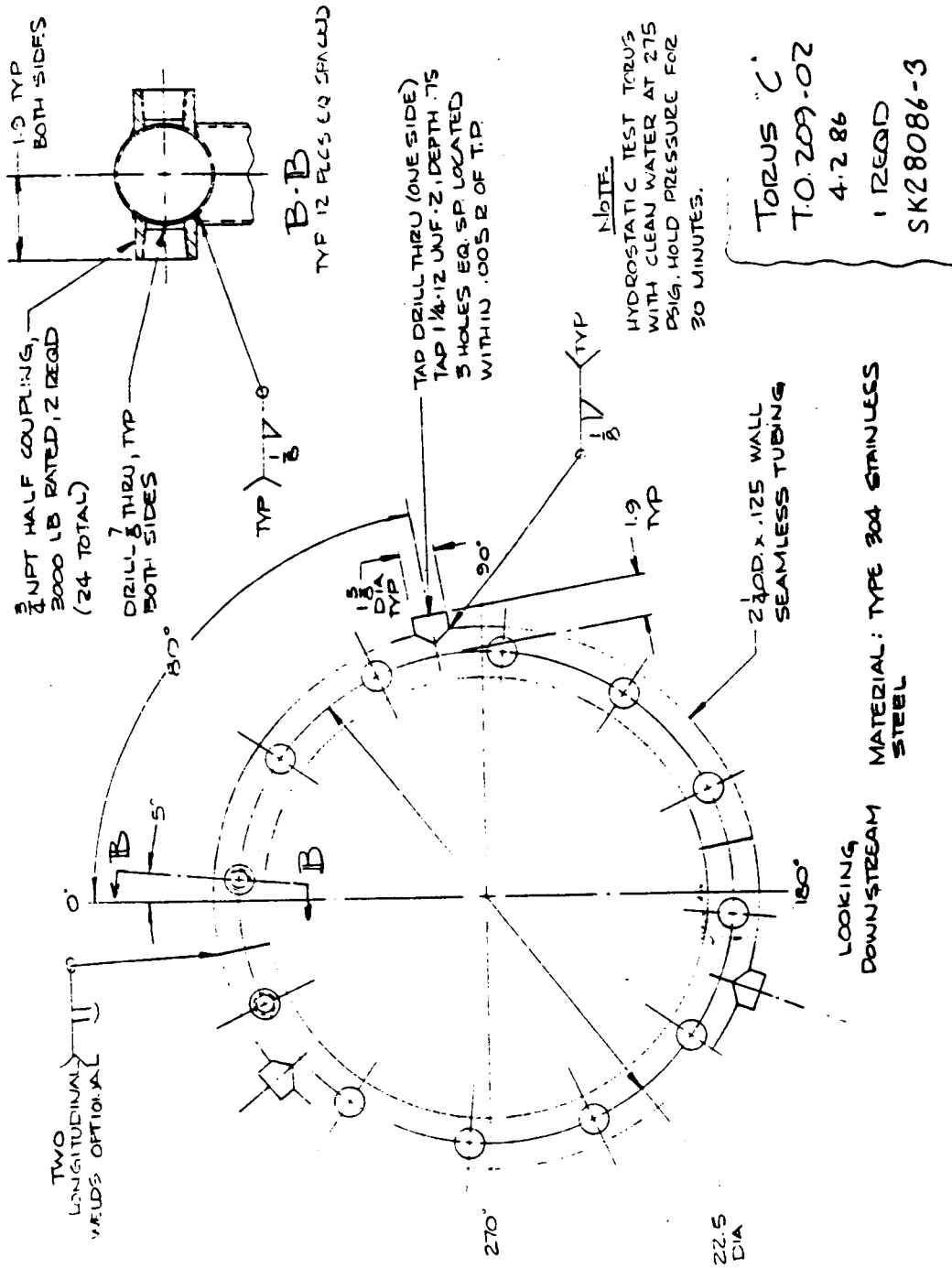


Figure D3: Manifold "C" Dimensions

ORIGINAL VIEW IS OF POOR QUALITY

ORIGINAL PAGE IS
OF POOR QUALITY

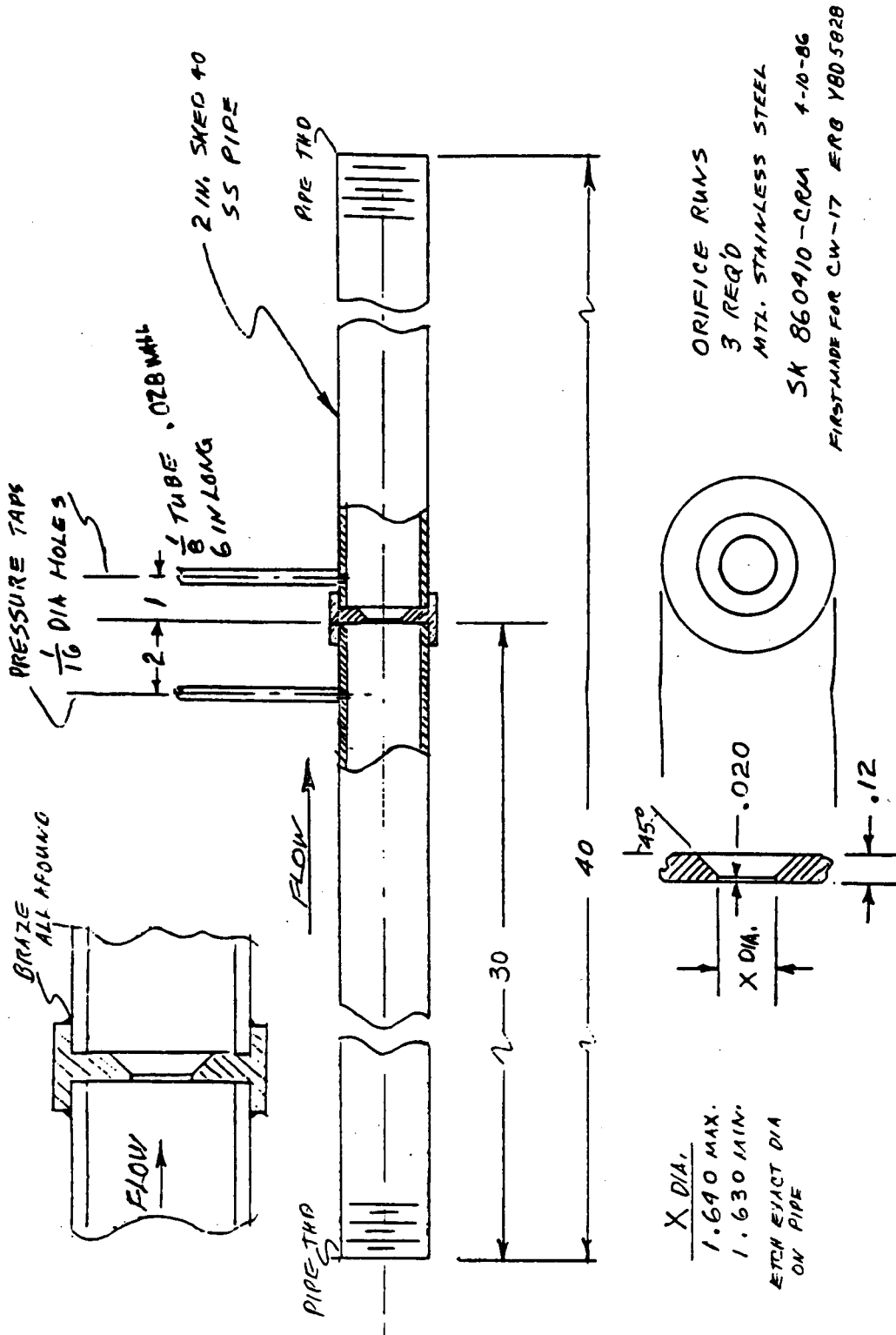


Figure D4: Orifice-Plate Dimensions

1. Report No. NASA CR-180895		2. Government Accession No.		3. Recipient's Catalog No.	
4. Title and Subtitle Turbulent Swirling Jets With Excitation				5. Report Date March 1988	
				6. Performing Organization Code	
7. Author(s) Rahmat Taghavi and Saeed Farokhi				8. Performing Organization Report No. None	
				10. Work Unit No. 505-62-21	
9. Performing Organization Name and Address Flight Research Laboratory The University of Kansas Center for Research, Inc. Lawrence, Kansas 66045				11. Contract or Grant No. NCC-3-56	
				13. Type of Report and Period Covered Contractor Report Interim	
12. Sponsoring Agency Name and Address National Aeronautics and Space Administration Lewis Research Center Cleveland, Ohio 44135-3191				14. Sponsoring Agency Code	
15. Supplementary Notes Project Manager, Edward J. Rice, Internal Fluid Mechanics Division, NASA Lewis Research Center.					
16. Abstract An existing cold-jet facility at NASA Lewis Research Center was modified to produce swirling flows with controllable initial tangential velocity distribution. Two extreme swirl profiles, i.e., one with solid-body rotation and the other predominated by a free-vortex distribution, were produced at identical swirl number of 0.48. Mean centerline velocity decay characteristics of the solid-body rotation jet flow exhibited classical decay features of a swirling jet with $S \approx 0.48$ reported in the literature. However, the predominantly free-vortex distribution case was on the verge of vortex breakdown, a phenomenon associated with the rotating flows of significantly higher swirl numbers, i.e., $S_{crit} \geq 0.6$. This remarkable result leads to the conclusion that the integrated swirl effect, reflected in the swirl number, is inadequate in describing the mean swirling jet behavior in the near field. The relative size (i.e., diameter) of the vortex core emerging from the nozzle and the corresponding tangential velocity distribution are also controlling factors. Excitability of swirling jets is also investigated by exciting a flow with a swirl number of 0.35 by plane acoustic waves at a constant sound pressure level and at various frequencies. It is observed that the cold swirling jet is excitable by plane waves, and that the instability waves grow about 50 percent less in peak r.m.s. amplitude and saturate further upstream compared to corresponding waves in a jet without swirl having the same axial mass flux. The preferred Strouhal number based on the mass-averaged axial velocity and nozzle exit diameter for both swirling and nonswirling flows is 0.4.					
17. Key Words (Suggested by Author(s)) Swirl, Swirling jet, Turbulent, Instability wave, Jet			18. Distribution Statement Unclassified - Unlimited Subject Category 02		
19. Security Classif. (of this report) Unclassified		20. Security Classif. (of this page) Unclassified		21. No of pages 229	22. Price* A07